A Snapshot of Tevatron Flying Wire and Synchrotron Light Detector Transverse Emittance Measurements at 980GeV

Krzysztof Genser
June 3rd 2003

Computing Division, Fermilab

Abstract

This note compares Tevatron Transverse Emittance measurements done using Flying Wire and Synchrotron Light detectors. It also describes performance and self consistency of the above detectors.

1 Introduction

We study Tevatron Transverse Emittance measurements done using Flying Wires (FW) (See ref [2]) and Synchrotron Light (SL)(See ref [3]) detectors. The above detectors were used to measure the transverse beam spread. The Sampled Bunch Display (SBD) system was used to measure longitudinal beam spread. In the case of the Vertical Emittance comparison between FW at the E11 location and SL detectors is done. In the case of the Horizontal Emittance the comparison also includes FW detector at E17.

2 Data Selection

The stores for this analysis were selected from May 2003 running period when the detector parameters were believed to be constant. This resulted in stores: 2502, 2503, 2505, 2507, 2509, 2511, 2521, 2523, 2529, 2536, 2538, 2540, 2542, 2546, 2549, 2551, 2555, 2557. The Tevatron Case chosen for analysis was "Remove Halo" (with the beam energy of 980GeV) as this is one of the cases where both FW and SL systems are activated. The requirements imposed on the data were:

1. The FW freshness number (ACcelerator NETwork (ACNET) variable T:FWFRSH) in case "Remove Halo" had to be incremented by at least one with respect to the case "Initiate Collisions".

2. The Transverse Emittance as measured by the FW E11 (combined with SBD in the Horizontal cases) had to be between 0 and 40 ($\pi \cdot mm \cdot mrad$) in the vertical cases and between 0 and 25 ($\pi \cdot mm \cdot mrad$) in the horizontal cases (to avoid both nonphysical or difficult to measure cases).

3. The antiprotons intensity had to be greater than 15E9 (to avoid difficult to measure cases)

3 Emittance calculations

The following formulas were used to calculate the Horizontal and Vertical (Normalized) Emittances:

$$\varepsilon_h = 6\left(\sigma^2 - (\frac{\delta p}{p})^2 D^2\right)\frac{\gamma_L}{\beta} \qquad \varepsilon_v = 6\sigma^2\frac{\gamma_L}{\beta}$$

where

$$\delta p = \delta t * (83.293 + \delta t * (-10.562 + \delta t * 0.8023)) \text{ (See ref [1])}$$

δt is the T:SBD[A,P]SS ACNET variable (longitudinal beam bunch spread in ns), p is the beam momentum in GeV, γ_L is the Lorentz gamma, σ are bunch width as measured by each of the detectors (ACNET variables T:SL[A,P]S[H,V], T:FW[H,V,E][A,P]SG). In the FW case the width is the arithmetic average of the two measurements (for both of the wire passes trough the beam). The dispersion (D) and β lattice functions at E11, E17, C11 (location of the SL detector) are shown in Table 1.

Detector	beta Function [m]	dispersion Function [m]
FW E11H p & $\overline{p}$	80.161	2.030
FW E11V p & $\overline{p}$	80.804	
FW E17H p & $\overline{p}$	68.157	5.278
SL C11H p	50.005	1.517
SL C11H $\overline{p}$	34.040	1.182
SL C11V p	107.862	
SL C11V $\overline{p}$	101.648	

Table 1: Tevatron beta and dispersion functions for corresponding measurement locations

4 Performance of Individual Detectors

4.1 Flying Wire Detectors at E11 and E17 locations

Results related to the performance of the Horizontal Flying Wire Detector at the E11 location are shown on figures 1 to 4 for antiprotons and on figures 20 to 23 for protons. Figures 39 to 42 show the same quantities related to the Vertical Flying Wire Detector at E11 for antiprotons, and figures 49 to 52 correspond to the protons. Similarly, results related to the performance of the Horizontal Flying Wire Detector at the E17 location are shown on figures 11 to 14 for antiprotons, and on figures 30 to 33 for protons.
The quantities plotted on the first figure from each set are (1 – top left, 2 – top right, 3 – bottom left, 4 – bottom right):

1. amplitude (in arbitrary units) times sigma (square root of variance) of the bunch width distribution (in *mm*) of the front end FW detector data versus bunch intensity (ACNET variables T:FBI[A,P]NG) (in E9) with an overlaid horizontal profile of the previous distribution with a straight line fit;

2. amplitude times sigma of the bunch width distribution of the front end FW detector data over bunch intensity versus bunch centroid (in *mm*) (based on the T:FW[E,H,V][A,P]CE ACNET variable) with an overlaid horizontal profile of that distribution with a straight line fit;

3. bunch intensity;

4. amplitude times sigma of the bunch width distribution (in *mm*) of the raw FW detector distribution over bunch intensity versus store number.

In the second figure of each set quantities plotted are as follows:

1. sigma of the bunch width distribution (in *mm*) as measured by the FW detector versus front end measure of the goodness of fit;

2. sigma itself;

3. goodness of fit itself;

4. goodness of fit versus bunch intensity.

The third figure of each set shows:

1. amplitude (in arbitrary units) times sigma of the bunch width distribution (in *mm*) of the pass 1 over pass 2 of the front end FW detector data versus bunch intensity (ACNET variables T:FBI[A,P]NG) (in E9) with an overlaid horizontal profile of that distribution with a straight line fit;

2. sigma of the bunch width distribution versus bunch centroid (in *mm*) (based on the T:FW[E,H,V][A,P]CE ACNET variable) with an overlaid horizontal profile of that distribution with a straight line fit;

3. amplitude times sigma of the bunch width distribution (in *mm*) of the pass 1 over pass 2 of the front end FW detector data;

4. bunch emittance (in $\pi \cdot mm \cdot mrad$) versus store number.

The fourth figure of each set shows:

1. sigma of the bunch width distribution (in *mm*) of the pass 1 versus pass 2 of the FW detector;

2. sigma of the bunch width distribution (in *mm*) of the pass 1 over pass 2 of the FW detector versus bunch intensity (ACNET variables T:FBI[A,P]NG) (in E9);

3. sigma of the beam width distribution (in *mm*) of the bunch width distribution of the pass 1 over pass 2 of the FW detector itself;

4. sigma of the bunch width distribution (in *mm*) of the pass 1 over pass 2 of the FW detector versus front end measure of the goodness of fit.

4.2 Flying Wire Detectors at E11

From the plots related to the Flying Wire Detectors at the E11 location one can see that for horizontal antiproton detector the ratio of amplitude times sigma to bunch intensity is quite stable with no significant dependence on bunch centroid position for the stores considered, with an overall rms of 7.4% (Fig 1-4). There is an indication of the detector saturation for higher bunch intensities (Fig 3-1) and some sigma on centroid position dependence. There also seems to be a correlation between sigma and χ^2 (Fig 2-1) and a strong correlation between χ^2 and bunch intensity (Fig 2-4). There seems to be some grouping in the amplitude times sigma of pass 1 over pass 2 versus bunch intensity (Fig 3-1). The difference between sigmas from two passes and the asymmetric shape of the distributions is leading to the bunch width measurement accuracy of about 1.7%/2 with assymetric tails up to 5%/2, giving sigma "rms of rms" of 1.3%/2 (Fig 4-3).

The distributions related to the horizontal proton detector show that there is some store to store instability of the amplitude times sigma to bunch intensity ratio due to significant dependence on bunch centroid position despite small overall fluctuations of the ratio (rms 3.3%) (Fig 20-4). As opposed to the horizontal antiproton detector, there is no obvious correlation between sigma and χ^2 and between χ^2 and bunch intensity, although there may be some for intensities smaller than 210E9 (Fig 21-1,4). Again, as in the horizontal antiproton case there seems to be some grouping in the amplitude times sigma of pass 1 over pass 2 versus bunch intensity plot (Fig 22-1). Given that grouping it is hard to conclude if this detector saturates or not however sigma dependence on centroid position is even stronger than in the horizontal antiproton case. The difference between sigmas from two passes and the asymmetric shape of the distribution leads to the bunch width measurement accuracy of about 1.7%/2 with rms of 0.63%/2 (Fig 23-3).

From plots presenting vertical antiproton detector data one can see that the ratio of amplitude times sigma to bunch intensity is quite stable with an overall rms of 7.1% and there is no significant dependence on bunch centroid position (Fig 39-2,4). The detector does show signs of saturation as can be seen in Fig 39-1 and 41-1 and a significant trend in sigma on centroid position dependence. Similarly to the horizontal antiproton case there is a correlation between sigma and χ^2 and between χ^2 and bunch intensity (Fig 40-1,4). The difference between sigmas from two passes results in a bunch width measurement accuracy of about 2.3%/2 with rms of 0.89%/2 (Fig 42-3).

The distributions related to the vertical proton detector show that there is significant variation of the ratio of amplitude times sigma to bunch intensity with bunch centroid position for the range of stores involved with the overall rms of 3.5% (Fig 49-4). There is no visible correlation between sigma and χ^2 and between χ^2 and intensity (Fig 50-1,4). There is a possible saturation of the detector (Fig 51-1) and a significant sigma on centroid position dependence. There is distinct two peak structure in the distribution of the sigmas from two passes, but because the peaks are almost symmetric with respect to one there is still quite good measurement accuracy for each peak of about 1-1.5%/2 (Fig 52-3).

4.3 Flying Wire Detector at E17

The distributions related to the horizontal antiproton detector show that an rms of the ratio of amplitude times sigma to bunch intensity is about 2.1% and there is no significant dependence on the bunch centroid poistion (Fig 11). There is a strong sigma dependence on χ^2, and strong χ^2 dependence on intensity (Fig 12-1,4). There are no indications that the detector is saturating (Fig 13) and there may be some sigma dependence on bunch centroid position. Because of the structure of the distribution of the sigmas from two passes the width measurement accuracy is about 1%/2 with rms of about 1%/2 (Fig 14).

From plots presenting data of the horizontal proton detector one can see that the ratio of amplitude times sigma to bunch intensity is quite stable with the rms of 2.0% and there is no significant dependence on the bunch centroid poistion (Fig 30). There is some possible small correlation between sigma and χ^2 and a correlation between χ^2 and intensity (Fig 31-1,4). As in other FW detector cases there is some grouping in the amplitude times sigma of pass 1 over pass 2 versus bunch intensity plots. There may be some sigma dependence on bunch centroid position (Fig 32). Fig 33-2 seems to indicate that sigma ratio seems

to depend on the bunch intensity. Given the structure of the pass 1 versus pass 2 sigmas distribution the sigma measurement accuracy is about 1.0%/2 with an rms of 0.8%/2 (Fig 33-3).

4.4 Synchrotron Light Detectors at C11

Results related to the performance of the Synchrotron Light Detector at the C11 location are shown on figures 5 to 7 and 43 to 45 for antiprotons and on figures 24 to 26 and 53 to 55 for protons.

The quantities plotted on the first figure from each set are (top left, top right, bottom left, bottom right):

1. amplitude (in arbitrary units) times sigma of the bunch width distribution (in *mm*) of the raw SL detector distribution versus bunch intensity (ACNET variables T:FBI[A,P]NG) (in E9) with an overlaid horizontal profile of that distribution with a straight line fit;
2. amplitude times sigma of the bunch width distribution (in *mm*) of the raw SL detector distribution over bunch intensity versus bunch E11 centroid (in *mm*) (based on the T:FW[E,H,V][A,P]CE ACNET variable) with an overlaid horizontal profile of that distribution with a straight line fit;
3. bunch intensity;
4. amplitude times sigma of the bunch width distribution (in *mm*) of the raw SL detector distribution over bunch intensity versus store number.

In the second figure of each set quantities are as follows:

1. Sigma of the bunch width distribution (in *mm*) as measured by the SL detector versus front end measure of the goodness of fit;
2. sigma of the bunch width distribution (in *mm*) itself;
3. goodness of fit itself;
4. the goodness of fit versus bunch intensity.

The third figure of each set shows:

1. Bunch emittance (in $\pi \cdot mm \cdot mrad$) as measured by the front end SL detector versus bunch emittance as recalculated using front end sigma of the bunch width distribution (in *mm*) (combined with SBD timing information in the horizontal cases) with an overlaid horizontal profile of that distribution with a straight line fit;
2. sigma of the bunch width distribution versus bunch E11 centroid (in *mm*) (based on the T:FW[E,H,V][A,P]CE ACNET variable) with an overlaid horizontal profile of that distribution with a straight line fit;
3. bunch emittance;
4. bunch emittance versus store number.

The distributions related to the horizontal antiproton case show that the ratio of amplitude times sigma to bunch intensity has an rms of about 4.0% with some dependence on bunch centroid position (Fig 5-4,2). There are no signs of strong correlations between sigmas, χ^2 and bunch intensity (Fig 6). There is a good agreement between front end and offline calculations and almost no indication of sigma dependence on bunch centroid position (Fig 7).

From plots presenting data of the horizontal proton case one can see that the ratio of amplitude times sigma to bunch intensity has an quite large rms of 7.2% with strong dependence on bunch centroid position wich may be resposible for large portion of the store to store variations (Fig 24-1,2,4). There are no signs of strong correlations between sigmas, χ^2 and bunch intensity (Fig 25). There is a good agreement between front end and offline calculations but there is a significant sigma dependence on bunch centroid position (Fig 26).

The distributions related to the vertical antiproton case show that the ratio of amplitude times sigma to bunch intensity is quite stable with overall rms of about 4.1% with some dependence on bunch centroid position (Fig 43-1,2,4). As in other Synchrotron Light detector cases there are no correlation between sigma and χ^2 and between χ^2 and intensity (Fig 44). There is a good agreement between front end and offline calculations but there is a significant sigma dependence on bunch centroid position (Fig 45).

Plots showing data for the vertical proton case are similar to the ones in horizontal proton case in that the instability of the ratio of amplitude times sigma to bunch intensity is large (rms of 7.4%) and there is strong dependence on bunch centroid position. (Fig 53-1,2,4). There is no correlation between sigma and χ^2 and between χ^2 and intensity (Fig 54). The agreement between front end and offline calculations is good but there is a significant sigma dependence on bunch centroid position (Fig 55).

5 Comparisons of Emittance measurements as done using Synchrotron Light Detectors and Flying Wire Detectors at E17 to the Measurements done using Flying Wire Detectors at E11

5.1 Comparison between Synchrotron Light Detectors at C11 and Flying Wire Detectors at E11

Data relating Emittances measurements as done using Synchrotron Light Detectors at C11 and Flying Wire Detectors at E11 are presented on figures 8 to 10 for antiprotons and on figures 27 to 29 for protons. Whereas figures 46 to 48 show the same quantities related to the Vertical Flying Wire Detector for antiprotons and figures 56 to 58 correspond to the protons.

The quantities plotted on the first figure from each set are:

1. Bunch emittance (in $\pi \cdot mm \cdot mrad$) as measured by Synchrotron Light Detector versus bunch emittance as measured by the Flying Wire Detector at E11;
2. horizontal profile of the previous distribution with a straight line fit;
3. Bunch emittance as measured by Synchrotron Light Detector over bunch emittance as measured by the Flying Wire Detector at E11 versus bunch intensity (ACNET variables T:FBI[A,P]NG) (in E9);
4. Bunch emittance as measured by Synchrotron Light Detector over bunch emittance as measured by the Flying Wire Detector at E11 versus store number.

In the second figure of each set quantities plotted are as follows:

1. Bunch emittance as measured by Synchrotron Light Detector over bunch emittance as measured by the Flying Wire Detector at E11 versus recalculated $\delta p/p$ (based on δt the T:SBD[A,P]SS ACNET variable);
2. horizontal profile of the previous distribution with a straight line fit;
3. $\delta p/p$ itself;
4. $\delta p/p$ versus store number.

The third figure of each set shows:

1. Bunch emittance as measured by Synchrotron Light Detector over bunch emittance as measured by the Flying Wire Detector at E11 versus bunch E11 centroid (in *mm*) (based on the T:FW[E,H,V][A,P]CE ACNET variable);
2. horizontal profile of the previous distribution with a straight line fit;
3. bunch E11 centroid itself;
4. bunch E11 centroid versus store number;

The horizontal antiproton emittance case shows that there is large non zero offset of 38.6 (See Table 3) and slope different from one of 0.43 in the SL v FW dependence, the overall ratio is 2.6 and strongly depends on bunch intensity (Fig 8-1,2,3). There is no obvious dependence of the ratio on $\delta p/p$ (Fig 9-1,2). But there is some dependence on the bunch centroid position (Fig 10-1,2,3). In the case of horizontal proton emittance SL v FW dependence the offset is 6.4 and slope 1.3. The emittance ratio is 1.6 with a weak dependence on the bunch intensity (Fig 27-1,2,3). There seems to be a weak dependence on $\delta p/p$ (Fig 28-1,2). There is a dependence on the bunch centroid position (Fig 29-1,2,3). The SL v FW dependence for the vertical antiproton emittance has offset of 12.7, slope of 0.73 the ratio is 1.17 with strong ratio intensity dependence (Fig 46-1,2,3). There do not seem to be any dependence on $\delta p/p$ (Fig 46-2). There is no significant dependence on the bunch centroid position (Fig 48-1,2,3). In the vertical proton emittance SL v FW dependence there is no significant offset (0.3), the slope is 1.25 and the ratio 1.26. There is little if any ratio dependence on the intensity and no signs of $\delta p/p$ dependence (Fig 56-1,2,3 and Fig 56-2). There is no significant dependence on the bunch centroid position (Fig 58-1,2,3).

5.2 Comparison between Flying Wire Detectors at E17 and E11

Data relating Emittances measurements as done by Synchrotron Light Detectors at C11 and Flying Wire Detectors at E11 are presented on figures 15 to 17 for antiprotons and on figures 34 to 36 for protons.

The quantities plotted on the first figure from each set are:

1. Bunch emittance (in $\pi \cdot mm \cdot mrad$) as measured by Flying Wire Detector at E17 versus bunch emittance as measured by the Flying Wire Detector at E11;
2. horizontal profile of the previous distribution with a straight line fit;
3. Bunch emittance as measured by Flying Wire Detector at E17over bunch emittance as measured by the Flying Wire Detector at E11 versus bunch intensity (ACNET variables T:FBI[A,P]NG) (in E9);
4. Bunch emittance as measured by Flying Wire Detector at E17 over bunch emittance as measured by the Flying Wire Detector at E11 versus store number.

In the second figure of each set quantities plotted are as follows:

1. Bunch emittance as measured by Flying Wire Detector at E17 Detector over bunch emittance as measured by the Flying Wire Detector at E11 versus recalculated $\delta p/p$ (based on δt the T:SBD[A,P]SS ACNET variable);
2. horizontal profile of the previous distribution with a straight line fit;
3. $\delta p/p$ itself;
4. δt versus store number.

The third figure of each set shows:

1. Bunch emittance as measured by Flying Wire Detector at E17 over bunch emittance as measured by the Flying Wire Detector at E11 versus bunch E11 centroid (in *mm*) (based on the T:FW[E,H,V][A,P]CE ACNET variable);
2. horizontal profile of the previous distribution with a straight line fit;
3. bunch E17 centroid itself;
4. bunch E17 centroid versus store number;

The FW E17 v E11 horizontal antiproton emittance dependence has a nonzero offset of 4.1, slope very different from one 0.4, ratio of 0.63 with some bunch intensity dependence and significant store to store variations with possible weak dependence on $\delta p/p$ (Fig 15 and 16). There is a weak dependence on bunch centroid position (Fig 17). The dependence of FW E17 v E11 in the horizontal proton emittance case has offset of 9.1 and slope of 0.7. The ratio is 1.20 with some dependence on intensity and large store to store variations. There is some possible weak dependence on $\delta p/p$ (Fig 34 and 35). There is a quite strong dependence on bunch centroid position (Fig 36).

6 Summary and Conclusions

We have studied performance of Tevatron transverse emittance detectors and made emittance measurement comparisons. The results are summarized in Tables 2 and 3.

It can be seen that the Flying Wire (FW) detectors saturate for large antiproton bunch intensities and that most of the FW detectors show signs of χ^2 dependence on bunch intensities. The statistical accuracy of FW detectors as estimated from two passes is about 1%. There is also some amplitude times sigma over bunch intensity dependence on the beam position for the E11 detector when measuring proton beam. The performance of Synchrotron Light (SL) detectors does not show χ^2 dependence on bunch intensities although the amplitude times sigma over bunch intensity depends significantly on the beam position especially for proton detector. We note a non negligible trend in the bunch width sigma distribution dependence on the centroid position especially in vertical antiproton and horizontal proton FW E11 and SL detector cases.

When comparing emittance measurements done by SL detectors v FW E11 detectors (Table 3) we note statistically significant disagreements. The largest one being discrepancy in the horizontal antiproton case. It shows itself in all measured

Detector	Ampl times Sigma over bunch intensity [AS/I] RMS [%]	AS/I Centroid Dependence [%/RMS]	Sigma Centroid Dependence [%/RMS]	Accuracy [%]	Saturation	Sigma Dependence on χ^2
FWE11 horizontal $\overline{p}$	7.4	-0.397 ± 0.093	1.455 ± 0.085	0.85 ± 0.65	yes	yes
FWE11 horizontal p	3.3	-2.442 ± 0.066	2.175 ± 0.046	0.85 ± 0.31	perhaps	some
FWE11 vertical $\overline{p}$	7.1	-0.08 ± 0.14	-3.31 ± 0.19	1.15 ± 0.45	yes	yes
FWE11 vertical p	3.5	3.029 ± 0.077	-1.679 ± 0.089	0.6 ± 0.30	yes	no
FWE17 horizontal $\overline{p}$	2.1	-0.570 ± 0.034	1.25 ± 0.16	0.5 ± 0.5	no	yes
FWE17 horizontal p	2.0	0.412 ± 0.056	-0.382 ± 0.065	0.5 ± 0.4	no	no
SL horizontal $\overline{p}$	4.0	-3.26 ± 0.11	0.286 ± 0.056	n/a	n/a	no
SL horizontal p	7.2	-5.43 ± 0.16	2.257 ± 0.071	n/a	n/a	no
SL vertical $\overline{p}$	4.1	2.52 ± 0.10	-2.53 ± 0.13	n/a	n/a	no
SL vertical p	7.4	5.50 ± 0.21	-1.72 ± 0.12	n/a	n/a	no

Table 2: Some characteristics of the Flying Wire and Synchrotron Light Detectors and their measurements. The errors quoted are statistical only.

Detectors	Intercept	Slope	Ratio	Correlation Factor	Intensity Dependence [%/RMS]	Centroid Dependence [%/RMS]
SL v FWE11 horizontal $\overline{p}$	$36.85^{+0.16}_{-2.1}$	$0.551^{+0.079}_{-0.009}$	$2.62^{+0.28}_{-0.27}$	0.49	-4.20 ± 0.36	-1.75 ± 0.20
SL v FWE11 horizontal p	$6.39^{+2.1}_{-0.27}$	$1.288^{+0.015}_{-0.11}$	$1.642^{+0.085}_{-0.085}$	0.78	-1.34 ± 0.13	-1.79 ± 0.15
SL v FWE11 vertical $\overline{p}$	$12.69^{+0.17}_{-3.9}$	$0.715^{+0.096}_{-0.006}$	$1.16^{+0.13}_{-0.12}$	0.88	-5.13 ± 0.34	0.86 ± 0.26
SL v FWE11 vertical p	$0.34^{+2.6}_{-0.97}$	$1.252^{+0.042}_{-0.077}$	$1.264^{+0.057}_{-0.057}$	0.82	0.53 ± 0.10	-0.44 ± 0.17
FWE17 v FWE11 horizontal $\overline{p}$	$4.1^{+4.1}_{-1.6}$	$0.397^{+0.103}_{-0.24}$	$0.626^{+0.085}_{-0.085}$	0.53	-2.23 ± 0.59	-0.35 ± 0.25
FWE17 v FWE11 horizontal p	$9.1^{+1.8}_{-1.7}$	$0.696^{+0.081}_{-0.114}$	$1.204^{+0.087}_{-0.087}$	0.54	-3.05 ± 0.15	-3.83 ± 0.12

Table 3: Statistical data related to correlation of emittance measurements by different detector pairs. The errors for slope, intercept and ratio are statistical and systematic combined in quadrature. The systematic errors were estimated by dividing the data sample into high and low intensity bins and taking the difference between the central and high or low value. The errors on the intensity and centroid position dependence are statistical only.

parameters together with a small correlation factor. The ratio of the remaining measurements varies from 1.16 to 1.64. Comparison of horizontal emittance measurements as done with FW E17 and E11 detectors show low correlation factors and large ratio discrepancy of 0.63 and 1.20. To bring these ratios to one it would require varying the E17 dispersion function in two opposite directions by about 5 to 7%.

Table 3 also quantifies emittance ratio dependence on the bunch intensity and bunch centroid position quoting % per one rms of the bunch intensity and bunch centroid position distributions correspondingly. It should be noted that for some emittance ratios the dependence on bunch centroid position is non negligible and sometimes larger than the dependence on bunch intensity.

Acknowledgments

We would like to thank Harry Cheung, Andreas Jansson, Paul Lebrun, Alberto Marchionni, Stephen Pordes and Jean Slaughter for their suggestions and comments.

References

[1] M. Church, *A Study of the Emittances of P1 during Proton Injections for Store 2070*, talk on 01/16/2003, http://www-bd.fnal.gov/sdahomepage/osda/devices/p1_2070_study_pdf.pdf

[2] S. Pordes et al, *Measurements of Proton and Antiproton beam intensities in the Tevatron*, Particle Accelerator Conference, Portland, Oregon, USA, May 12-16, 2003

[3] H. W. K. Cheung et al, *Performance of a Beam Monitor in the Fermilab Tevatron using Synchrotron Light*, Particle Accelerator Conference, Portland, Oregon, USA, May 12-16, 2003

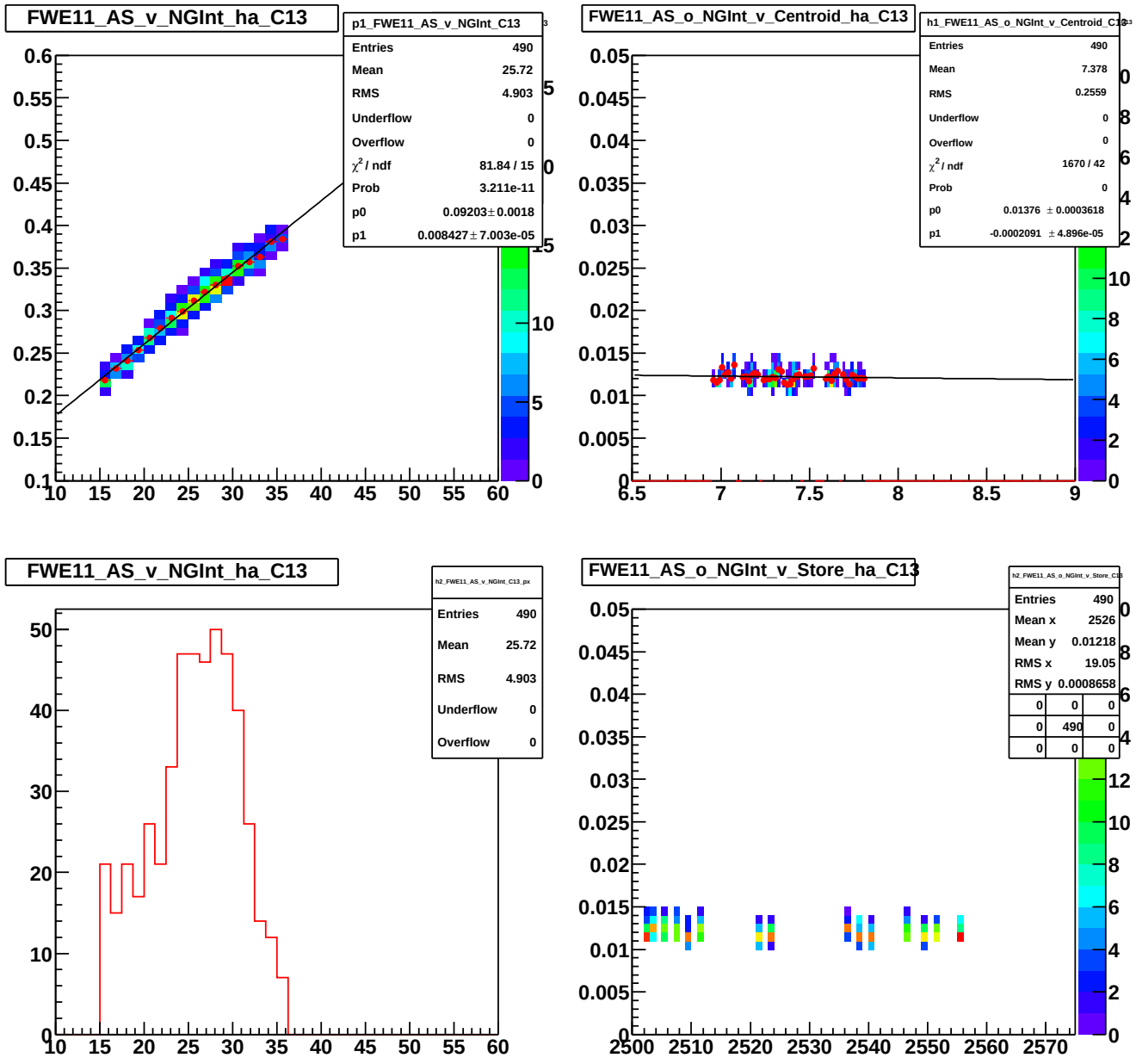

Figure 1: Antiproton beam, horizontal detectors: Performance of the Flying Wire Detector at the E11 location during Tevatron Remove Halo case: Amplitude (in arbitrary units) times sigma of the bunch width distribution (in *mm*) of the front end FW detector data versus bunch intensity (ACNET variables T:FBI[A,P]NG) (in E9) with an overlaid horizontal profile of that distribution with a straight line fit; Amplitude times sigma of the bunch width distribution of the front end FW detector data over bunch intensity versus bunch E11 centroid (in *mm*) (based on the T:FW[E,H,V][A,P]CE ACNET variable) with an overlaid horizontal profile of that distribution with a straight line fit; bunch intensity; amplitude times sigma of the bunch width distribution (in *mm*) of the raw FW detector distribution over bunch intensity versus store number.

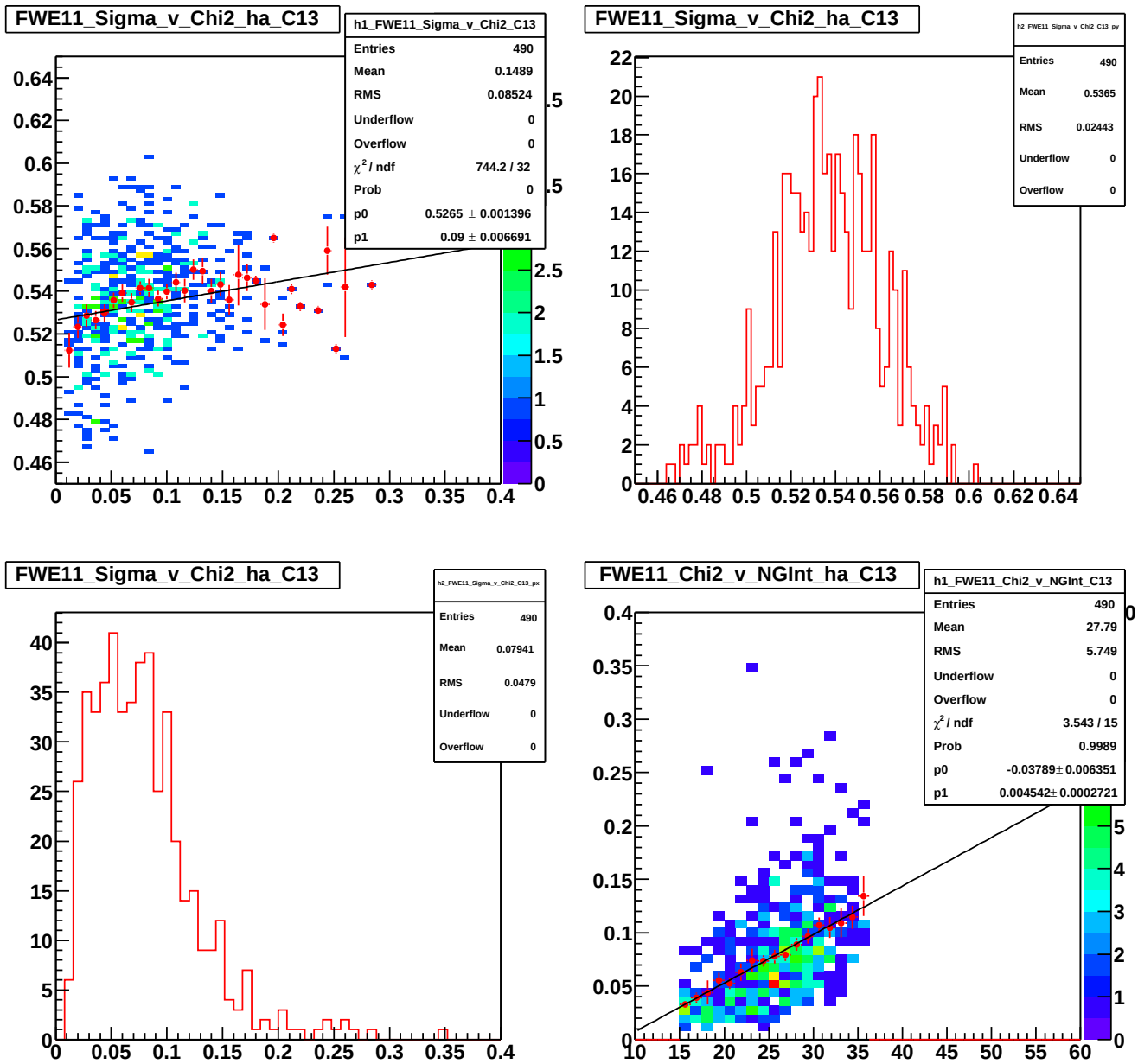

Figure 2: Antiproton beam, horizontal detectors: Performance of the Flying Wire Detector at the E11 location during Tevatron Remove Halo case: Sigma of the bunch width distribution (in *mm*) as measured by the FW detector versus front end measure of the goodness of fit together with an overlaid horizontal profile and a straight line fit; sigma itself, goodness of fit itself; goodness of fit versus bunch intensity together with an overlaid horizontal profile and a straight line fit;

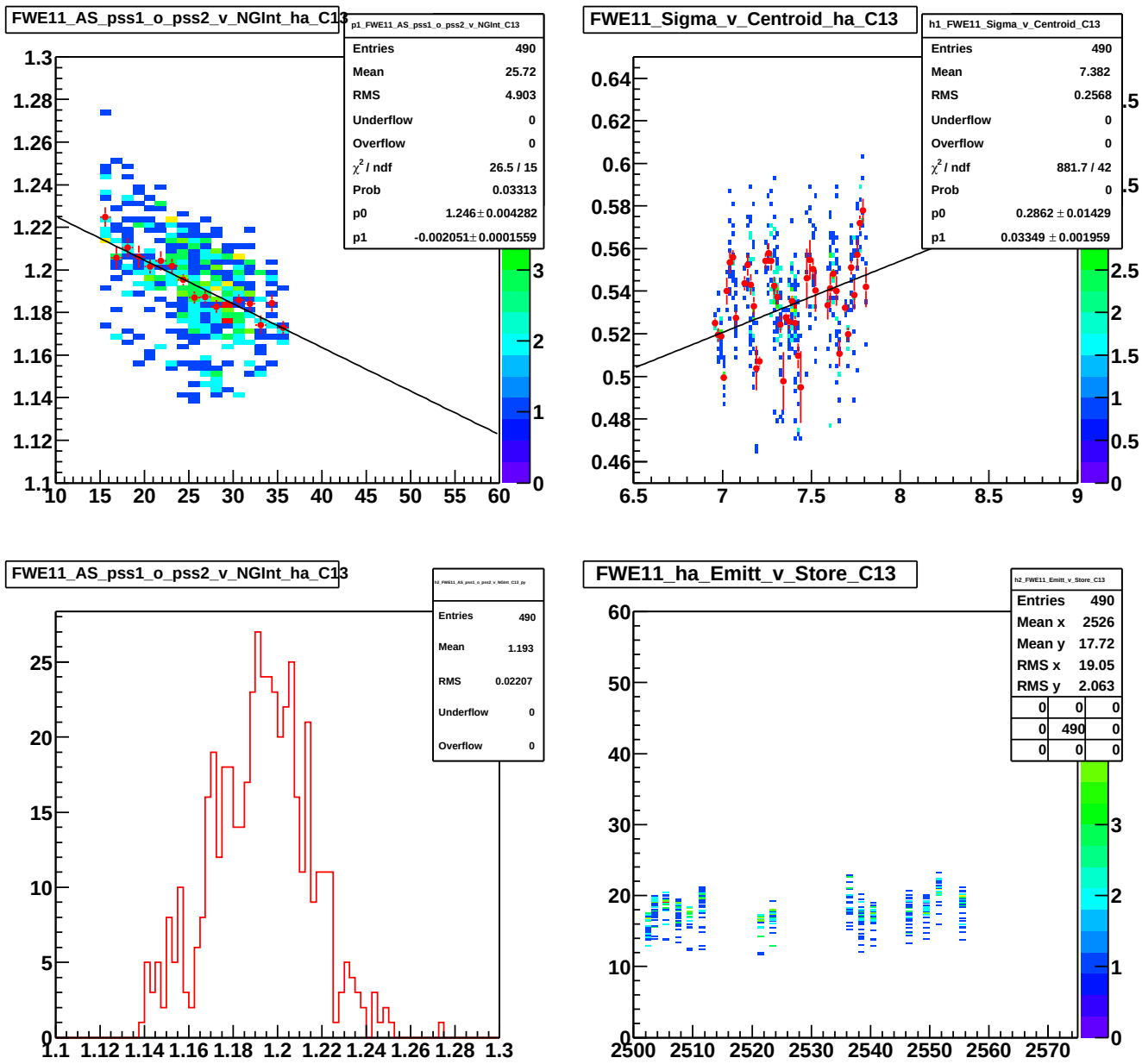

Figure 3: Antiproton beam, horizontal detectors: Performance of the Flying Wire Detector at the E11 location during Tevatron Remove Halo case: Amplitude (in arbitrary units) times sigma of the bunch width distribution (in *mm*) of the pass 1 over pass 2 of the front end FW detector data versus bunch intensity (ACNET variables T:FBI[A,P]NG) (in E9) together with an overlaid horizontal profile of that distribution with a straight line fit; sigma of the bunch width distribution versus bunch centroid (in *mm*) (based on the T:FW[E,H,V][A,P]CE ACNET variable) with an overlaid horizontal profile of that distribution with a straight line fit; amplitude (in arbitrary units) times sigma of the bunch width distribution (in *mm*) of the pass 1 over pass 2 of the front end FW detector data itself, bunch emittance (in $\pi \cdot mm \cdot mrad$) versus store number.

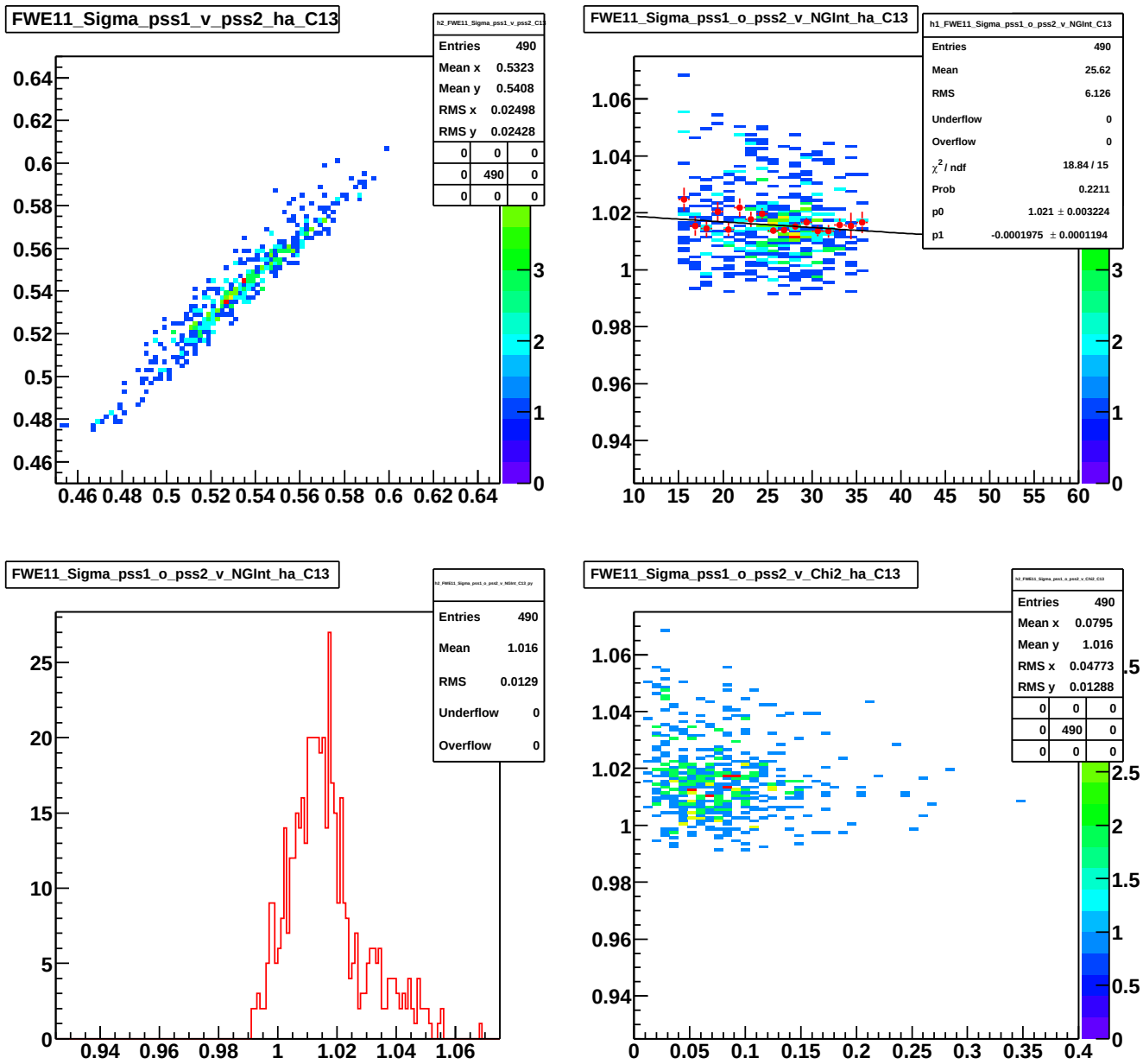

Figure 4: Antiproton beam, horizontal detectors: Performance of the Flying Wire Detector at the E11 location during Tevatron Remove Halo case: Sigma of the bunch width distribution (in *mm*) of the pass 1 versus pass 2 of the FW detector; sigma of the bunch width distribution (in *mm*) of the pass 1 over pass 2 of the FW detector versus bunch intensity (ACNET variables T:FBI[A,P]NG) (in E9) together with an overlaid horizontal profile and a straight line fit; sigma of the bunch width distribution (in *mm*) of the pass 1 over pass 2 of the FW detector itself, sigma of the bunch width distribution (in *mm*) of the pass 1 over pass 2 of the FW detector versus front end measure of the goodness of fit.

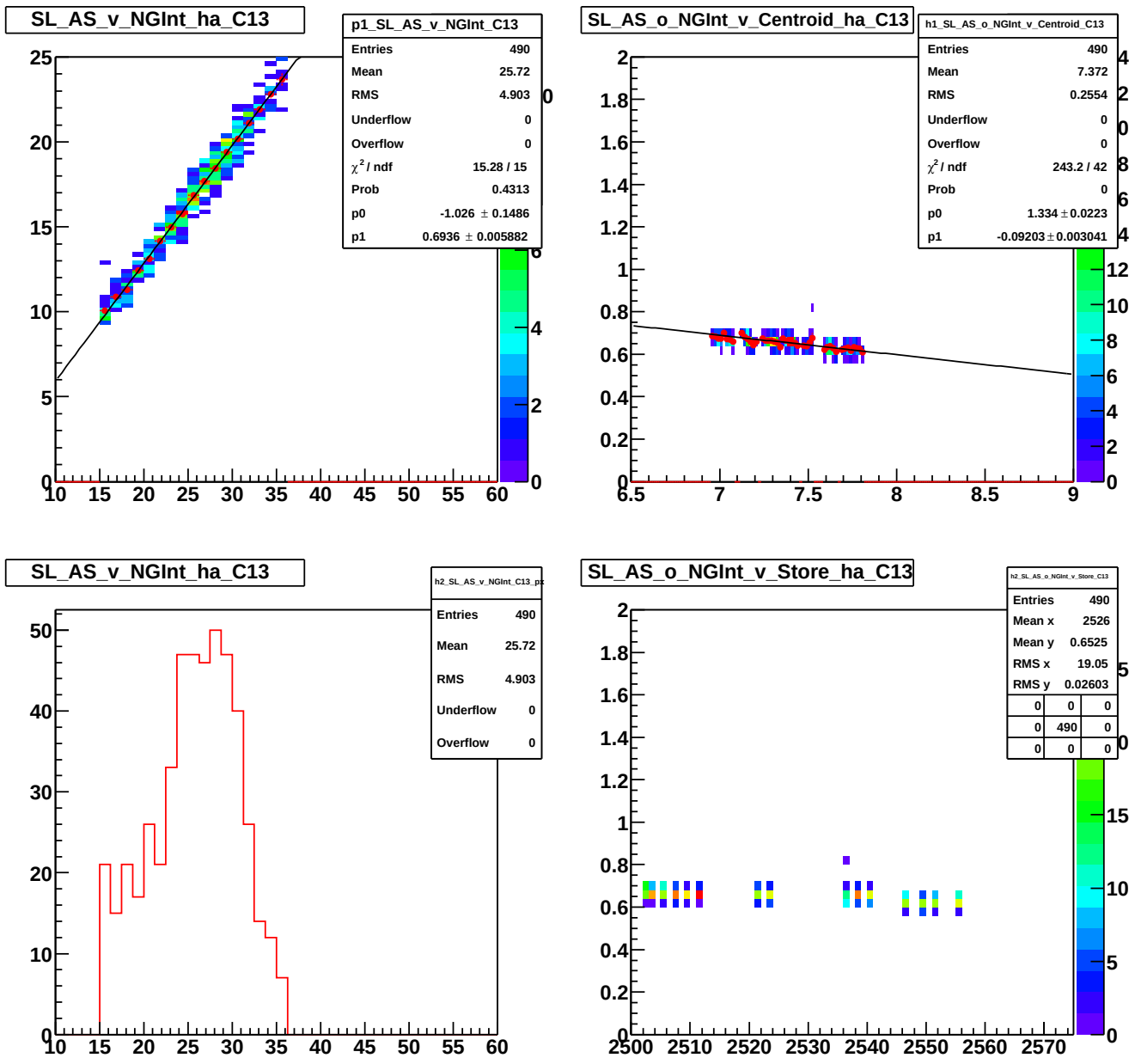

Figure 5: Antiproton beam, horizontal detectors: Performance of the Synchrotron Light Detector at the C11 location during Tevatron Remove Halo case: Amplitude (in arbitrary units) times sigma of the bunch width distribution (in *mm*) of the raw SL detector distribution versus bunch intensity (ACNET variables T:FBI[A,P]NG) (in E9) with an overlaid horizontal profile of that distribution with a straight line fit; amplitude times sigma of the bunch width distribution (in *mm*) of the raw SL detector distribution over bunch intensity versus bunch E11 centroid (in *mm*) (based on the T:FW[E,H,V][A,P]CE ACNET variable) with an overlaid horizontal profile of that distribution with a straight line fit; bunch intensity; amplitude times sigma of the bunch width distribution (in *mm*) of the raw SL detector distribution over bunch intensity versus store number.

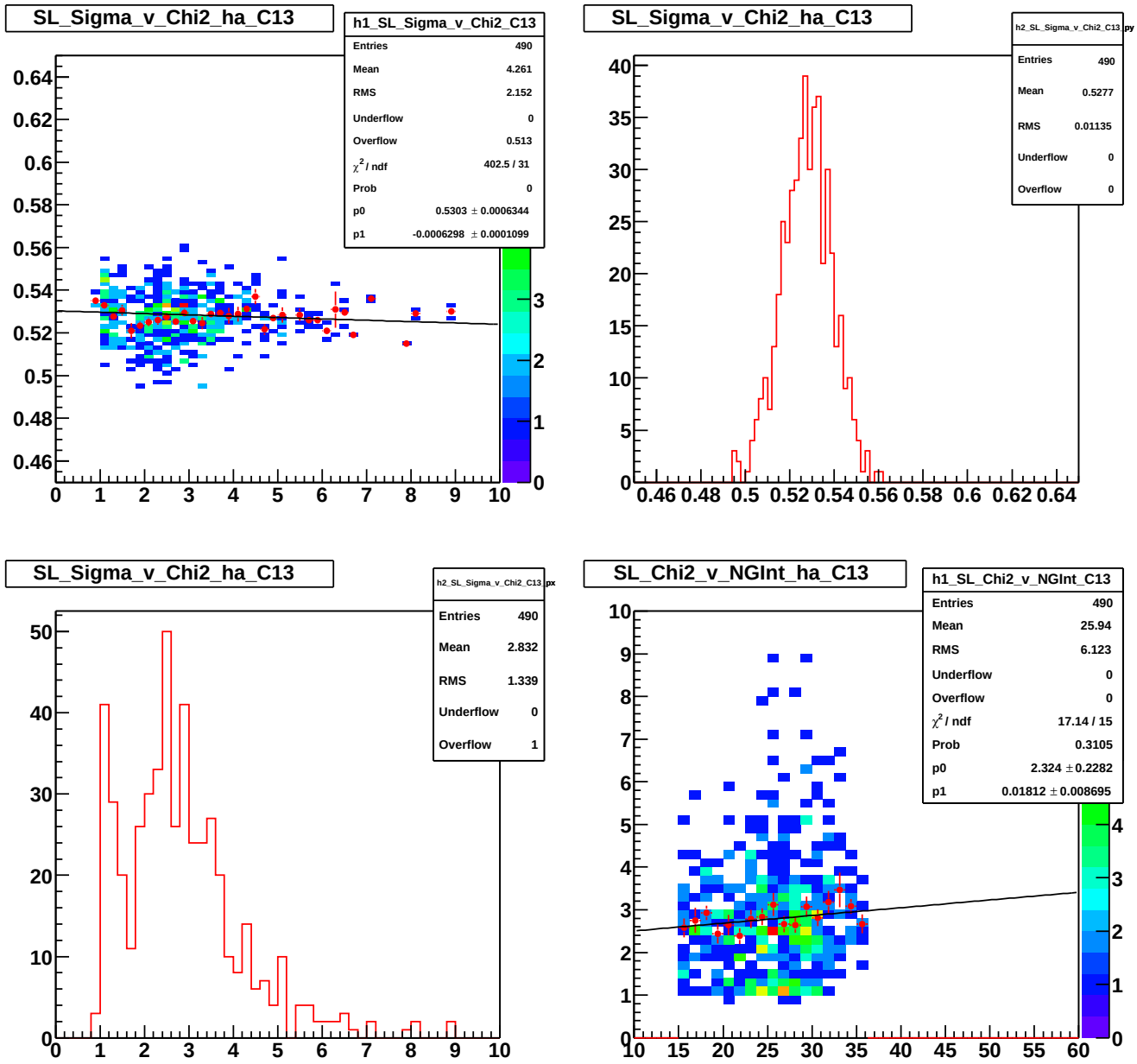

Figure 6: Antiproton beam, horizontal detectors: Performance of the Synchrotron Light Detector at the C11 location during Tevatron Remove Halo case: Sigma of the bunch width distribution (in *mm*) as measured by the SL detector versus front end measure of the goodness of fit together with an overlaid horizontal profile and a straight line fit; sigma of the bunch width distribution (in *mm*) itself; goodness of fit itself; goodness of fit versus bunch intensity together with an overlaid horizontal profile and a straight line fit.

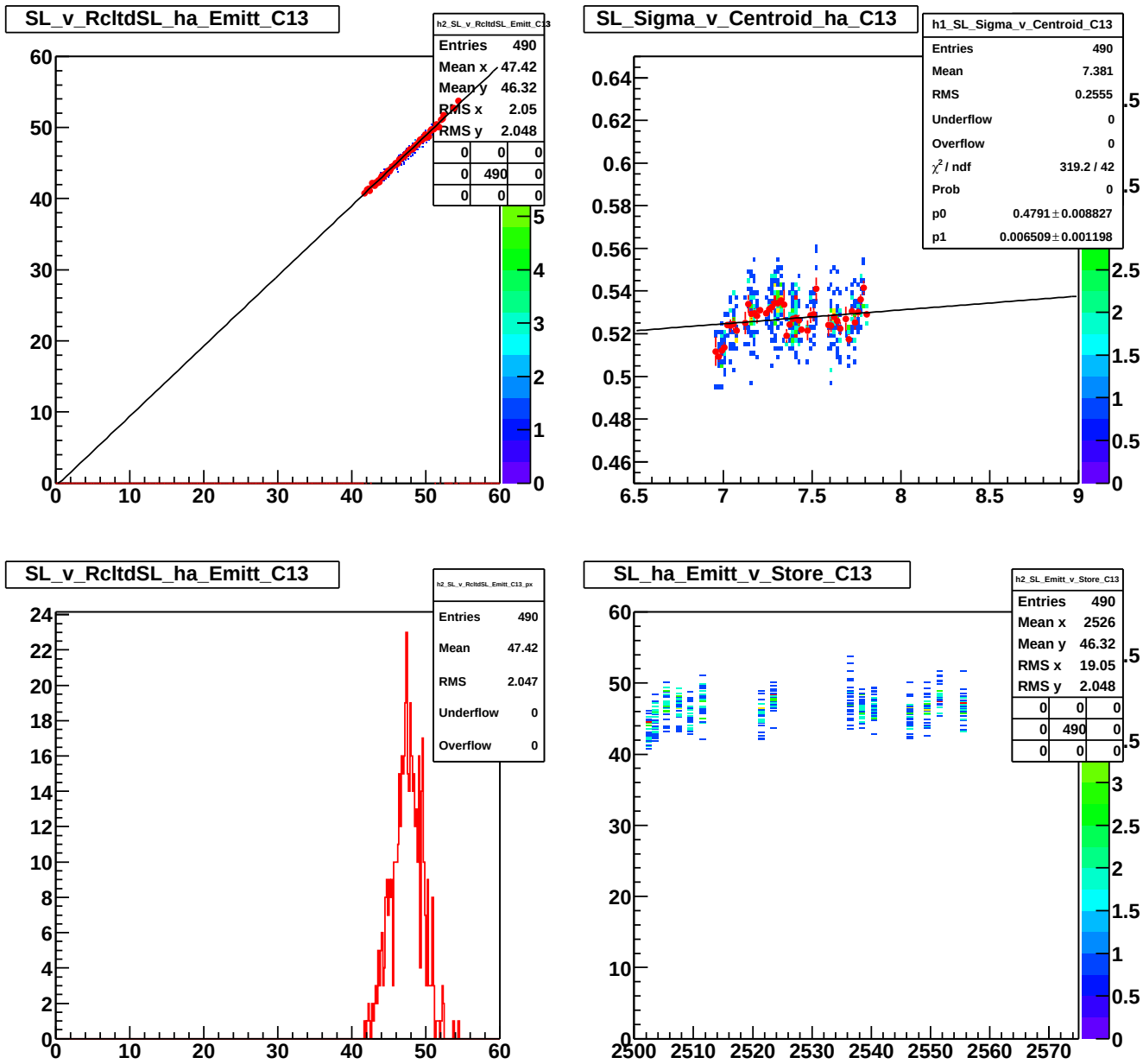

Figure 7: Antiproton beam, horizontal detectors: Performance of the Synchrotron Light Detector at the C11 location during Tevatron Remove Halo case: Bunch emittance (in $\pi \cdot mm \cdot mrad$) as measured by the front end SL detector versus bunch emittance as recalculated using front end sigma of the bunch width distribution (in *mm*) (combined with SBD timing information in the horizontal cases) together with an overlaid horizontal profile of that distribution with a straight line fit; sigma of the bunch width distribution versus bunch E11 centroid (in *mm*) (based on the T:FW[E,H,V][A,P]CE ACNET variable) with an overlaid horizontal profile of that distribution with a straight line fit; bunch emittance; bunch emittance versus store number.

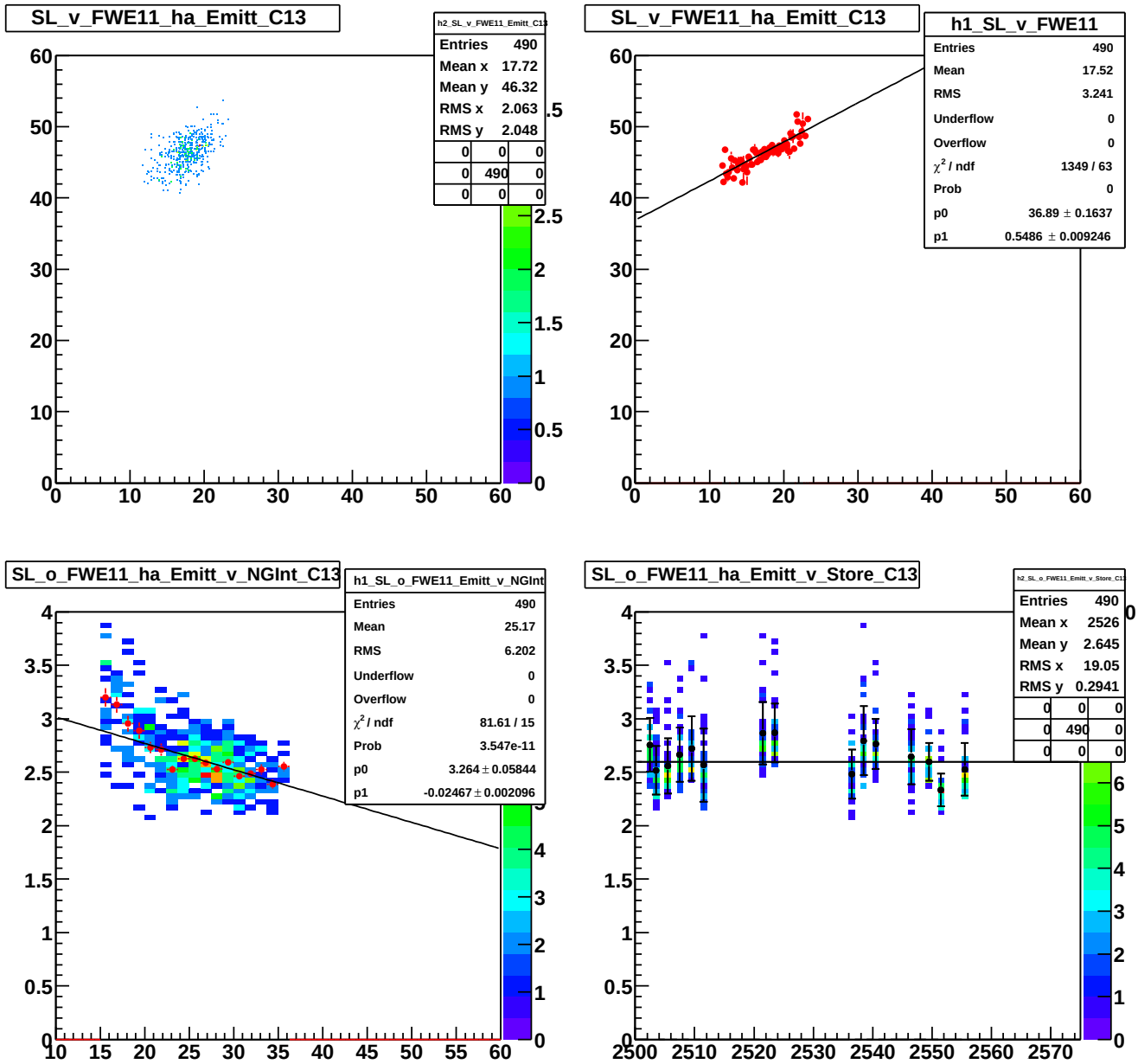

Figure 8: Antiproton beam, horizontal detectors: Comparisons of Emittance measurements as done by Synchrotron Light Detector at C11 and Flying Wire Detector at E11 during Tevatron Remove Halo case: Bunch emittance (in $\pi \cdot mm \cdot mrad$) as measured by Synchrotron Light Detector versus bunch emittance as measured by the Flying Wire Detector at E11; horizontal profile of the previous distribution with a straight line fit; bunch emittance as measured by Synchrotron Light Detector over bunch emittance as measured by the Flying Wire Detector at E11 versus bunch intensity (ACNET variables T:FBI[A,P]NG) (in E9) together with an overlaid horizontal profile and a straight line fit; bunch emittance as measured by Synchrotron Light Detector over bunch emittance as measured by the Flying Wire Detector at E11 versus store number with overlaid averaged ratios for each store and a horizontal line fit.

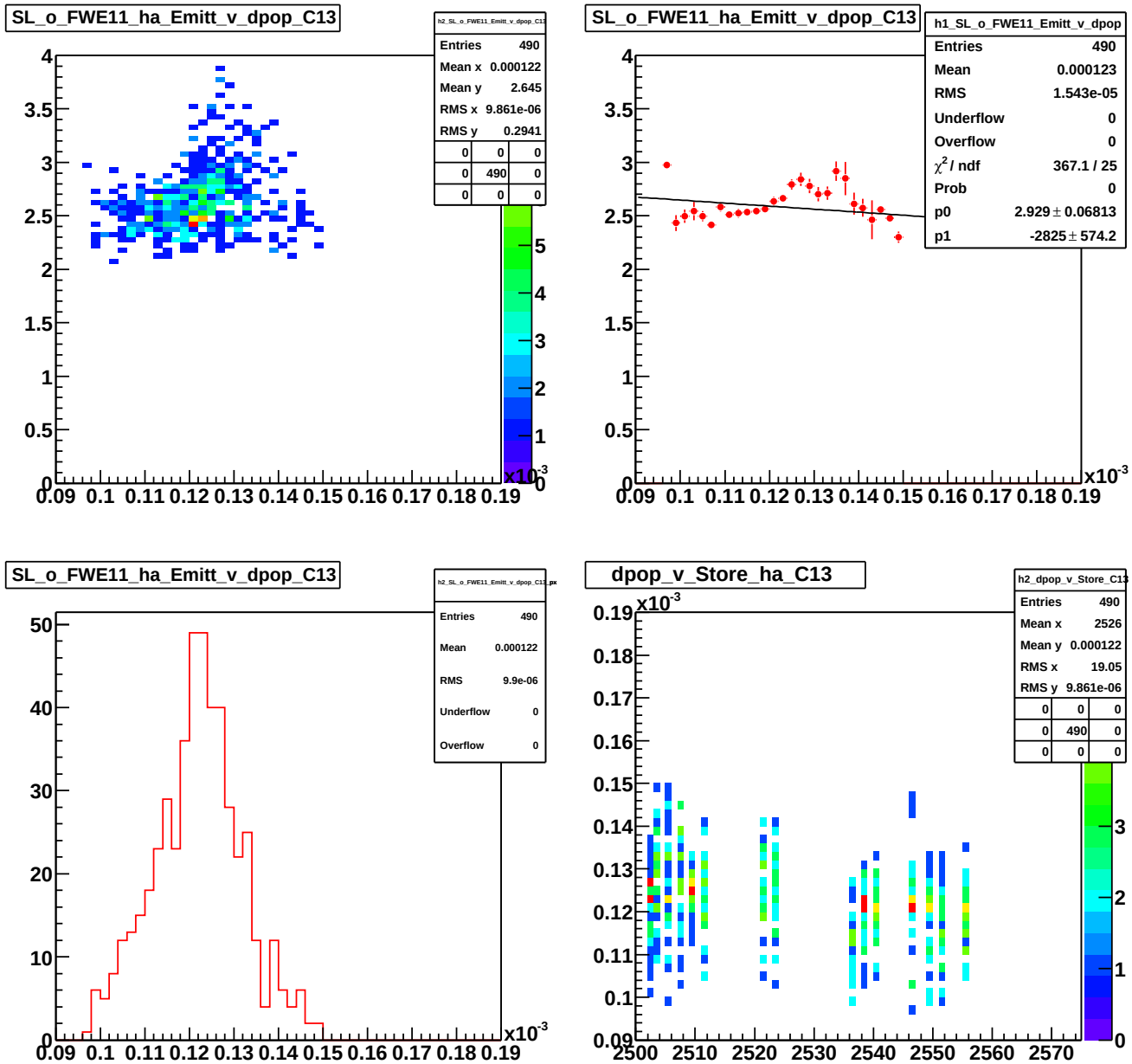

Figure 9: Antiproton beam, horizontal detectors: Comparisons of Emittance measurements as done by Synchrotron Light Detector at C11 and Flying Wire Detector at E11 during Tevatron Remove Halo case: Bunch emittance as measured by Synchrotron Light Detector over bunch emittance as measured by the Flying Wire Detector at E11 versus recalculated $\delta p/p$ (based on δt the T:SBD[A,P]SS ACNET variable); horizontal profile of the previous distribution with a straight line fit; $\delta p/p$ itself; $\delta p/p$ versus store number.

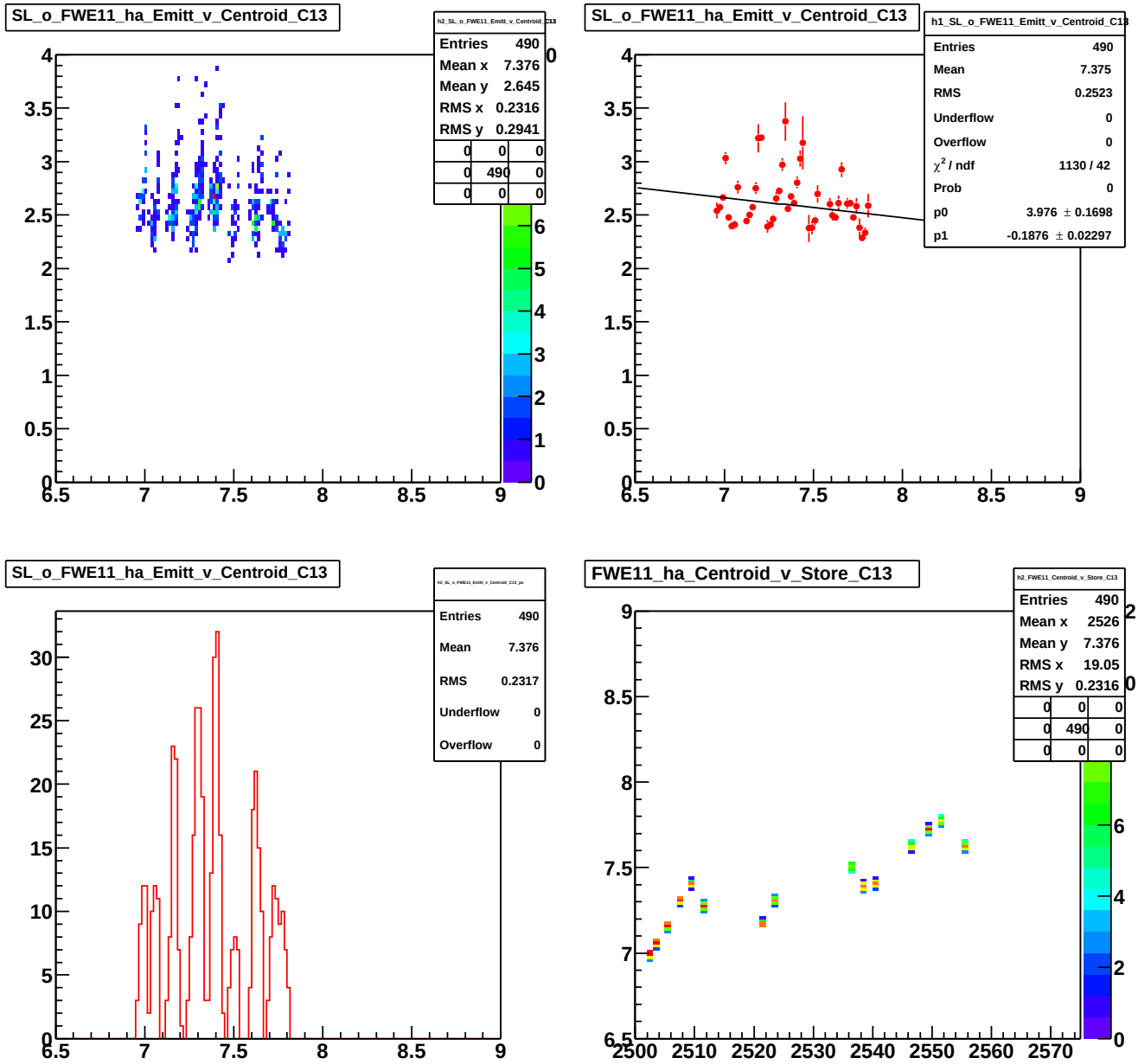

Figure 10: Antiproton beam, horizontal detectors: Comparisons of Emittance measurements as done by Synchrotron Light Detector at C11 and Flying Wire Detector at E11 during Tevatron Remove Halo case: Bunch emittance as measured by Synchrotron Light Detector over bunch emittance as measured by the Flying Wire Detector at E11 versus bunch E11 centroid (in *mm*) (based on the T:FW[E,H,V][A,P]CE ACNET variable); horizontal profile of the previous distribution with a straight line fit; bunch E11 centroid itself; bunch E11 centroid versus store number.

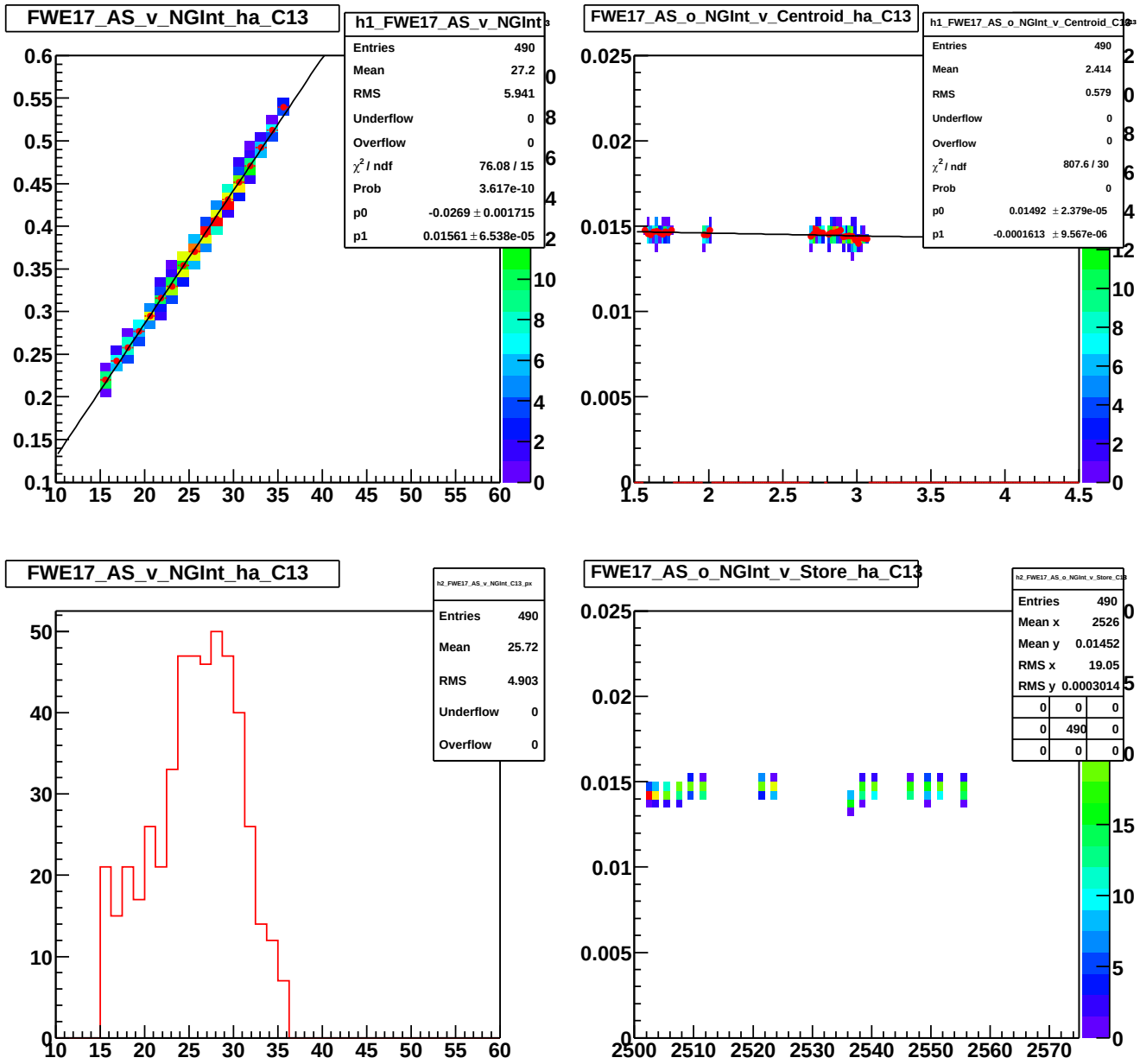

Figure 11: Antiproton beam, horizontal detectors: Performance of the Flying Wire Detector at the E17 location during Tevatron Remove Halo case: Amplitude (in arbitrary units) times sigma of the bunch width distribution (in *mm*) of the front end FW detector data versus bunch intensity (ACNET variables T:FBI[A,P]NG) (in E9) with an overlaid horizontal profile of that distribution with a straight line fit; Amplitude times sigma of the bunch width distribution of the front end FW detector data over bunch intensity versus bunch E17 centroid (in *mm*) (based on the T:FW[E,H,V][A,P]CE ACNET variable) with an overlaid horizontal profile of that distribution with a straight line fit; bunch intensity; amplitude times sigma of the bunch width distribution (in *mm*) of the raw FW detector distribution over bunch intensity versus store number.

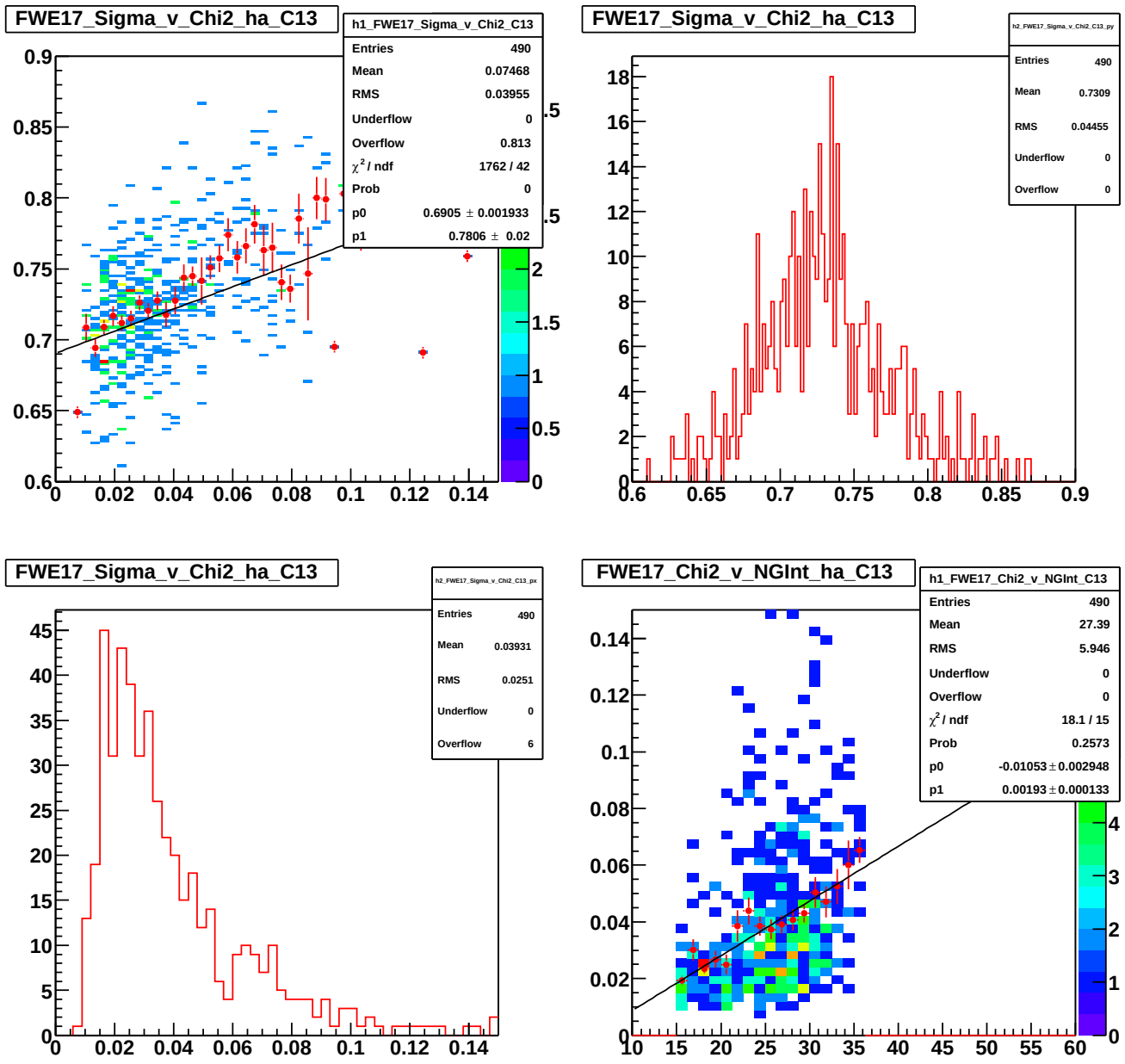

Figure 12: Antiproton beam, horizontal detectors: Performance of the Flying Wire Detector at the E17 location during Tevatron Remove Halo case: Sigma of the bunch width distribution (in *mm*) as measured by the FW detector versus front end measure of the goodness of fit together with an overlaid horizontal profile and a straight line fit; sigma itself, goodness of fit itself; goodness of fit versus bunch intensity together with an overlaid horizontal profile and a straight line fit.

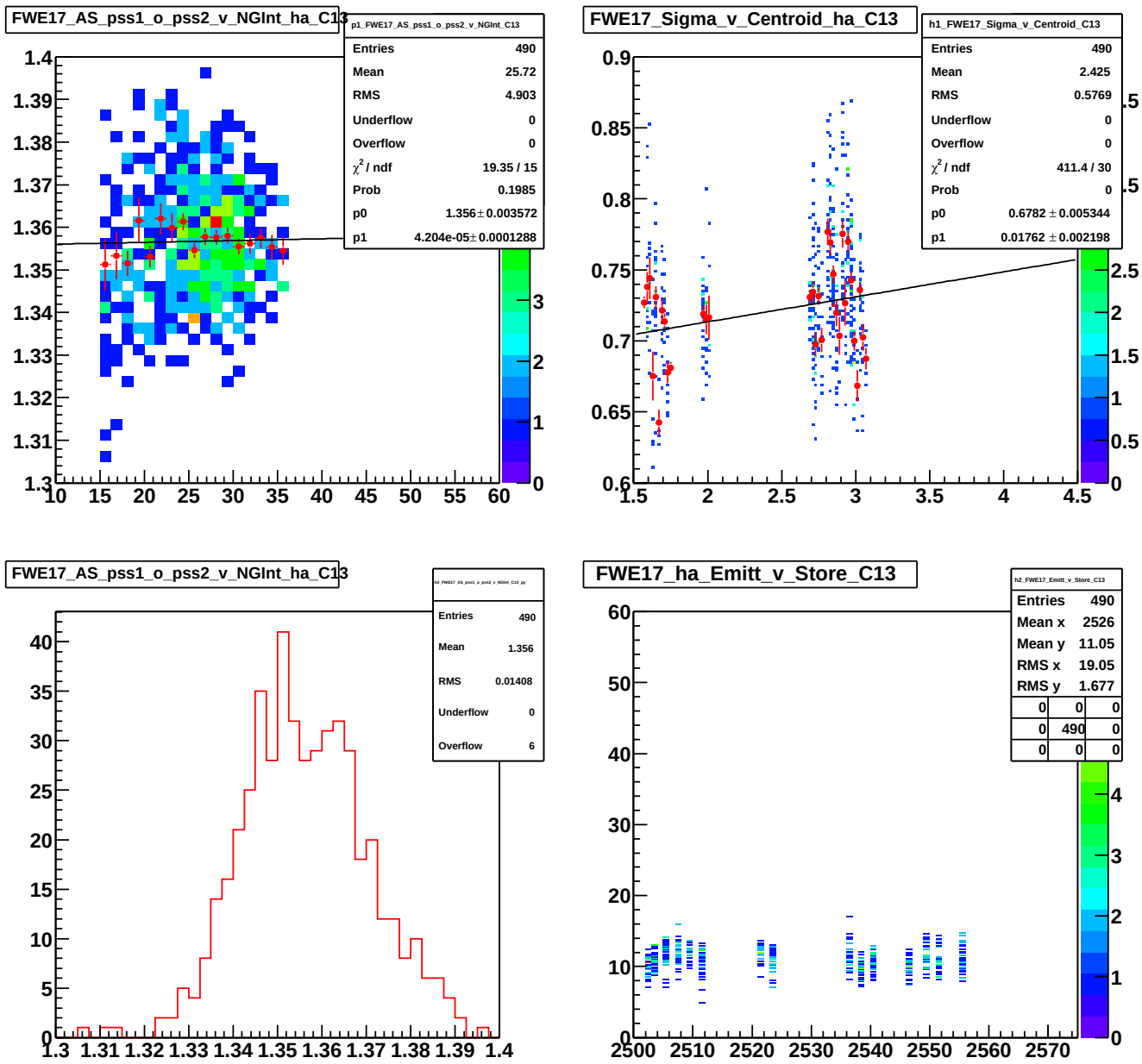

Figure 13: Antiproton beam, horizontal detectors: Performance of the Flying Wire Detector at the E17 location during Tevatron Remove Halo case: Amplitude (in arbitrary units) times sigma of the bunch width distribution (in *mm*) of the pass 1 over pass 2 of the front end FW detector data versus bunch intensity (ACNET variables T:FBI[A,P]NG) (in E9) together with an overlaid horizontal profile of that distribution with a straight line fit; sigma of the bunch width distribution versus bunch centroid (in *mm*) (based on the T:FW[E,H,V][A,P]CE ACNET variable) with an overlaid horizontal profile of that distribution with a straight line fit; amplitude (in arbitrary units) times sigma of the bunch width distribution (in *mm*) of the pass 1 over pass 2 of the front end FW detector data itself, bunch emittance (in $\pi \cdot mm \cdot mrad$) versus store number.

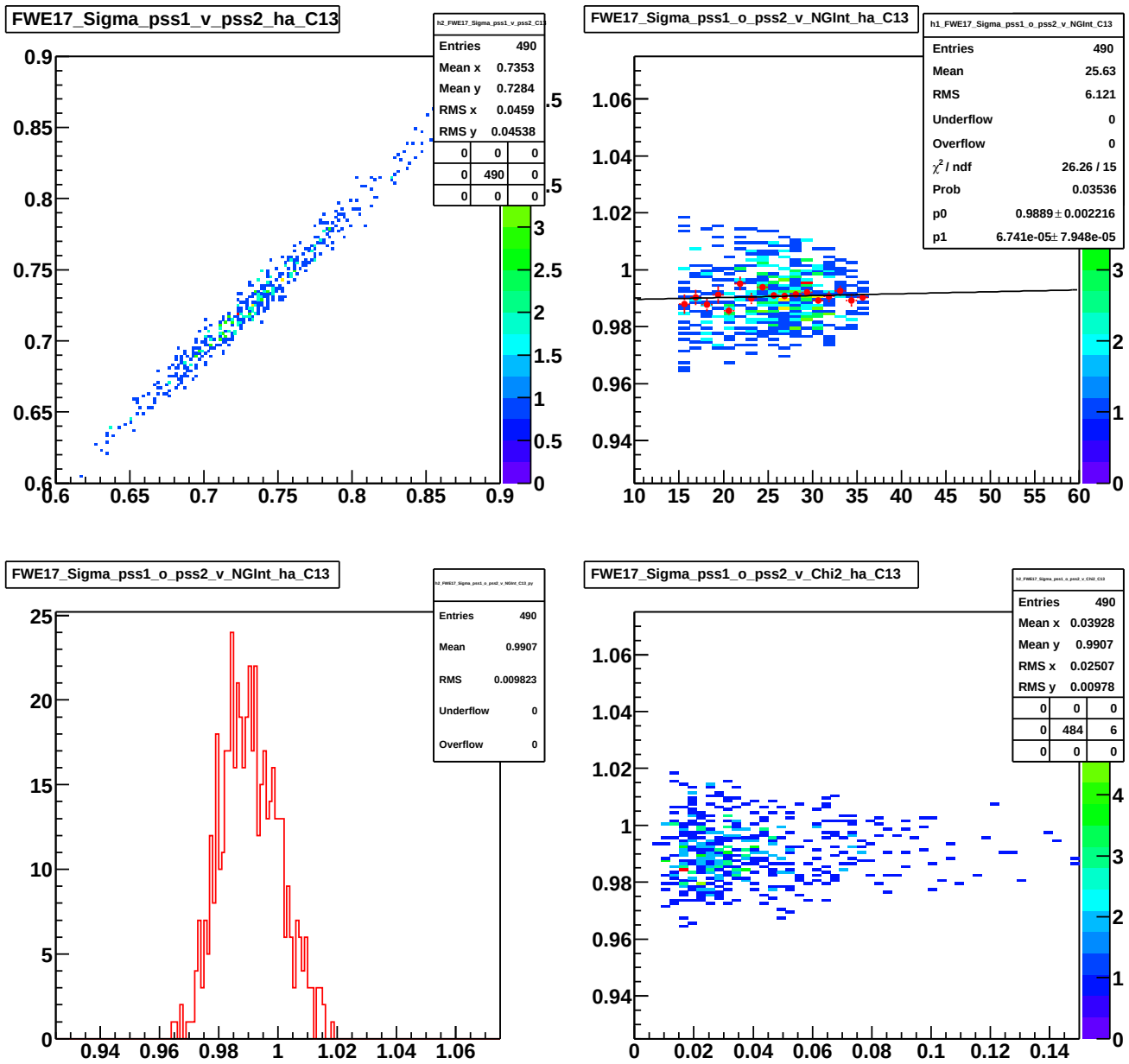

Figure 14: Antiproton beam, horizontal detectors: Performance of the Flying Wire Detector at the E17 location during Tevatron Remove Halo case: Sigma of the bunch width distribution (in *mm*) of the pass 1 versus pass 2 of the FW detector; sigma of the bunch width distribution (in *mm*) of the pass 1 over pass 2 of the FW detector versus bunch intensity (ACNET variables T:FBI[A,P]NG) (in E9) together with an overlaid horizontal profile and a straight line fit; sigma of the bunch width distribution (in *mm*) of the pass 1 over pass 2 of the FW detector itself, sigma of the bunch width distribution (in *mm*) of the pass 1 over pass 2 of the FW detector versus front end measure of the goodness of fit.

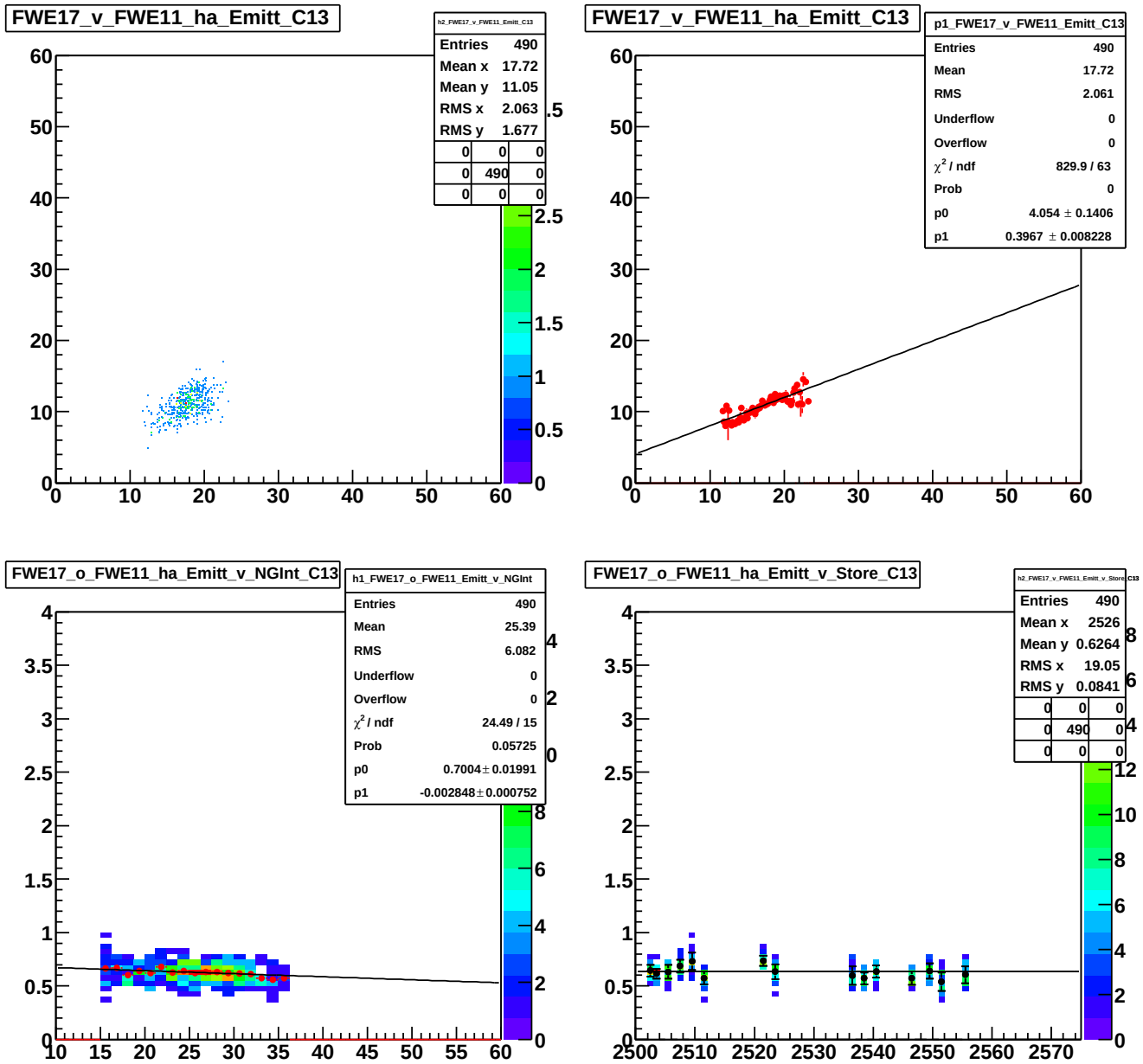

Figure 15: Antiproton beam, horizontal detectors: Comparisons of Emittance measurements as done by Flying Wire Detector at E17 and Flying Wire Detector at E11 during Tevatron Remove Halo case: Bunch emittance (in $\pi \cdot mm \cdot mrad$) as measured by Flying Wire Detector at E17 versus bunch emittance as measured by the Flying Wire Detector at E11; horizontal profile of the previous distribution with a straight line fit; bunch emittance as measured by Flying Wire Detector at E17over bunch emittance as measured by the Flying Wire Detector at E11 versus bunch intensity (ACNET variables T:FBI[A,P]NG) (in E9) together with an overlaid horizontal profile and a straight line fit; bunch emittance as measured by Flying Wire Detector at E17 over bunch emittance as measured by the Flying Wire Detector at E11 versus store number with overlaid averaged ratios for each store and a horizontal line fit.

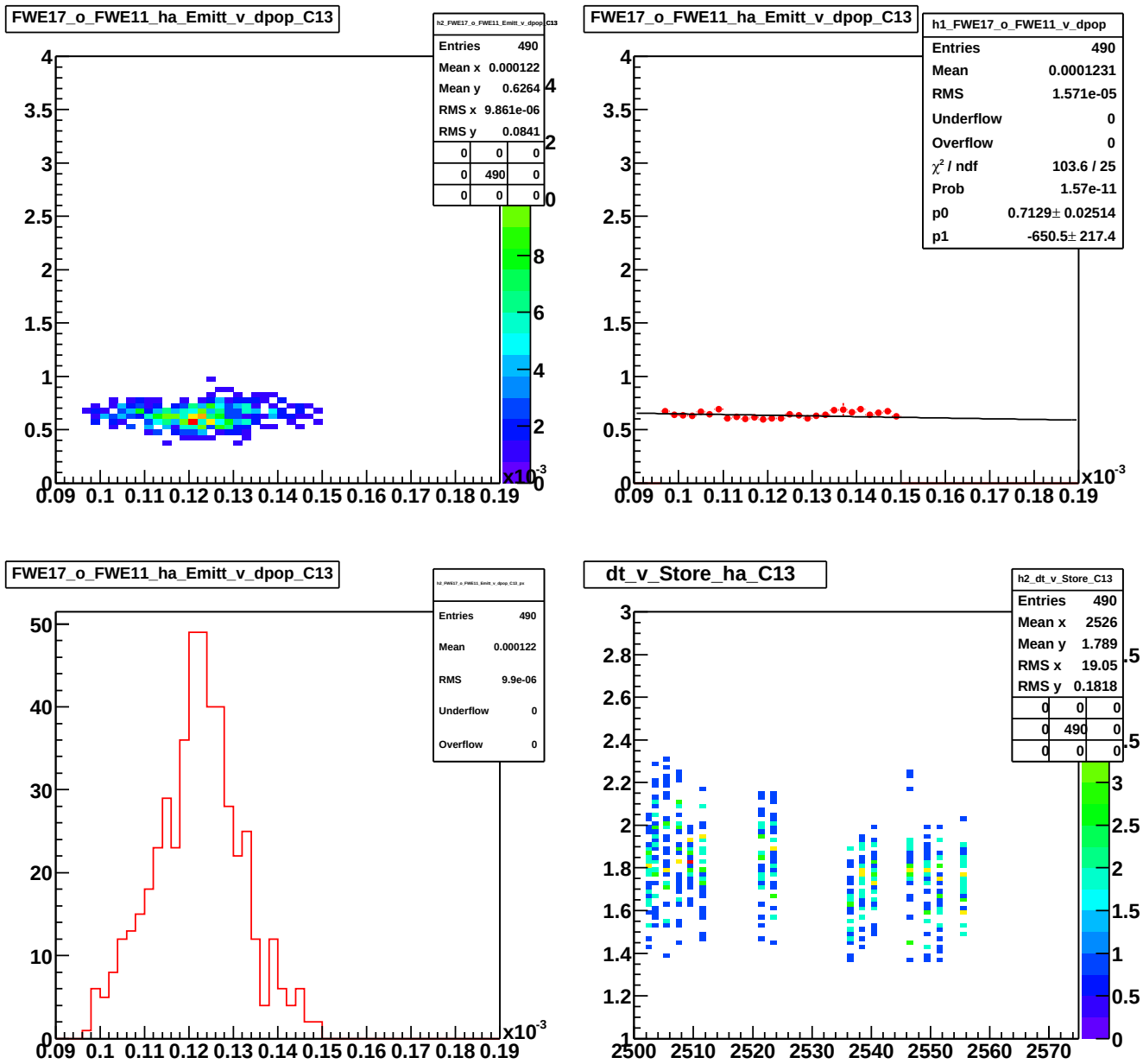

Figure 16: Antiproton beam, horizontal detectors: Comparisons of Emittance measurements as done by Flying Wire Detector at E17 and Flying Wire Detector at E11 during Tevatron Remove Halo case: Bunch emittance as measured by Flying Wire Detector at E17 over bunch emittance as measured by the Flying Wire Detector at E11 versus recalculated $\delta p/p$ (based on δt the T:SBD[A,P]SS ACNET variable); horizontal profile of the previous distribution with a straight line fit; $\delta p/p$ itself; δt versus store number.

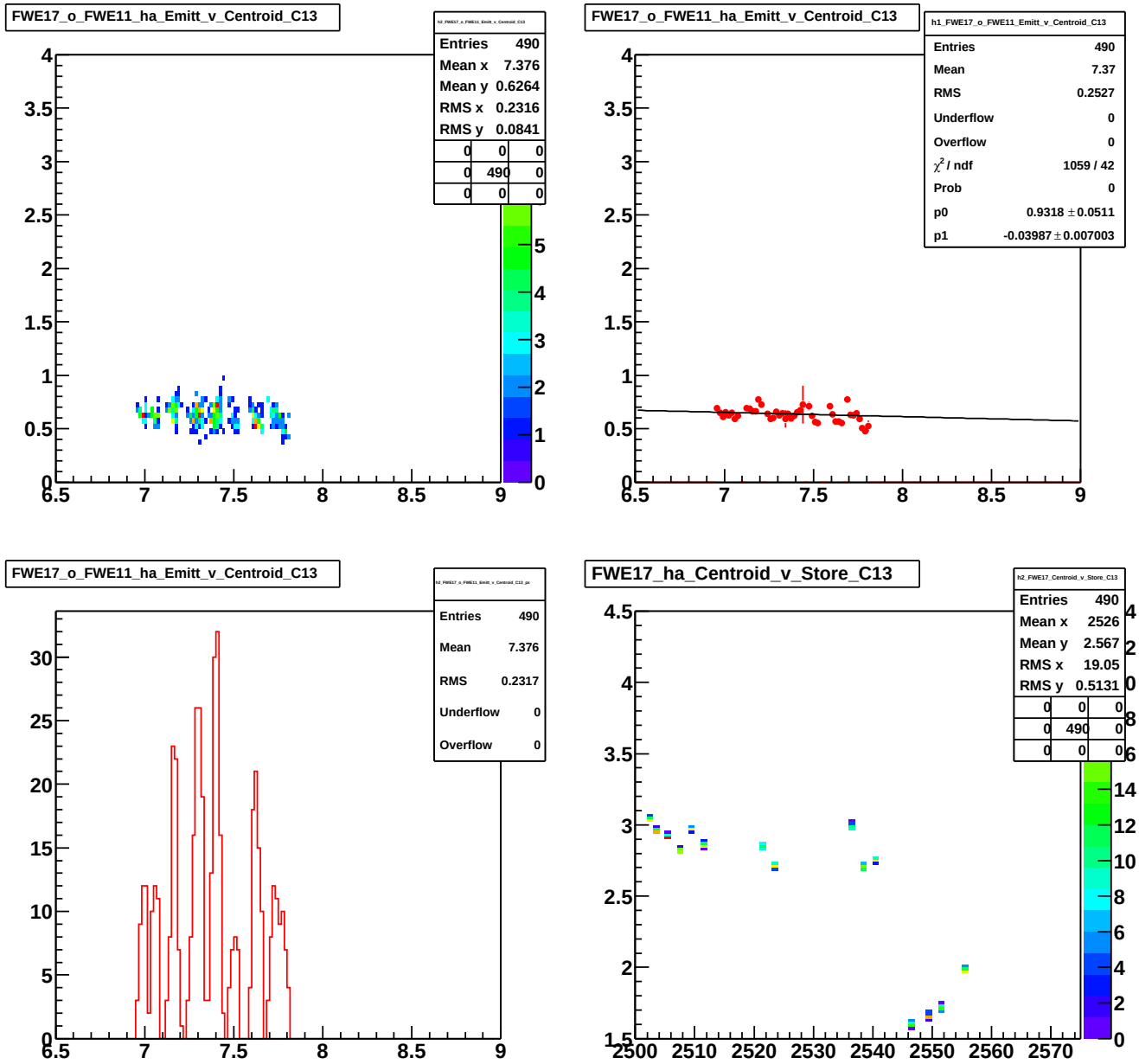

Figure 17: Antiproton beam, horizontal detectors: Comparisons of Emittance measurements as done by Flying Wire Detector at E17 and Flying Wire Detector at E11 during Tevatron Remove Halo case: Bunch emittance as measured by Flying Wire Detector at E17 over bunch emittance as measured by the Flying Wire Detector at E11 versus bunch E11 centroid (in *mm*) (based on the T:FW[E,H,V][A,P]CE ACNET variable); horizontal profile of the previous distribution with a straight line fit; bunch E17 centroid; bunch E17 centroid versus store number.

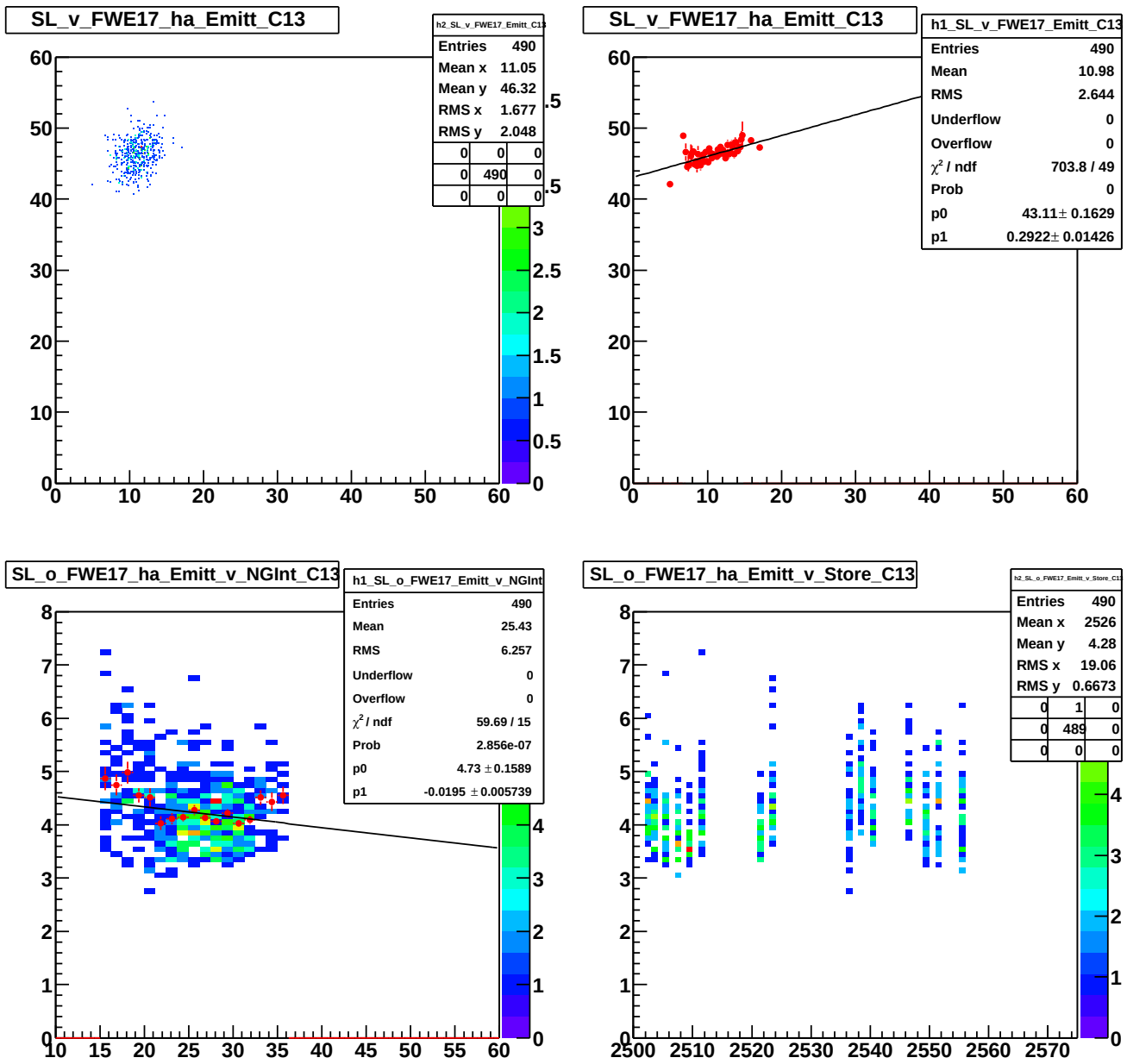

Figure 18: Antiproton beam, horizontal detectors: Comparisons of Emittance measurements as done by Synchrotron Light Detector at C11 and Flying Wire Detector at E17 during Tevatron Remove Halo case: Bunch emittance (in $\pi \cdot mm \cdot mrad$) as measured by Synchrotron Light Detector versus bunch emittance as measured by the Flying Wire Detector at E17; horizontal profile of the previous distribution with a straight line fit; bunch emittance as measured by Synchrotron Light Detector over bunch emittance as measured by the Flying Wire Detector at E17 versus bunch intensity (ACNET variables T:FBI[A,P]NG) (in E9) together with an overlaid horizontal profile and a straight line fit; bunch emittance as measured by Synchrotron Light Detector over bunch emittance as measured by the Flying Wire Detector at E17 versus store number.

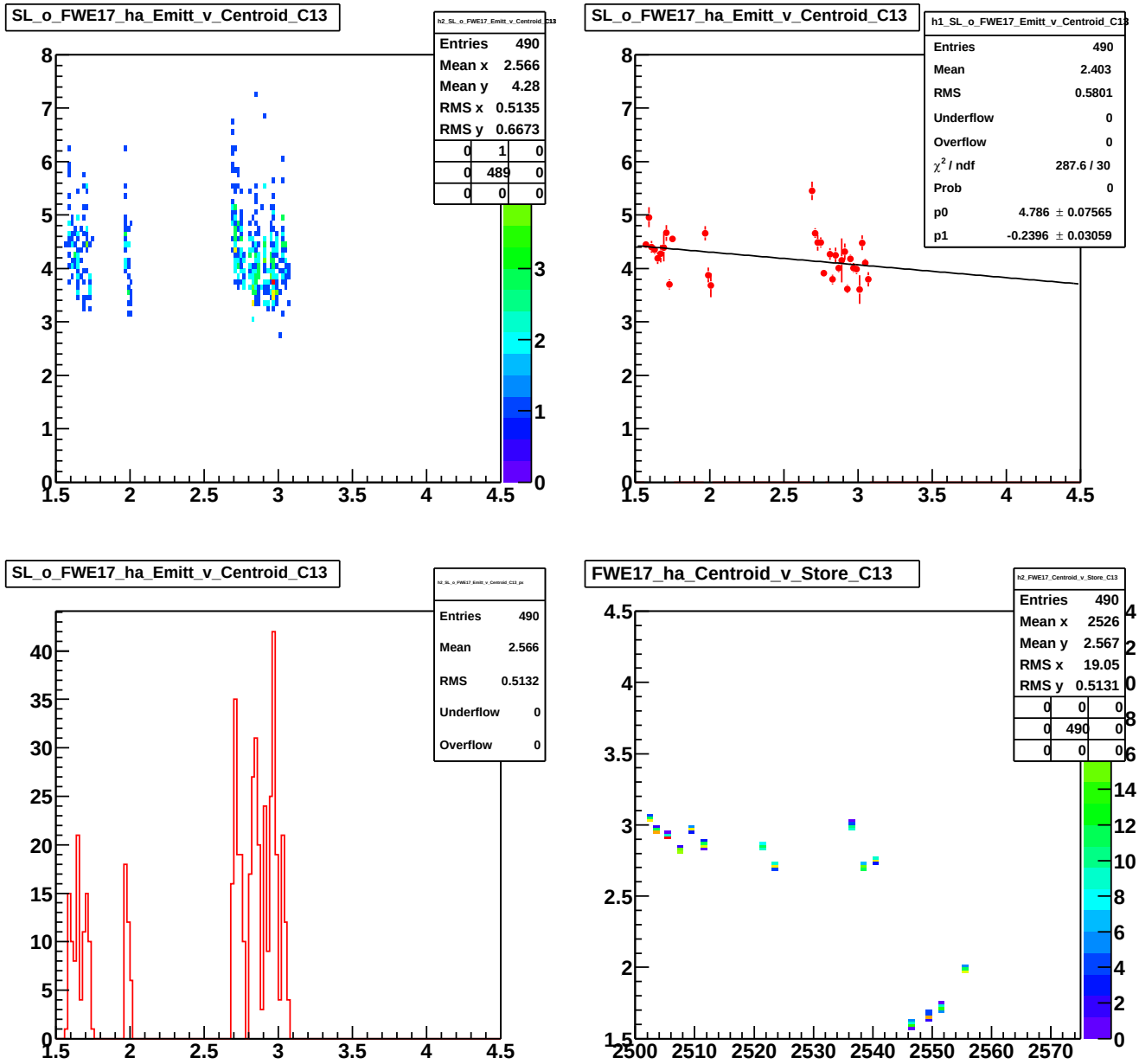

Figure 19: Antiproton beam, horizontal detectors: Comparisons of Emittance measurements as done by Synchrotron Light Detector at C11 and Flying Wire Detector at E17 during Tevatron Remove Halo case: Bunch emittance as measured by Synchrotron Light Detector over bunch emittance as measured by the Flying Wire Detector at E17 versus bunch E17 centroid (in *mm*) (based on the T:FW[E,H,V][A,P]CE ACNET variable); horizontal profile of the previous distribution with a straight line fit; bunch E17 centroid itself; bunch E17 centroid versus store number.

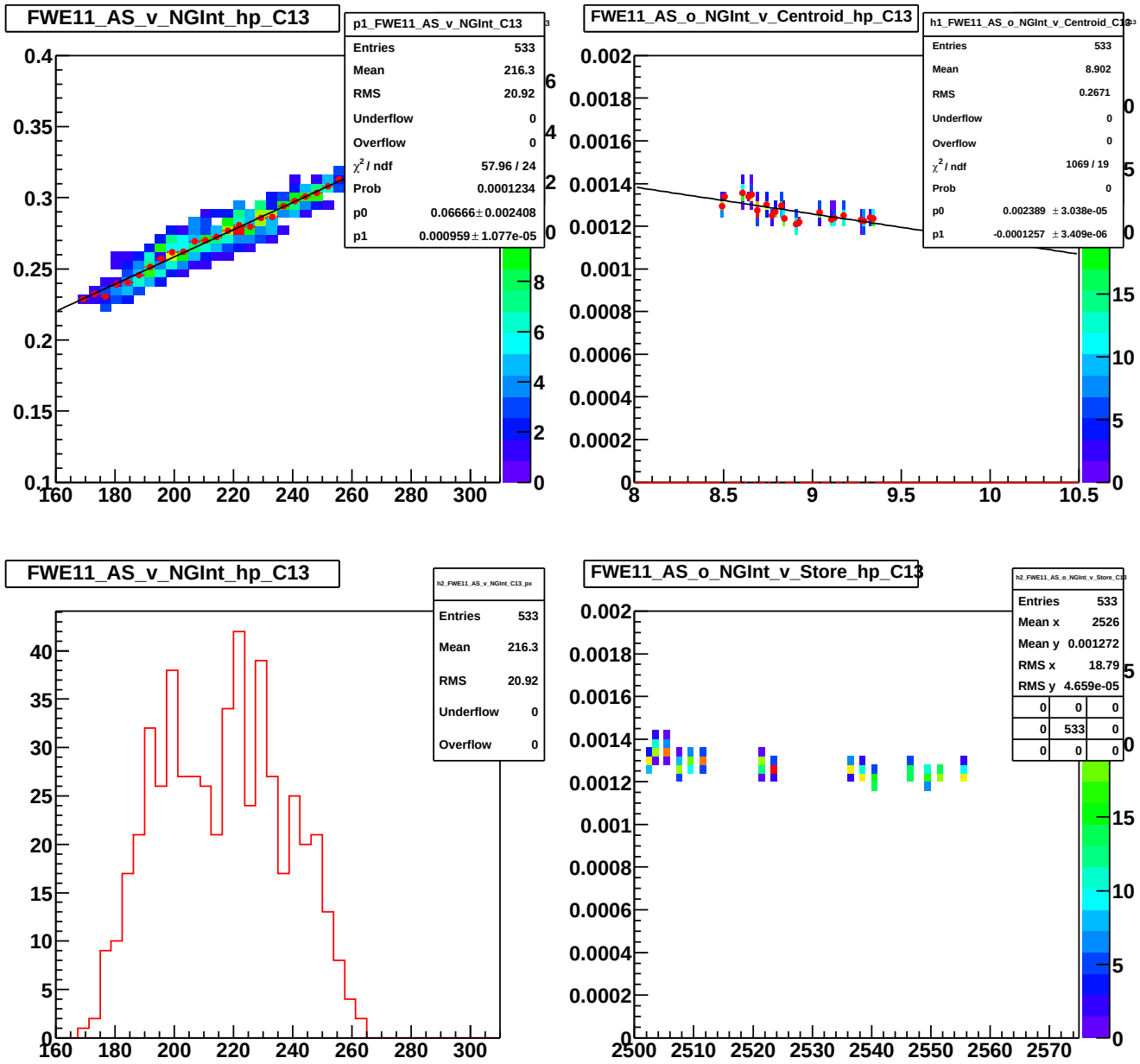

Figure 20: Proton beam, horizontal detectors: Performance of the Flying Wire Detector at the E11 location during Tevatron Remove Halo case: Amplitude (in arbitrary units) times sigma of the bunch width distribution (in *mm*) of the front end FW detector data versus bunch intensity (ACNET variables T:FBI[A,P]NG) (in E9) with an overlaid horizontal profile of that distribution with a straight line fit; Amplitude times sigma of the bunch width distribution of the front end FW detector data over bunch intensity versus bunch E11 centroid (in *mm*) (based on the T:FW[E,H,V][A,P]CE ACNET variable) with an overlaid horizontal profile of that distribution with a straight line fit; bunch intensity; amplitude times sigma of the bunch width distribution (in *mm*) of the raw FW detector distribution over bunch intensity versus store number.

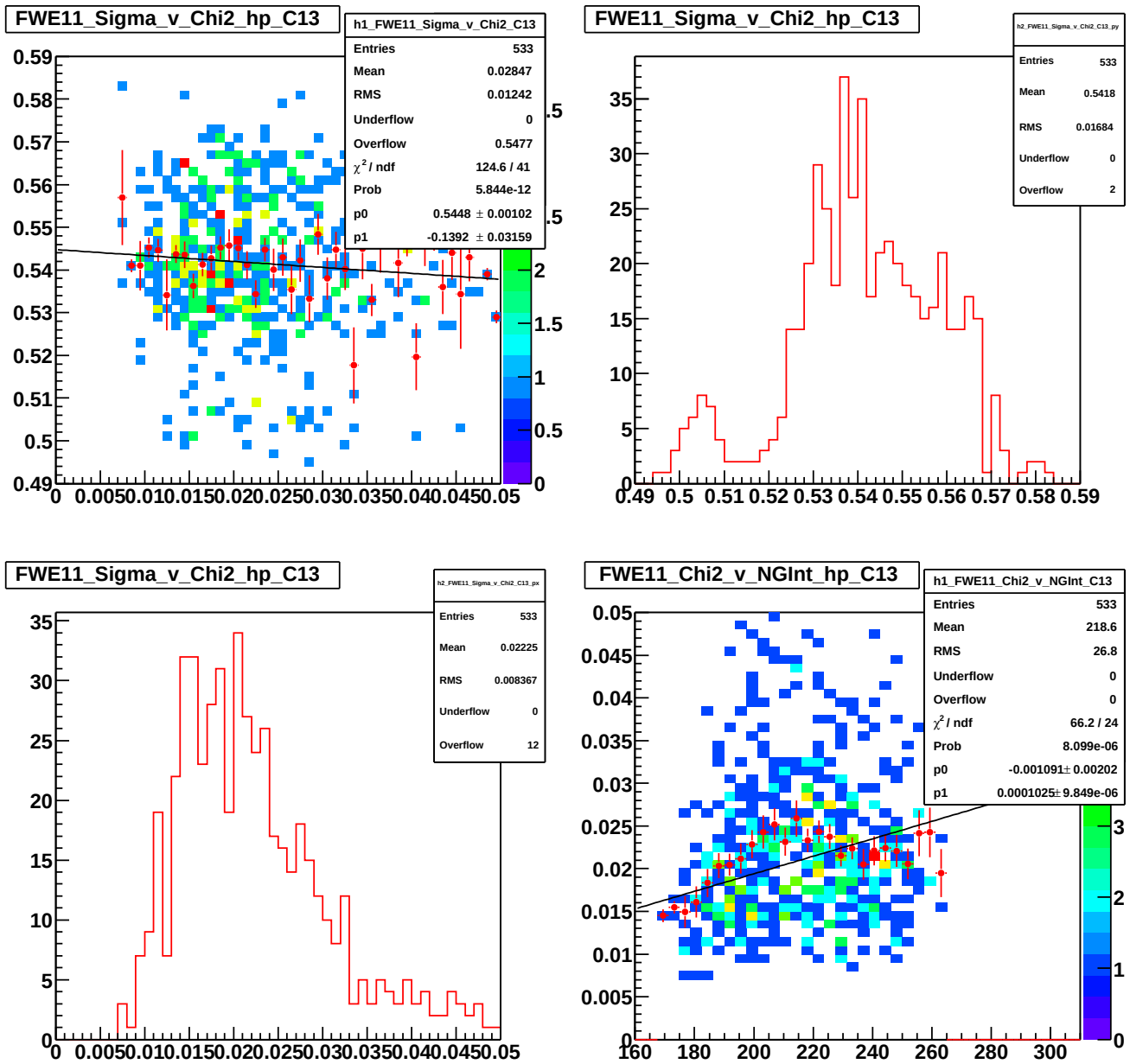

Figure 21: Proton beam, horizontal detectors: Performance of the Flying Wire Detector at the E11 location during Tevatron Remove Halo case: Sigma of the bunch width distribution (in *mm*) as measured by the FW detector versus front end measure of the goodness of fit together with an overlaid horizontal profile and a straight line fit; sigma itself, goodness of fit itself; goodness of fit versus bunch intensity together with an overlaid horizontal profile and a straight line fit;

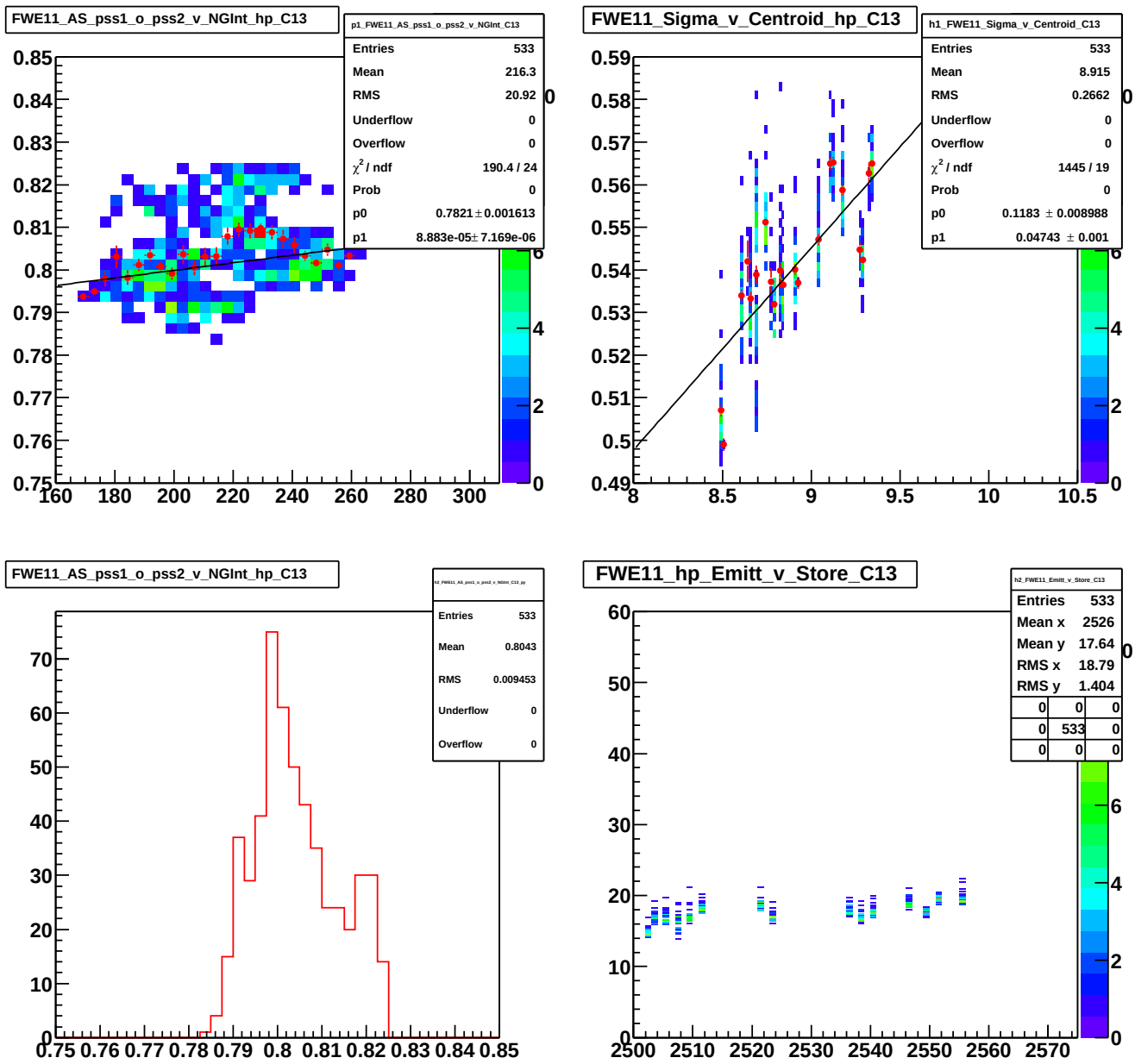

Figure 22: Proton beam, horizontal detectors: Performance of the Flying Wire Detector at the E11 location during Tevatron Remove Halo case: Amplitude (in arbitrary units) times sigma of the bunch width distribution (in *mm*) of the pass 1 over pass 2 of the front end FW detector data versus bunch intensity (ACNET variables T:FBI[A,P]NG) (in E9) together with an overlaid horizontal profile of that distribution with a straight line fit; sigma of the bunch width distribution versus bunch centroid (in *mm*) (based on the T:FW[E,H,V][A,P]CE ACNET variable) with an overlaid horizontal profile of that distribution with a straight line fit; amplitude (in arbitrary units) times sigma of the bunch width distribution (in *mm*) of the pass 1 over pass 2 of the front end FW detector data itself, bunch emittance (in $\pi \cdot mm \cdot mrad$) versus store number.

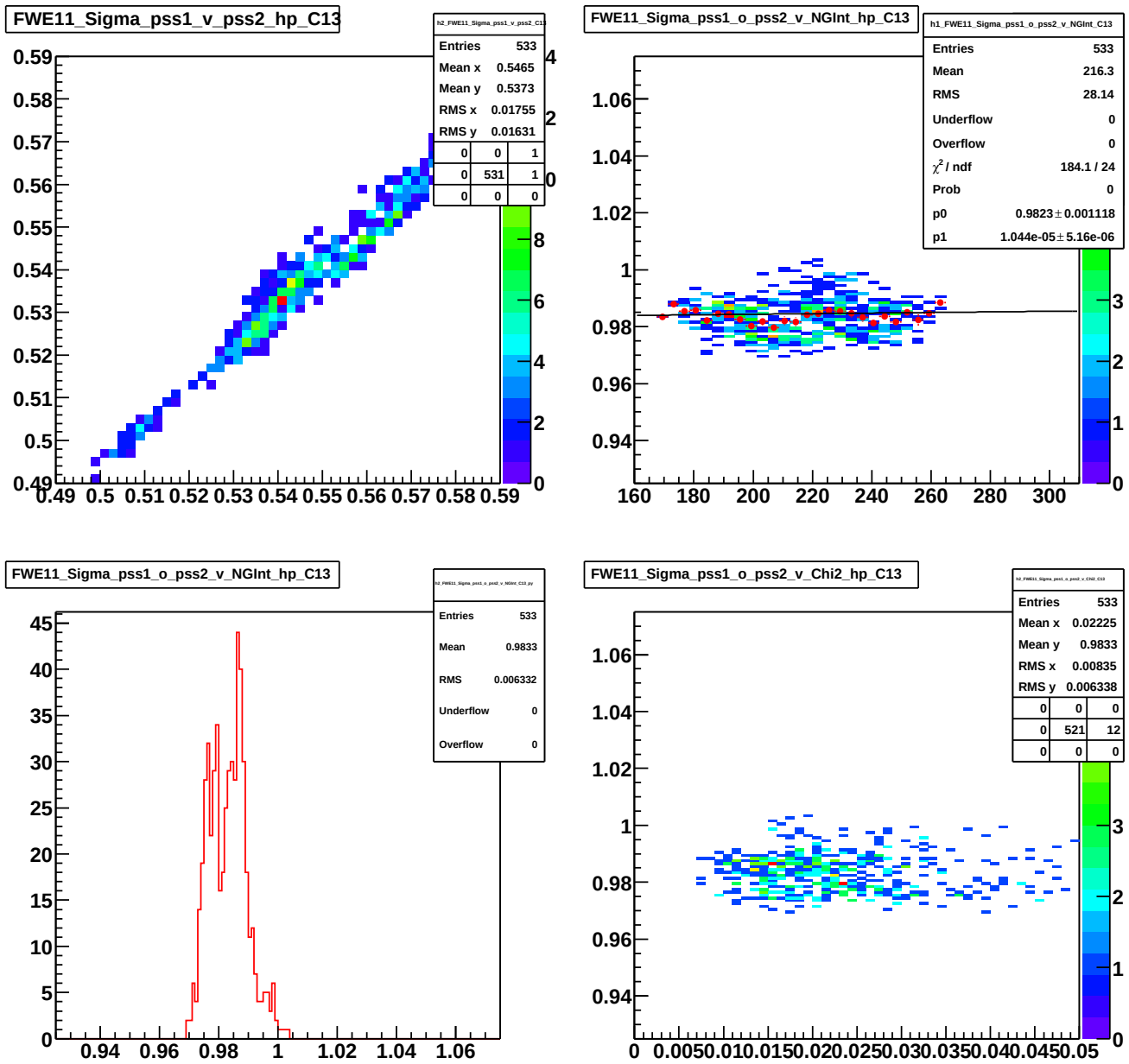

Figure 23: Proton beam, horizontal detectors: Performance of the Flying Wire Detector at the E11 location during Tevatron Remove Halo case: Sigma of the bunch width distribution (in *mm*) of the pass 1 versus pass 2 of the FW detector; sigma of the bunch width distribution (in *mm*) of the pass 1 over pass 2 of the FW detector versus bunch intensity (ACNET variables T:FBI[A,P]NG) (in E9) together with an overlaid horizontal profile and a straight line fit; sigma of the bunch width distribution (in *mm*) of the pass 1 over pass 2 of the FW detector itself, sigma of the bunch width distribution (in *mm*) of the pass 1 over pass 2 of the FW detector versus front end measure of the goodness of fit.

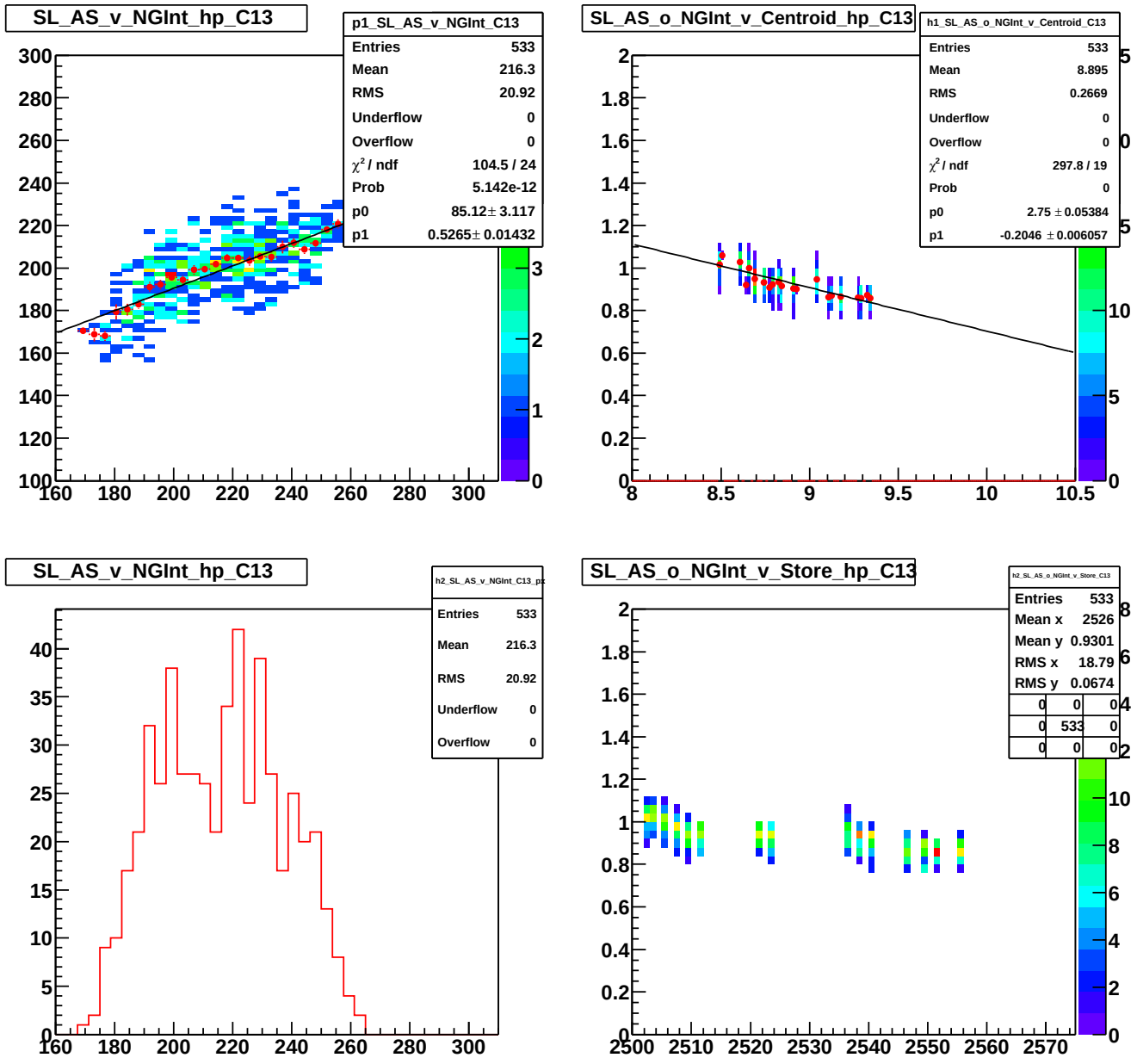

Figure 24: Proton beam, horizontal detectors: Performance of the Synchrotron Light Detector at the C11 location during Tevatron Remove Halo case: Amplitude (in arbitrary units) times sigma of the bunch width distribution (in *mm*) of the raw SL detector distribution versus bunch intensity (ACNET variables T:FBI[A,P]NG) (in E9) with an overlaid horizontal profile of that distribution with a straight line fit; amplitude times sigma of the bunch width distribution (in *mm*) of the raw SL detector distribution over bunch intensity versus bunch E11 centroid (in *mm*) (based on the T:FW[E,H,V][A,P]CE ACNET variable) with an overlaid horizontal profile of that distribution with a straight line fit; bunch intensity; amplitude times sigma of the bunch width distribution (in *mm*) of the raw SL detector distribution over bunch intensity versus store number.

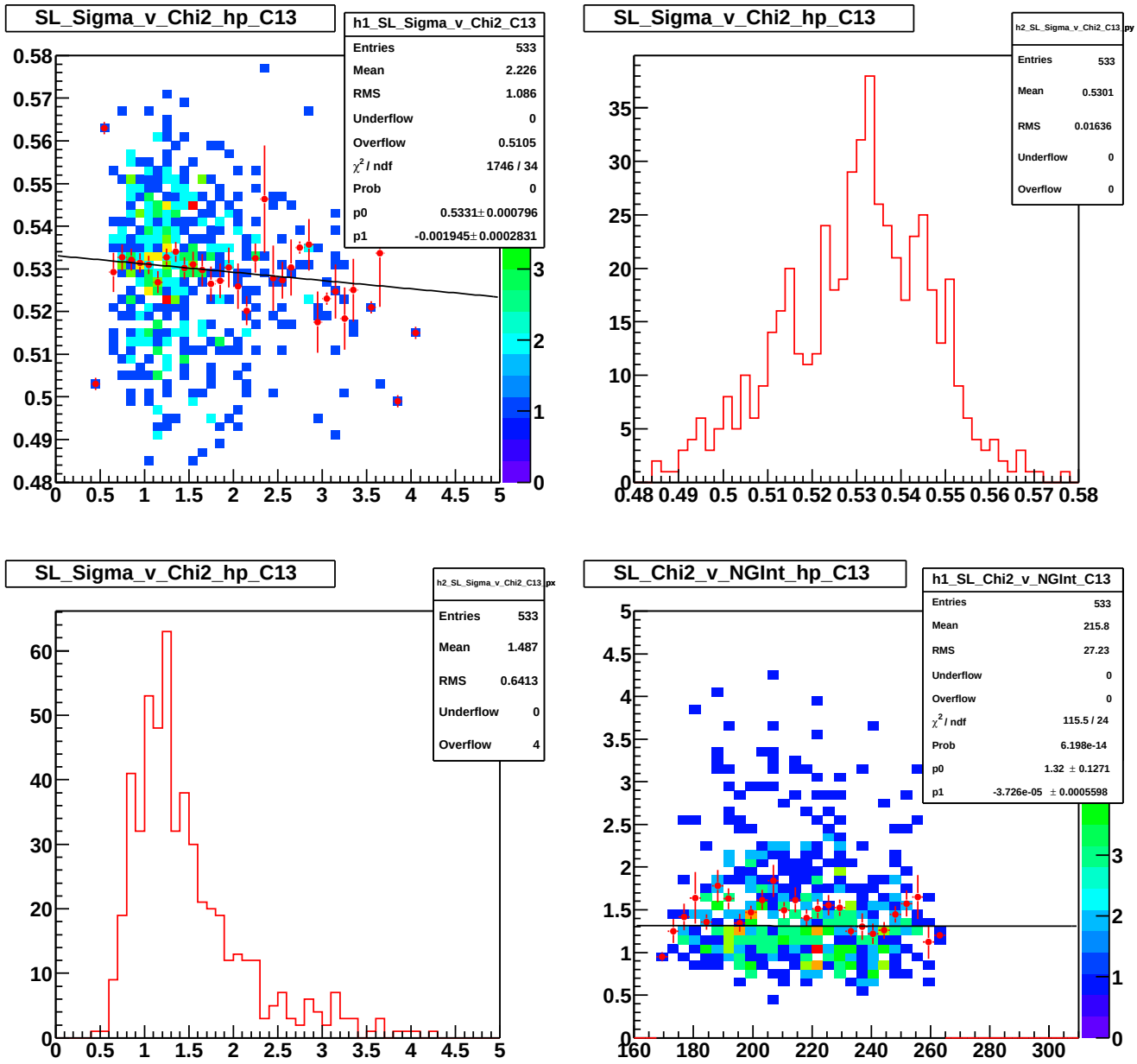

Figure 25: Proton beam, horizontal detectors: Performance of the Synchrotron Light Detector at the C11 location during Tevatron Remove Halo case: Sigma of the bunch width distribution (in *mm*) as measured by the SL detector versus front end measure of the goodness of fit together with an overlaid horizontal profile and a straight line fit; sigma of the bunch width distribution (in *mm*) itself; goodness of fit itself; goodness of fit versus bunch intensity together with an overlaid horizontal profile and a straight line fit.

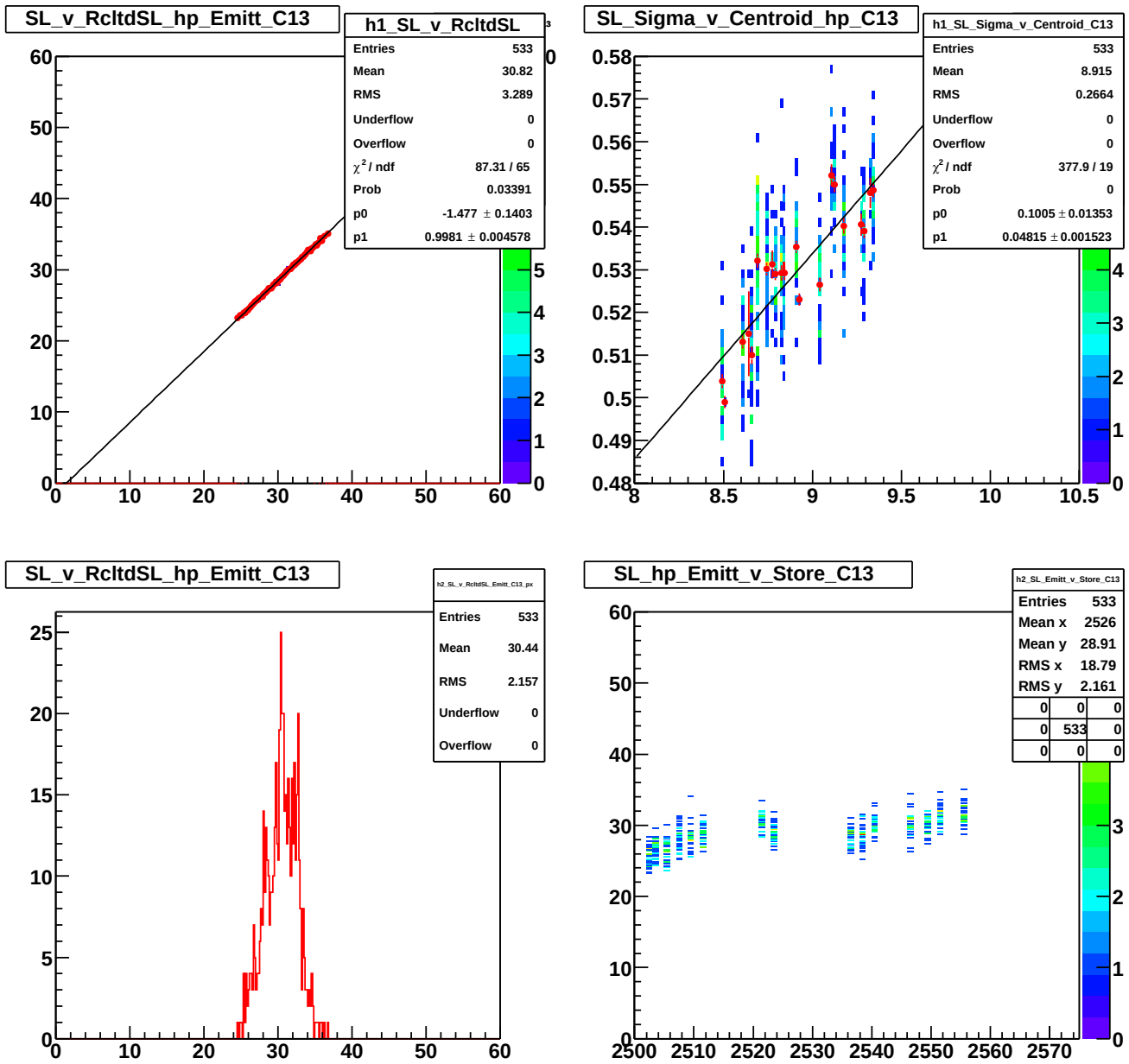

Figure 26: Proton beam, horizontal detectors: Performance of the Synchrotron Light Detector at the C11 location during Tevatron Remove Halo case: Bunch emittance (in $\pi \cdot mm \cdot mrad$) as measured by the front end SL detector versus bunch emittance as recalculated using front end sigma of the bunch width distribution (in *mm*) (combined with SBD timing information in the horizontal cases) together with an overlaid horizontal profile of that distribution with a straight line fit; sigma of the bunch width distribution versus bunch E11 centroid (in *mm*) (based on the T:FW[E,H,V][A,P]CE ACNET variable) with an overlaid horizontal profile of that distribution with a straight line fit; bunch emittance; bunch emittance versus store number.

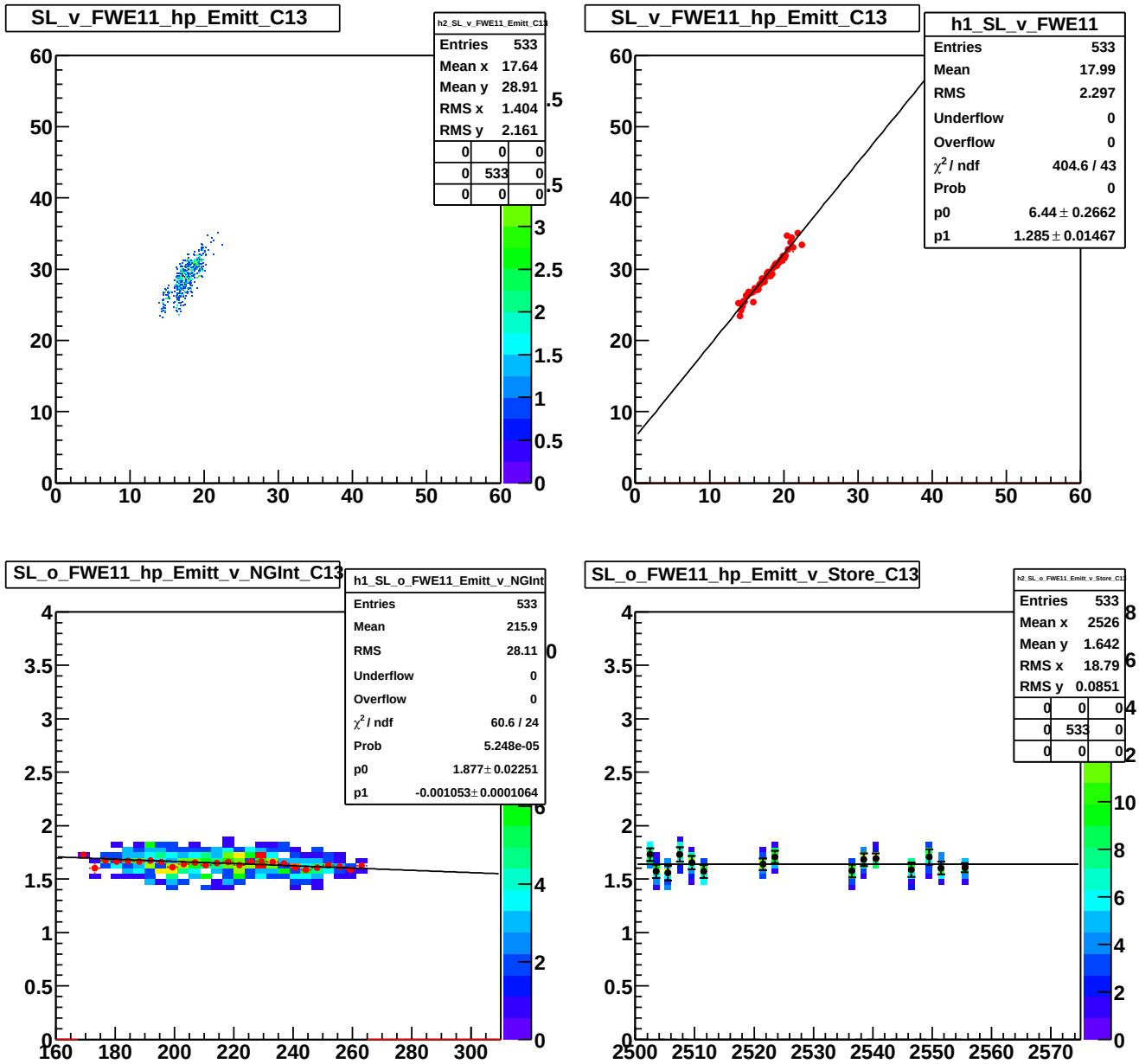

Figure 27: Proton beam, horizontal detectors: Comparisons of Emittance measurements as done by Synchrotron Light Detector at C11 and Flying Wire Detector at E11 during Tevatron Remove Halo case: Bunch emittance (in $\pi \cdot mm \cdot mrad$) as measured by Synchrotron Light Detector versus bunch emittance as measured by the Flying Wire Detector at E11; horizontal profile of the previous distribution with a straight line fit; bunch emittance as measured by Synchrotron Light Detector over bunch emittance as measured by the Flying Wire Detector at E11 versus bunch intensity (ACNET variables T:FBI[A,P]NG) (in E9) together with an overlaid horizontal profile and a straight line fit; bunch emittance as measured by Synchrotron Light Detector over bunch emittance as measured by the Flying Wire Detector at E11 versus store number with overlaid averaged ratios for each store and a horizontal line fit.

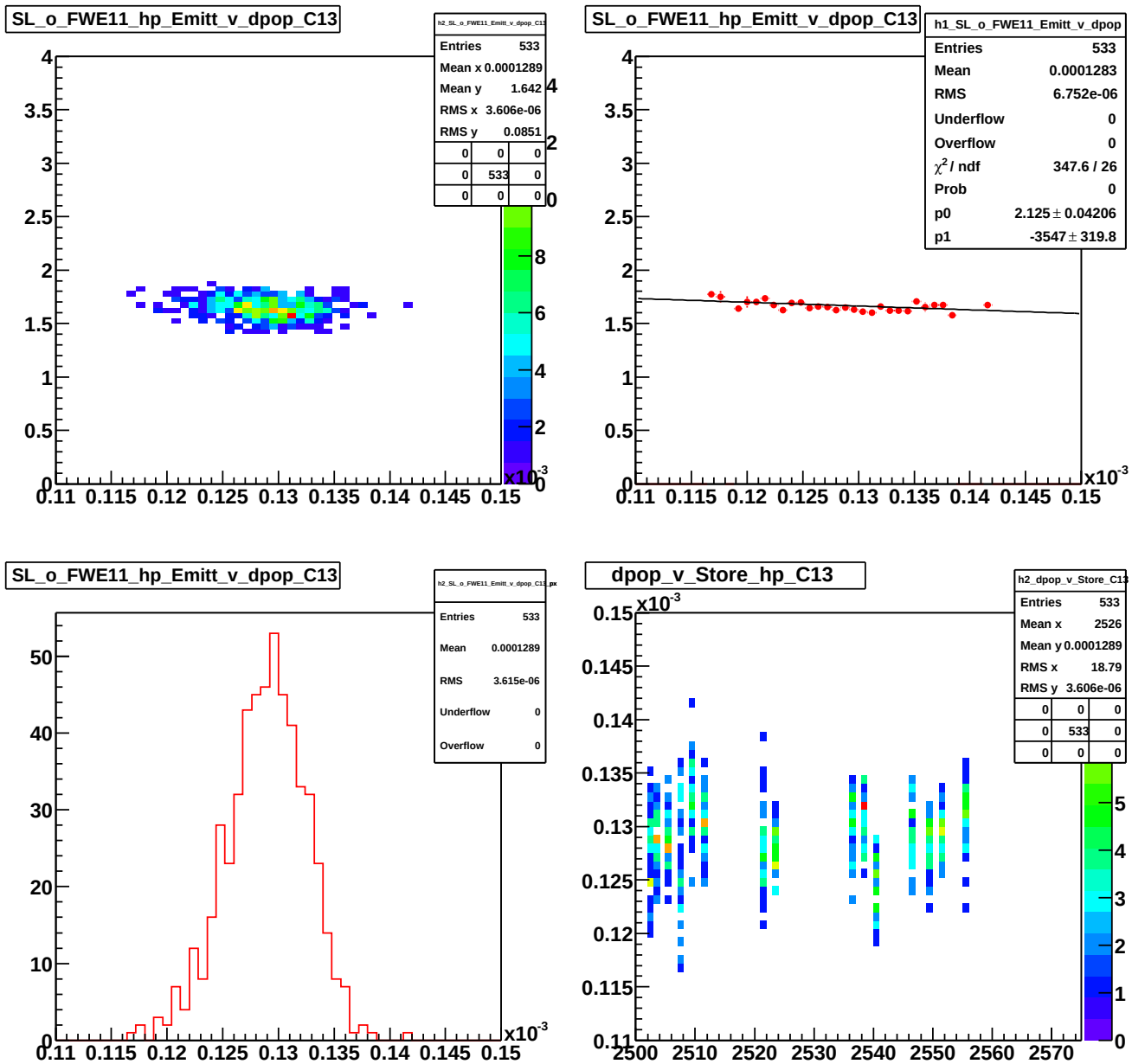

Figure 28: Proton beam, horizontal detectors: Comparisons of Emittance measurements as done by Synchrotron Light Detector at C11 and Flying Wire Detector at E11 during Tevatron Remove Halo case: Bunch emittance as measured by Synchrotron Light Detector over bunch emittance as measured by the Flying Wire Detector at E11 versus recalculated $\delta p/p$ (based on δt the T:SBD[A,P]SS ACNET variable); horizontal profile of the previous distribution with a straight line fit; $\delta p/p$ itself; $\delta p/p$ versus store number.

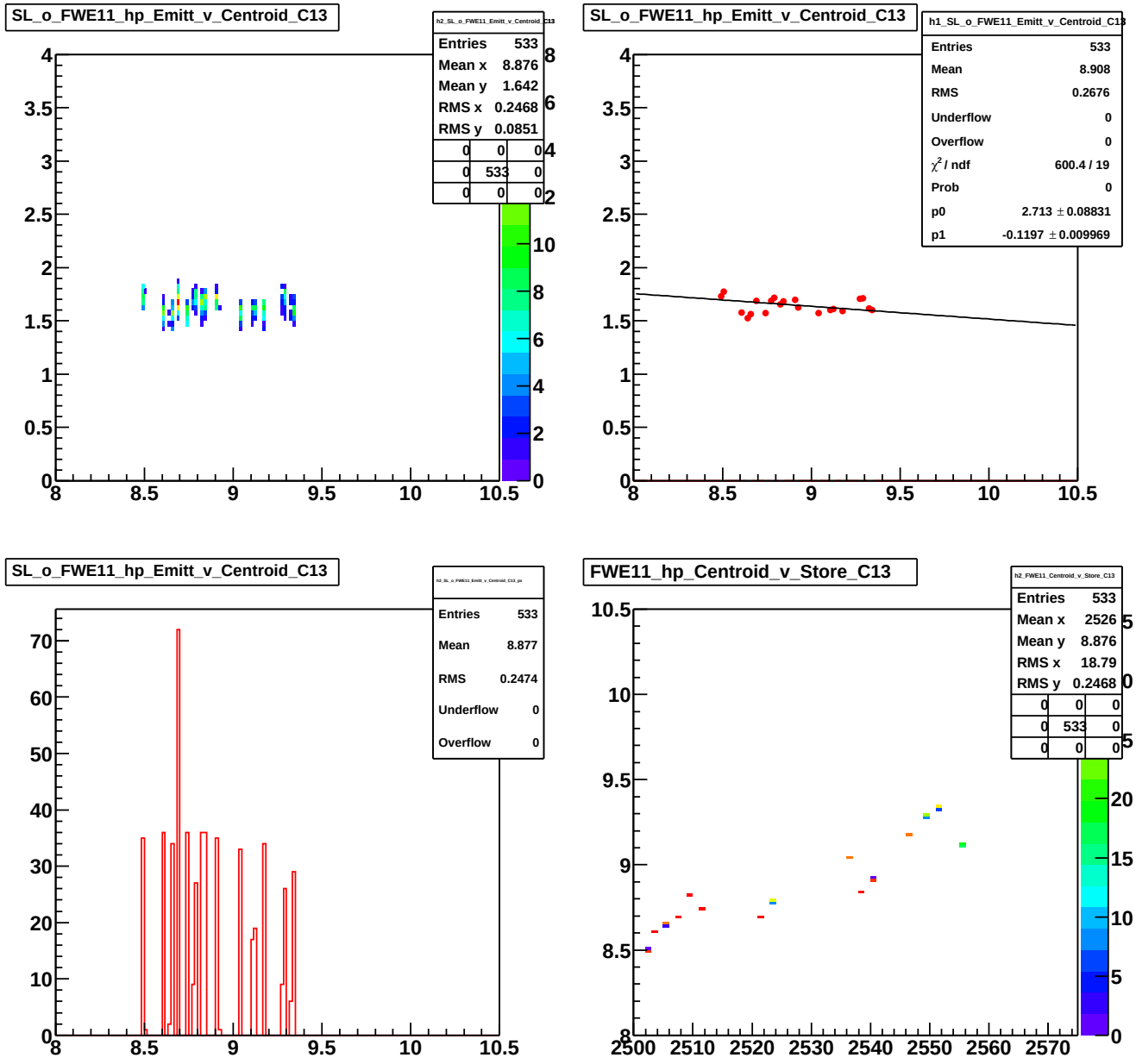

Figure 29: Proton beam, horizontal detectors: Comparisons of Emittance measurements as done by Synchrotron Light Detector at C11 and Flying Wire Detector at E11 during Tevatron Remove Halo case: Bunch emittance as measured by Synchrotron Light Detector over bunch emittance as measured by the Flying Wire Detector at E11 versus bunch E11 centroid (in *mm*) (based on the T:FW[E,H,V][A,P]CE ACNET variable); horizontal profile of the previous distribution with a straight line fit; bunch E11 centroid itself; bunch E11 centroid versus store number.

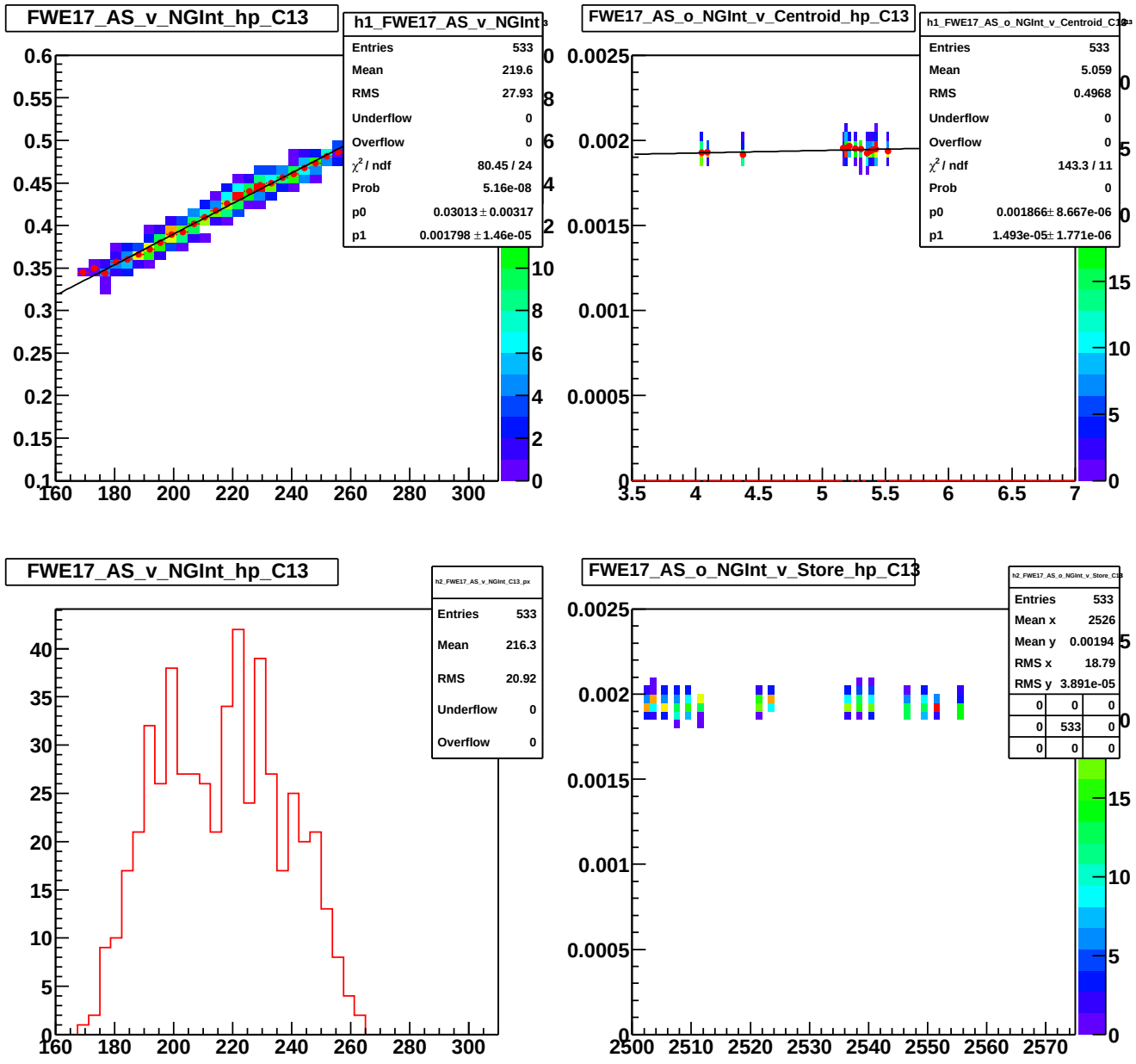

Figure 30: Proton beam, horizontal detectors: Performance of the Flying Wire Detector at the E17 location during Tevatron Remove Halo case: Amplitude (in arbitrary units) times sigma of the bunch width distribution (in *mm*) of the front end FW detector data versus bunch intensity (ACNET variables T:FBI[A,P]NG) (in E9) with an overlaid horizontal profile of that distribution with a straight line fit; Amplitude times sigma of the bunch width distribution of the front end FW detector data over bunch intensity versus bunch E17 centroid (in *mm*) (based on the T:FW[E,H,V][A,P]CE ACNET variable) with an overlaid horizontal profile of that distribution with a straight line fit; bunch intensity; amplitude times sigma of the bunch width distribution (in *mm*) of the raw FW detector distribution over bunch intensity versus store number.

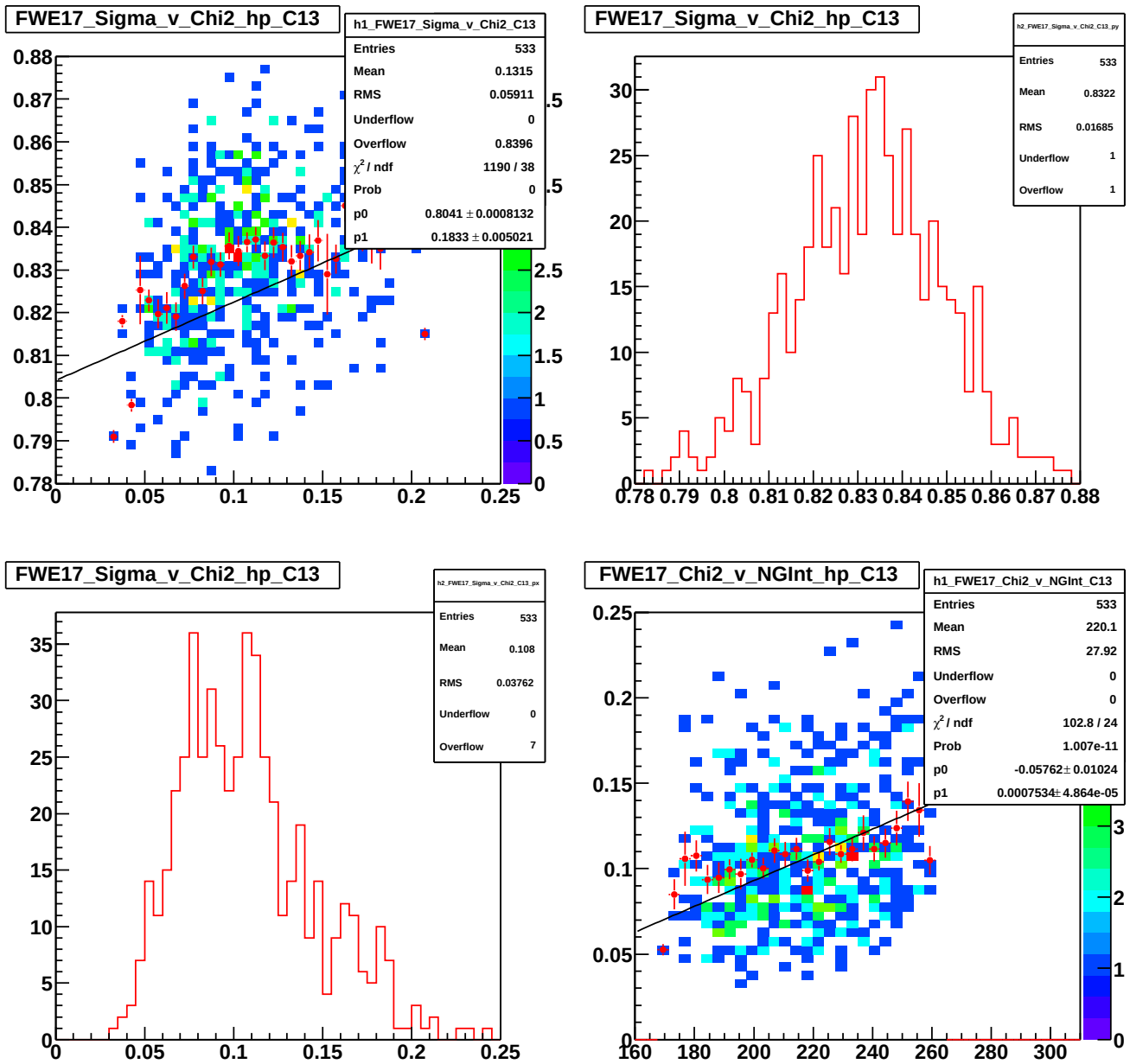

Figure 31: Proton beam, horizontal detectors: Performance of the Flying Wire Detector at the E17 location during Tevatron Remove Halo case: Sigma of the bunch width distribution (in *mm*) as measured by the FW detector versus front end measure of the goodness of fit together with an overlaid horizontal profile and a straight line fit; sigma itself, goodness of fit itself; goodness of fit versus bunch intensity together with an overlaid horizontal profile and a straight line fit.

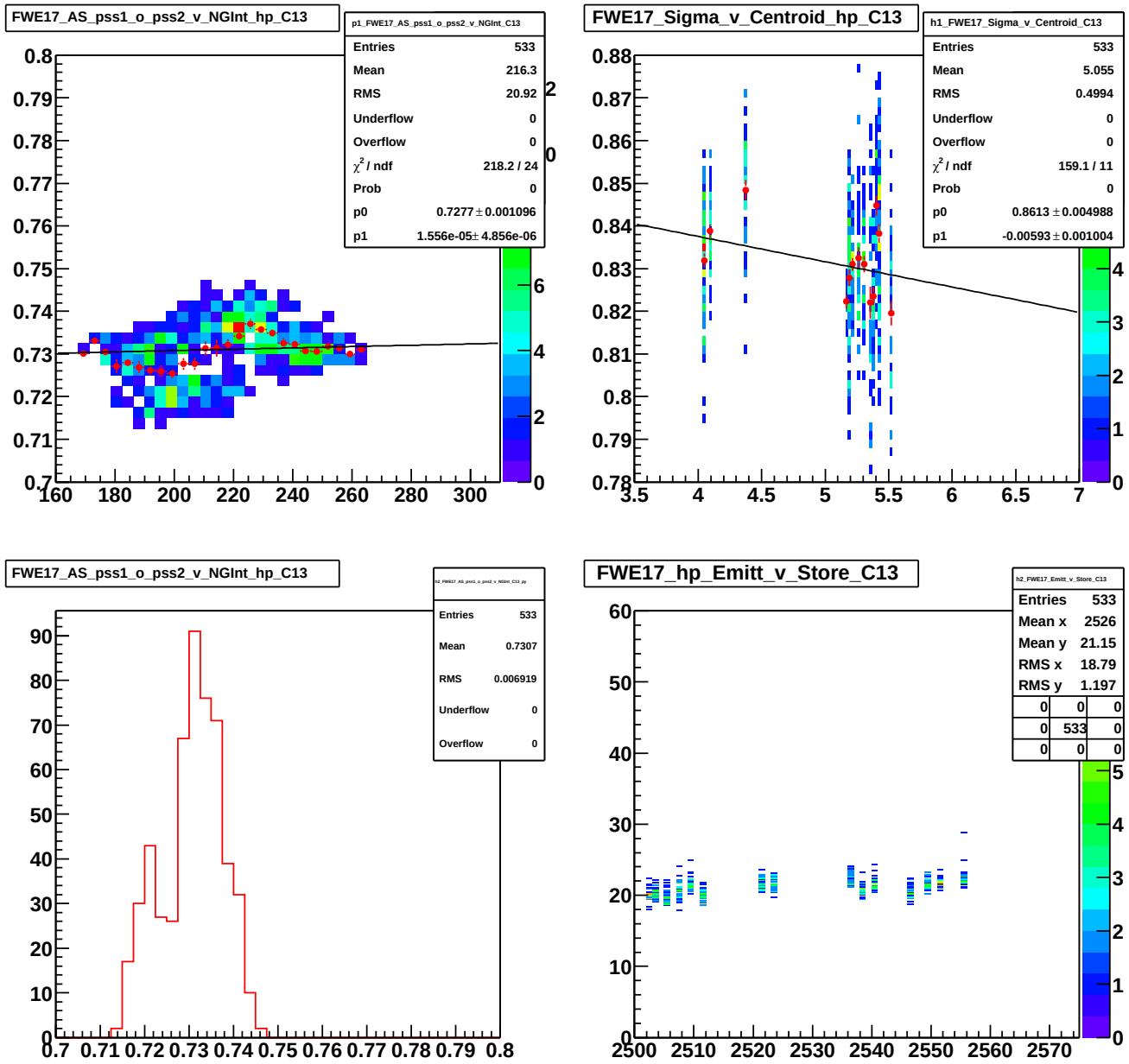

Figure 32: Proton beam, horizontal detectors: Performance of the Flying Wire Detector at the E17 location during Tevatron Remove Halo case: Amplitude (in arbitrary units) times sigma of the bunch width distribution (in *mm*) of the pass 1 over pass 2 of the front end FW detector data versus bunch intensity (ACNET variables T:FBI[A,P]NG) (in E9) together with an overlaid horizontal profile of that distribution with a straight line fit; sigma of the bunch width distribution versus bunch centroid (in *mm*) (based on the T:FW[E,H,V][A,P]CE ACNET variable) with an overlaid horizontal profile of that distribution with a straight line fit; amplitude (in arbitrary units) times sigma of the bunch width distribution (in *mm*) of the pass 1 over pass 2 of the front end FW detector data itself, bunch emittance (in $\pi \cdot mm \cdot mrad$) versus store number.

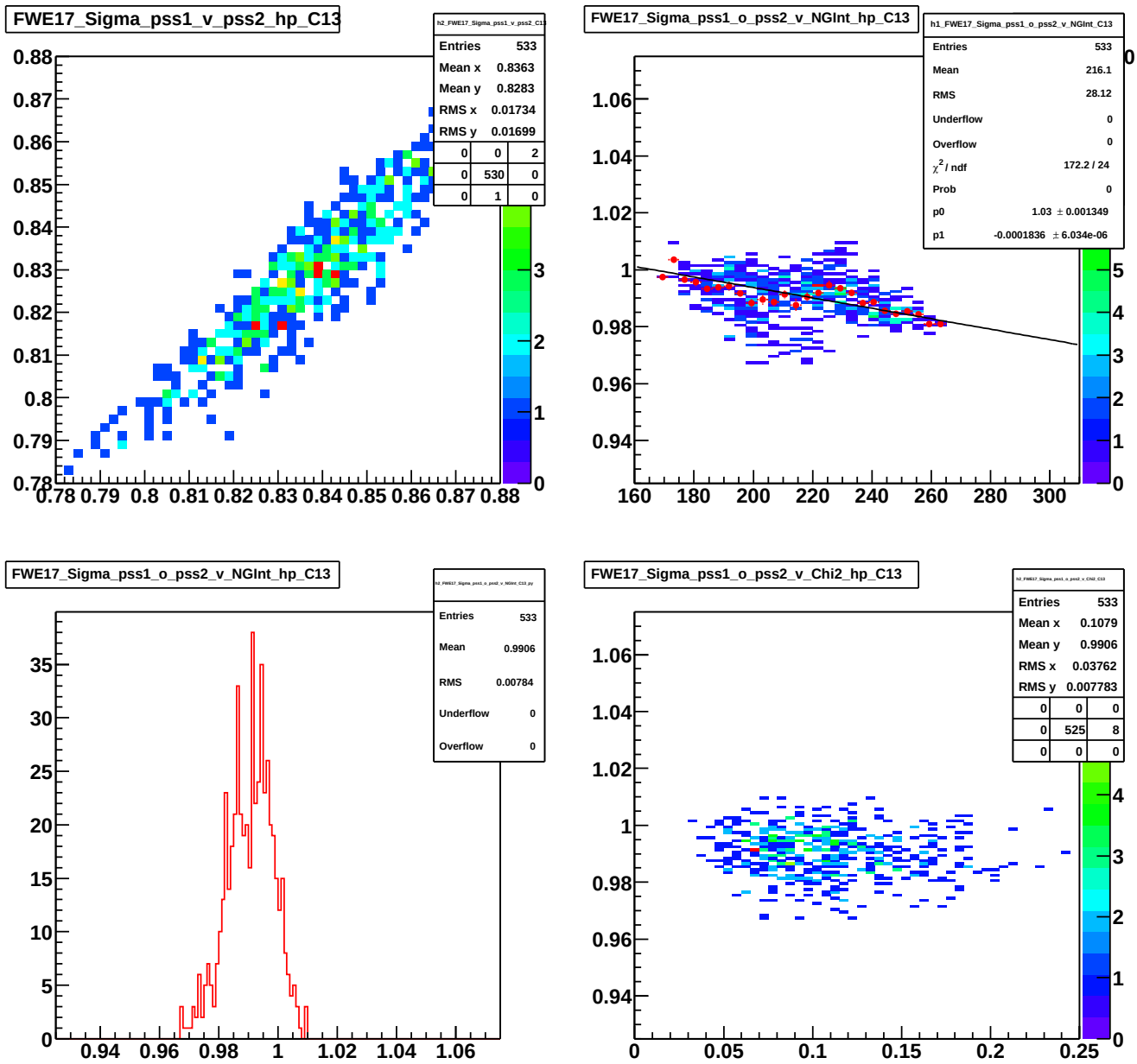

Figure 33: Proton beam, horizontal detectors: Performance of the Flying Wire Detector at the E17 location during Tevatron Remove Halo case: Sigma of the bunch width distribution (in *mm*) of the pass 1 versus pass 2 of the FW detector; sigma of the bunch width distribution (in *mm*) of the pass 1 over pass 2 of the FW detector versus bunch intensity (ACNET variables T:FBI[A,P]NG) (in E9) together with an overlaid horizontal profile and a straight line fit; sigma of the bunch width distribution (in *mm*) of the pass 1 over pass 2 of the FW detector itself, sigma of the bunch width distribution (in *mm*) of the pass 1 over pass 2 of the FW detector versus front end measure of the goodness of fit.

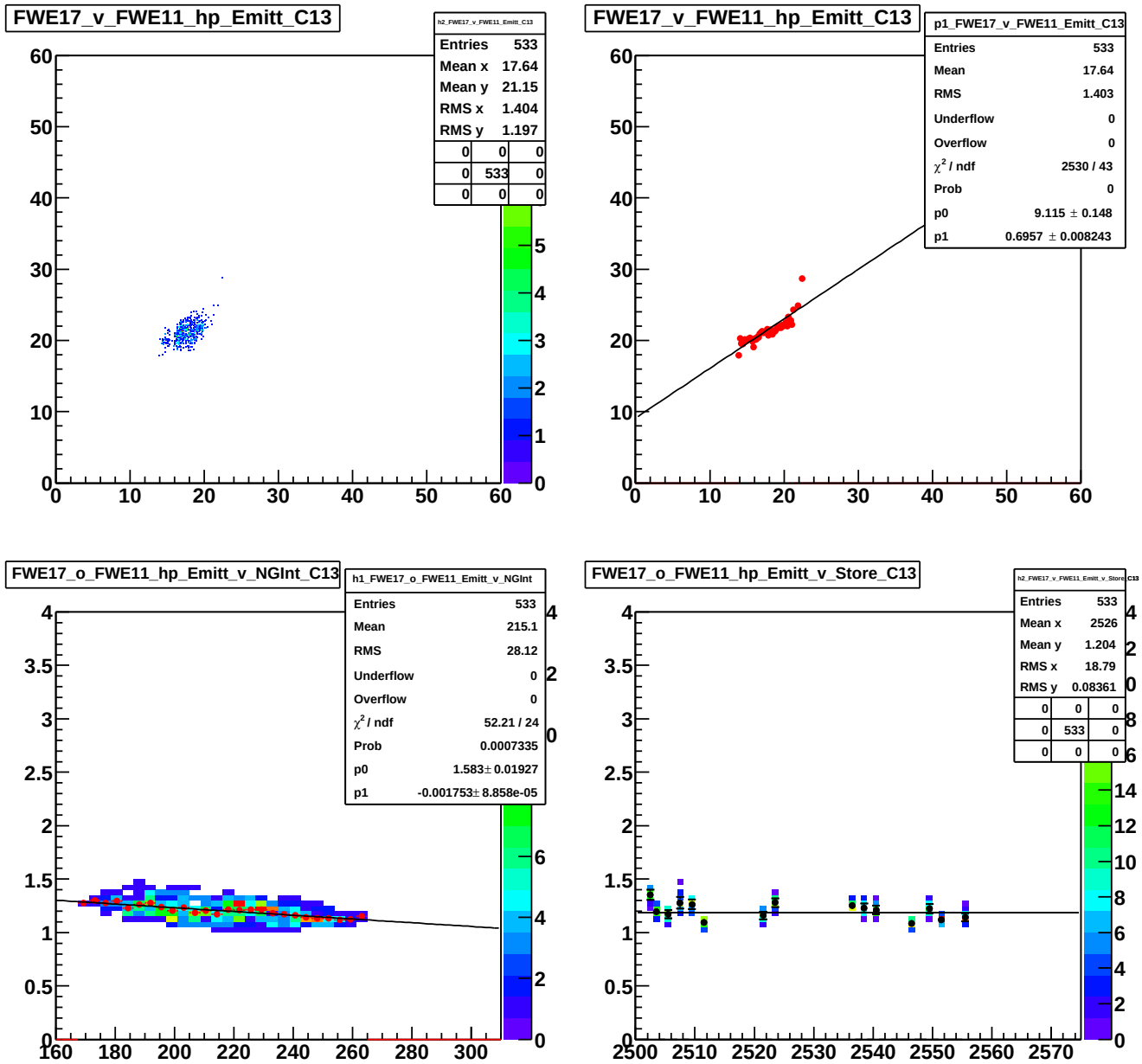

Figure 34: Proton beam, horizontal detectors: Comparisons of Emittance measurements as done by Flying Wire Detector at E17 and Flying Wire Detector at E11 during Tevatron Remove Halo case: Bunch emittance (in $\pi \cdot mm \cdot mrad$) as measured by Flying Wire Detector at E17 versus bunch emittance as measured by the Flying Wire Detector at E11; horizontal profile of the previous distribution with a straight line fit; bunch emittance as measured by Flying Wire Detector at E17over bunch emittance as measured by the Flying Wire Detector at E11 versus bunch intensity (ACNET variables T:FBI[A,P]NG) (in E9) together with an overlaid horizontal profile and a straight line fit; bunch emittance as measured by Flying Wire Detector at E17 over bunch emittance as measured by the Flying Wire Detector at E11 versus store number with overlaid averaged ratios for each store and a horizontal line fit.

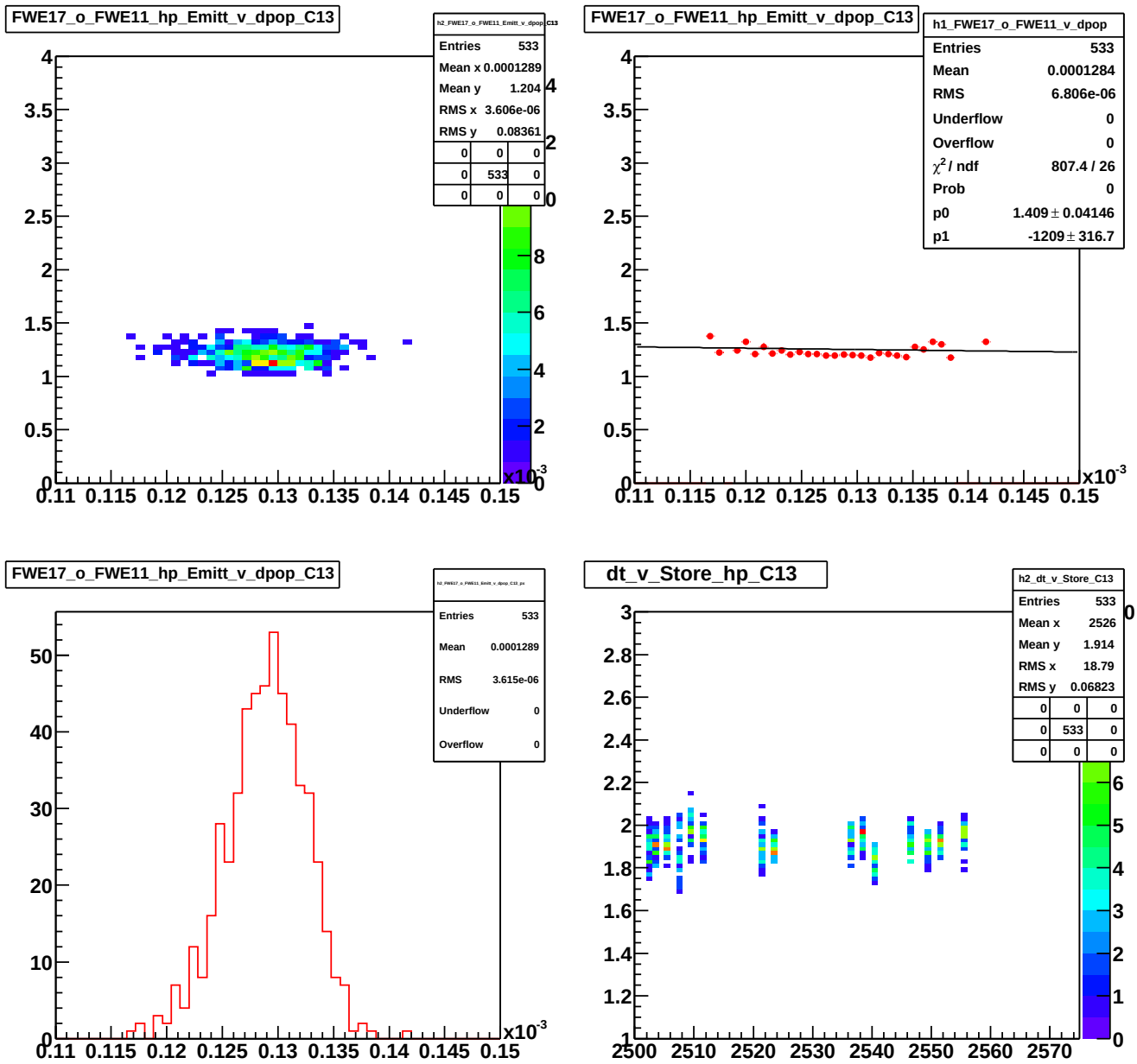

Figure 35: Proton beam, horizontal detectors: Comparisons of Emittance measurements as done by Flying Wire Detector at E17 and Flying Wire Detector at E11 during Tevatron Remove Halo case: Bunch emittance as measured by Flying Wire Detector at E17 over bunch emittance as measured by the Flying Wire Detector at E11 versus recalculated $\delta p/p$ (based on δt the T:SBD[A,P]SS ACNET variable); horizontal profile of the previous distribution with a straight line fit; $\delta p/p$ itself; δt versus store number.

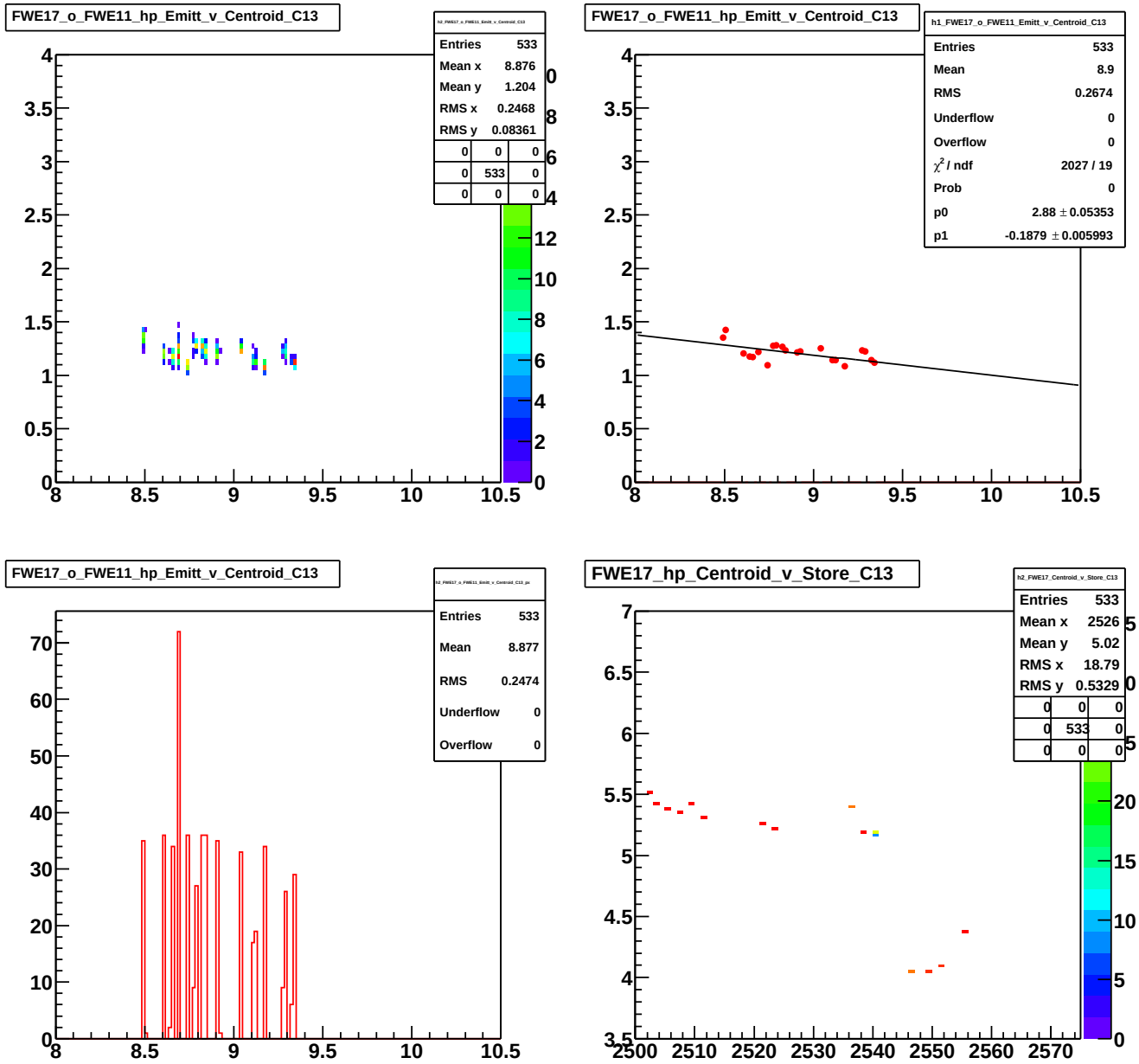

Figure 36: Proton beam, horizontal detectors: Comparisons of Emittance measurements as done by Flying Wire Detector at E17 and Flying Wire Detector at E11 during Tevatron Remove Halo case: Bunch emittance as measured by Flying Wire Detector at E17 over bunch emittance as measured by the Flying Wire Detector at E11 versus bunch E11 centroid (in *mm*) (based on the T:FW[E,H,V][A,P]CE ACNET variable); horizontal profile of the previous distribution with a straight line fit; bunch E17 centroid; bunch E17 centroid versus store number.

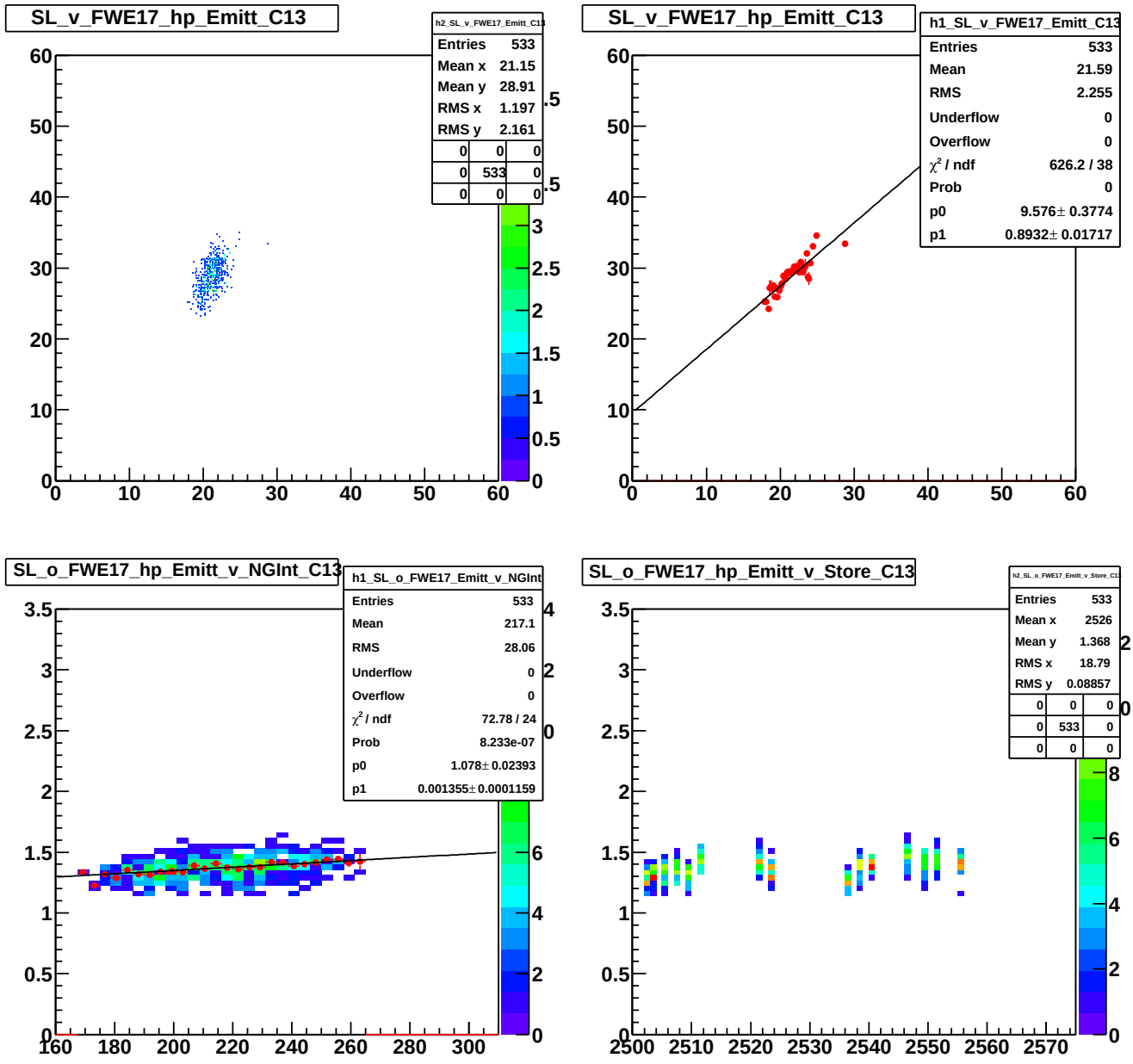

Figure 37: Proton beam, horizontal detectors: Comparisons of Emittance measurements as done by Synchrotron Light Detector at C11 and Flying Wire Detector at E17 during Tevatron Remove Halo case: Bunch emittance (in $\pi \cdot mm \cdot mrad$) as measured by Synchrotron Light Detector versus bunch emittance as measured by the Flying Wire Detector at E17; horizontal profile of the previous distribution with a straight line fit; bunch emittance as measured by Synchrotron Light Detector over bunch emittance as measured by the Flying Wire Detector at E17 versus bunch intensity (ACNET variables T:FBI[A,P]NG) (in E9) together with an overlaid horizontal profile and a straight line fit; bunch emittance as measured by Synchrotron Light Detector over bunch emittance as measured by the Flying Wire Detector at E17 versus store number.

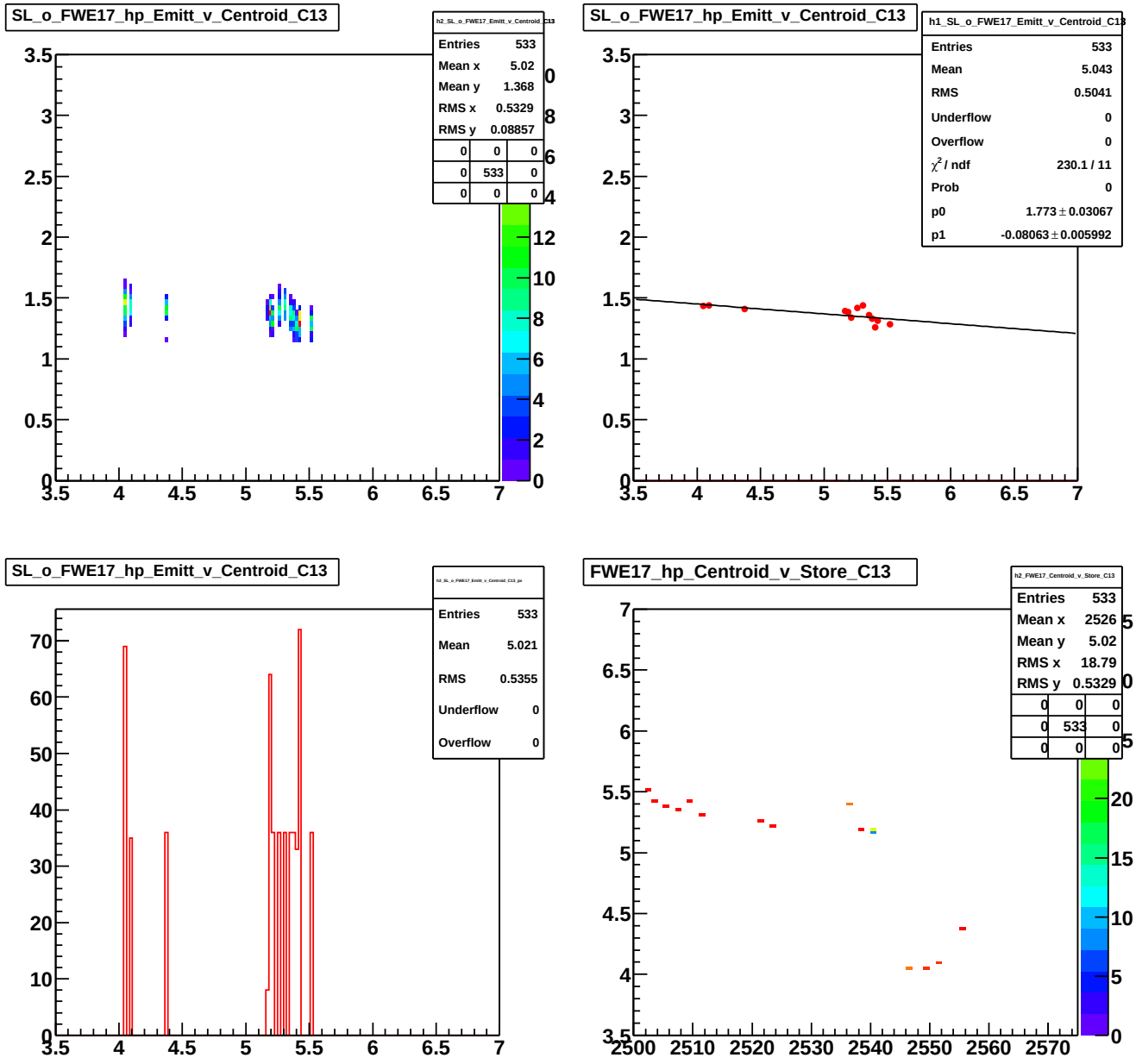

Figure 38: Proton beam, horizontal detectors: Comparisons of Emittance measurements as done by Synchrotron Light Detector at C11 and Flying Wire Detector at E17 during Tevatron Remove Halo case: Bunch emittance as measured by Synchrotron Light Detector over bunch emittance as measured by the Flying Wire Detector at E17 versus bunch E17 centroid (in *mm*) (based on the T:FW[E,H,V][A,P]CE ACNET variable); horizontal profile of the previous distribution with a straight line fit; bunch E17 centroid itself; bunch E17 centroid versus store number.

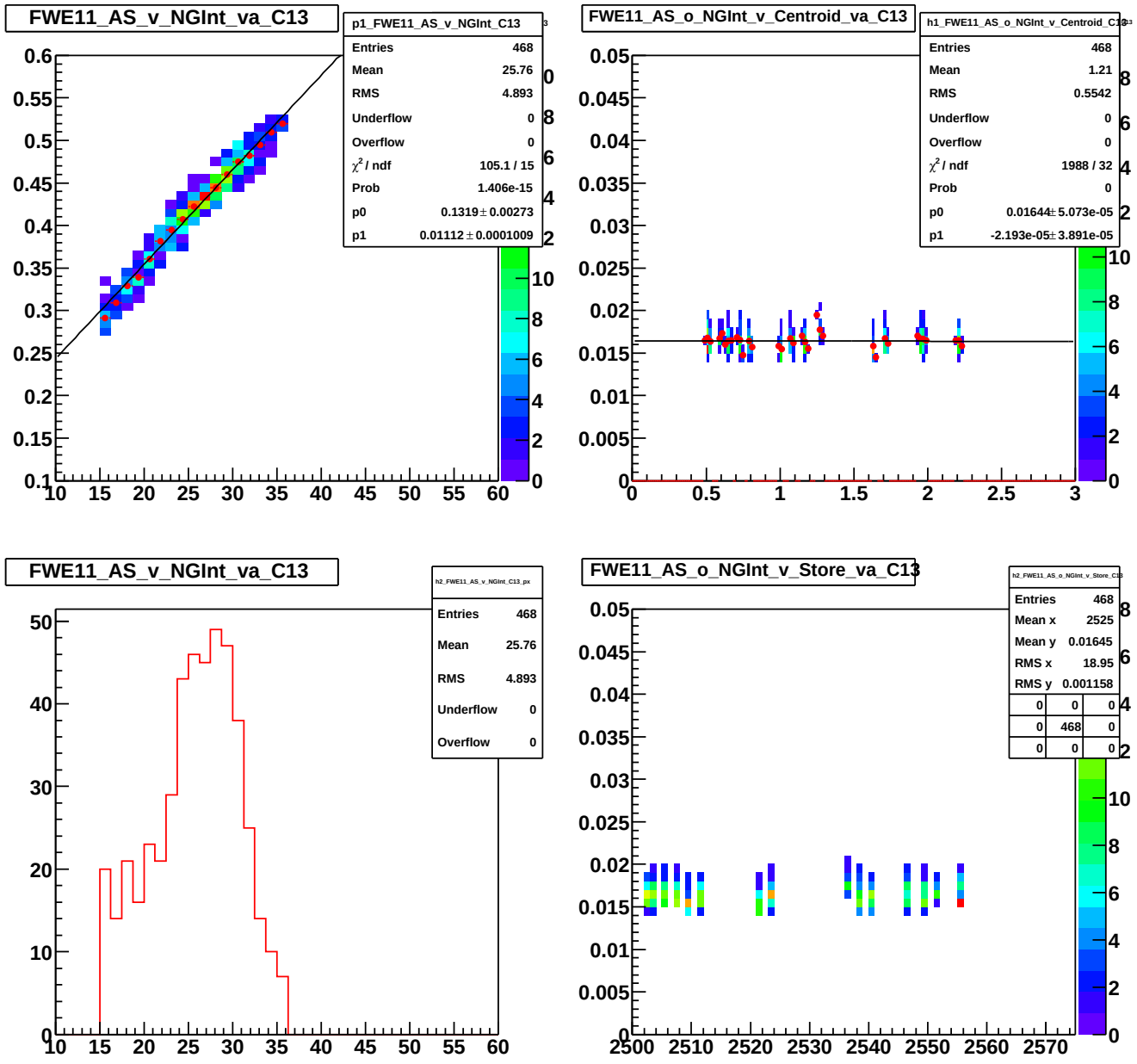

Figure 39: Antiproton beam, vertical detectors: Performance of the Flying Wire Detector at the E11 location during Tevatron Remove Halo case: Amplitude (in arbitrary units) times sigma of the bunch width distribution (in *mm*) of the front end FW detector data versus bunch intensity (ACNET variables T:FBI[A,P]NG) (in E9) with an overlaid horizontal profile of that distribution with a straight line fit; Amplitude times sigma of the bunch width distribution of the front end FW detector data over bunch intensity versus bunch E11 centroid (in *mm*) (based on the T:FW[E,H,V][A,P]CE ACNET variable) with an overlaid horizontal profile of that distribution with a straight line fit; bunch intensity; amplitude times sigma of the bunch width distribution (in *mm*) of the raw FW detector distribution over bunch intensity versus store number.

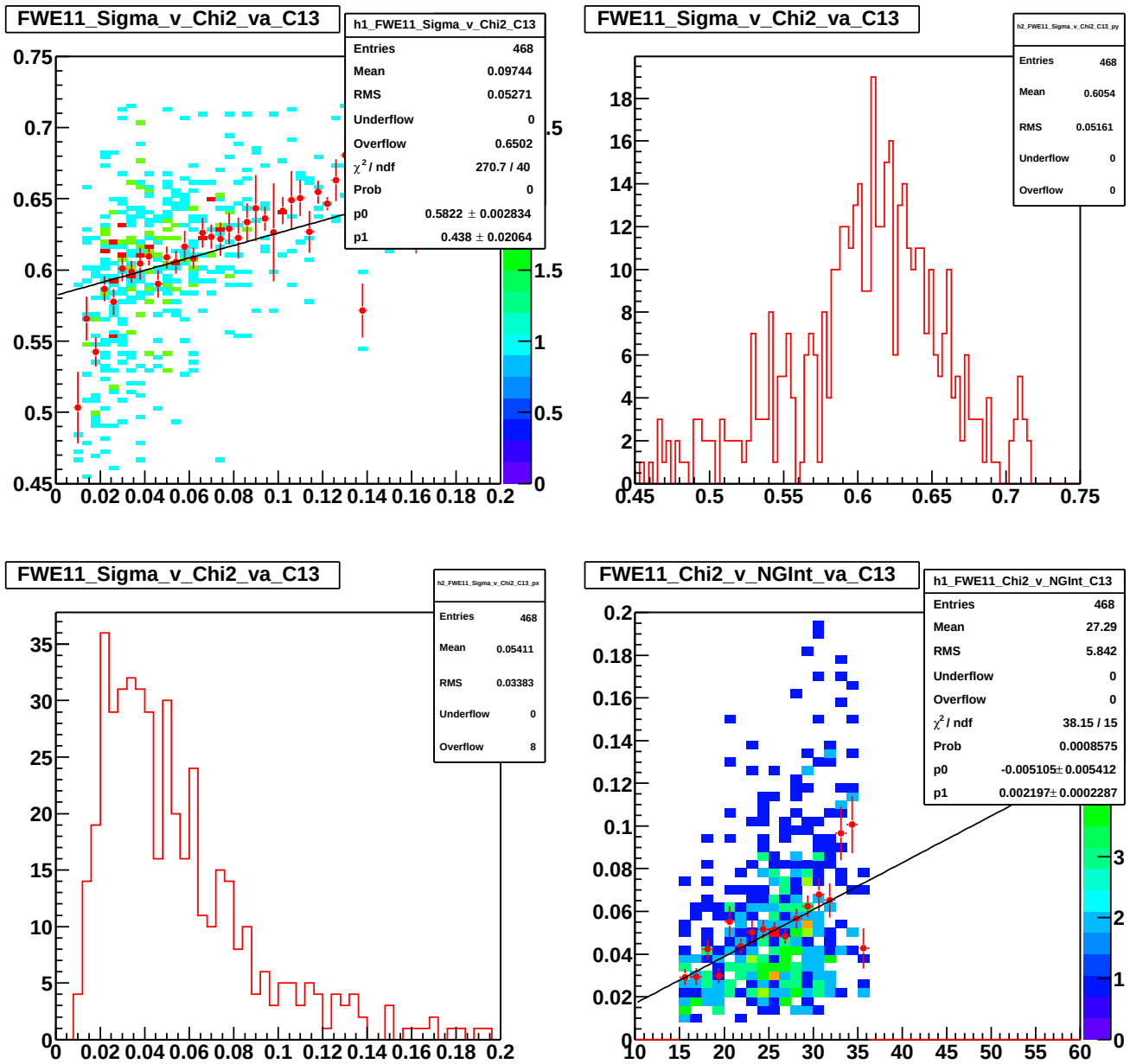

Figure 40: Antiproton beam, vertical detectors: Performance of the Flying Wire Detector at the E11 location during Tevatron Remove Halo case: Sigma of the bunch width distribution (in *mm*) as measured by the FW detector versus front end measure of the goodness of fit together with an overlaid horizontal profile and a straight line fit; sigma itself, goodness of fit itself; goodness of fit versus bunch intensity together with an overlaid horizontal profile and a straight line fit;

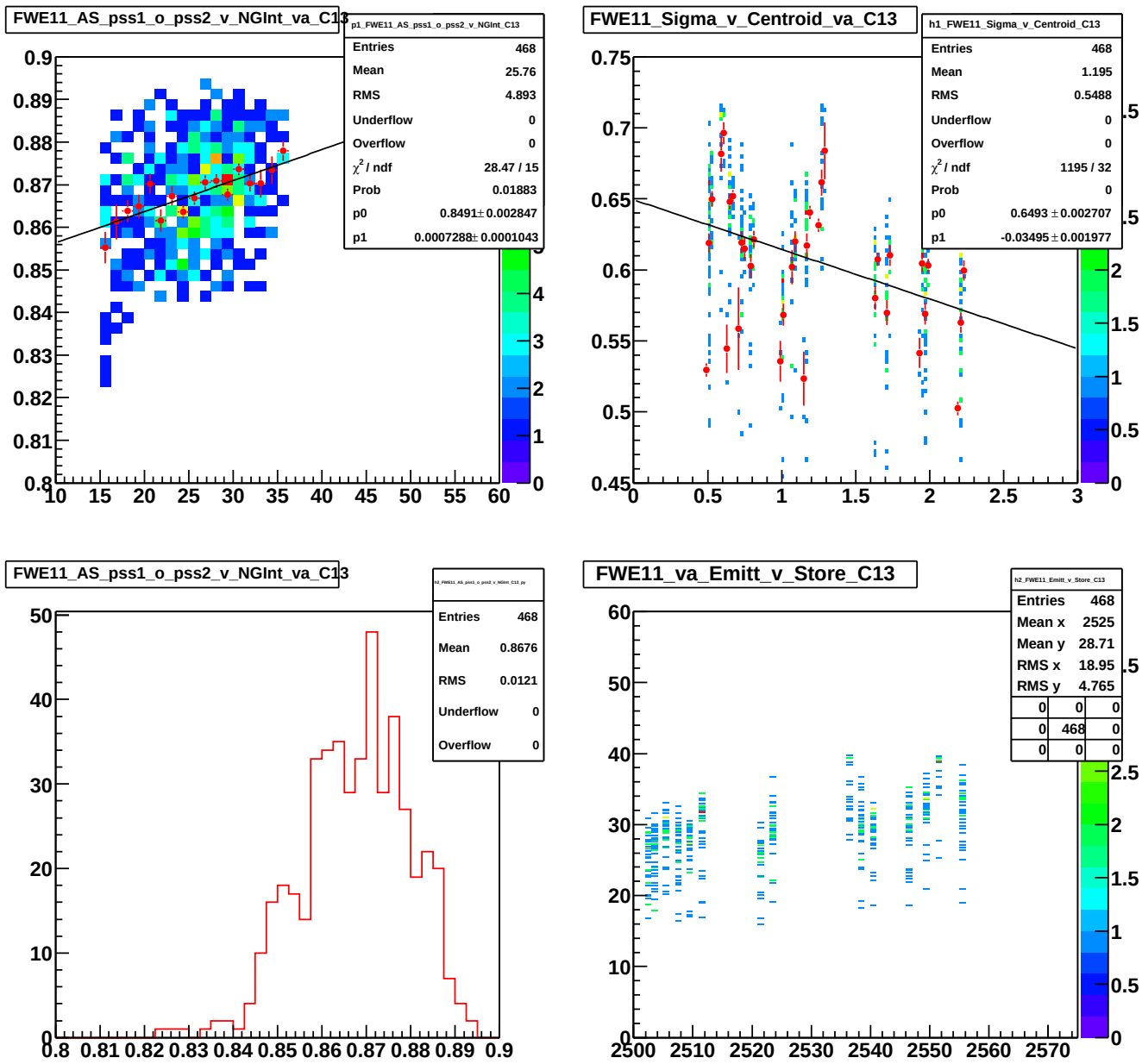

Figure 41: Antiproton beam, vertical detectors: Performance of the Flying Wire Detector at the E11 location during Tevatron Remove Halo case: Amplitude (in arbitrary units) times sigma of the bunch width distribution (in *mm*) of the pass 1 over pass 2 of the front end FW detector data versus bunch intensity (ACNET variables T:FBI[A,P]NG) (in E9) together with an overlaid horizontal profile of that distribution with a straight line fit; sigma of the bunch width distribution versus bunch centroid (in *mm*) (based on the T:FW[E,H,V][A,P]CE ACNET variable) with an overlaid horizontal profile of that distribution with a straight line fit; amplitude (in arbitrary units) times sigma of the bunch width distribution (in *mm*) of the pass 1 over pass 2 of the front end FW detector data itself, bunch emittance (in $\pi \cdot mm \cdot mrad$) versus store number.

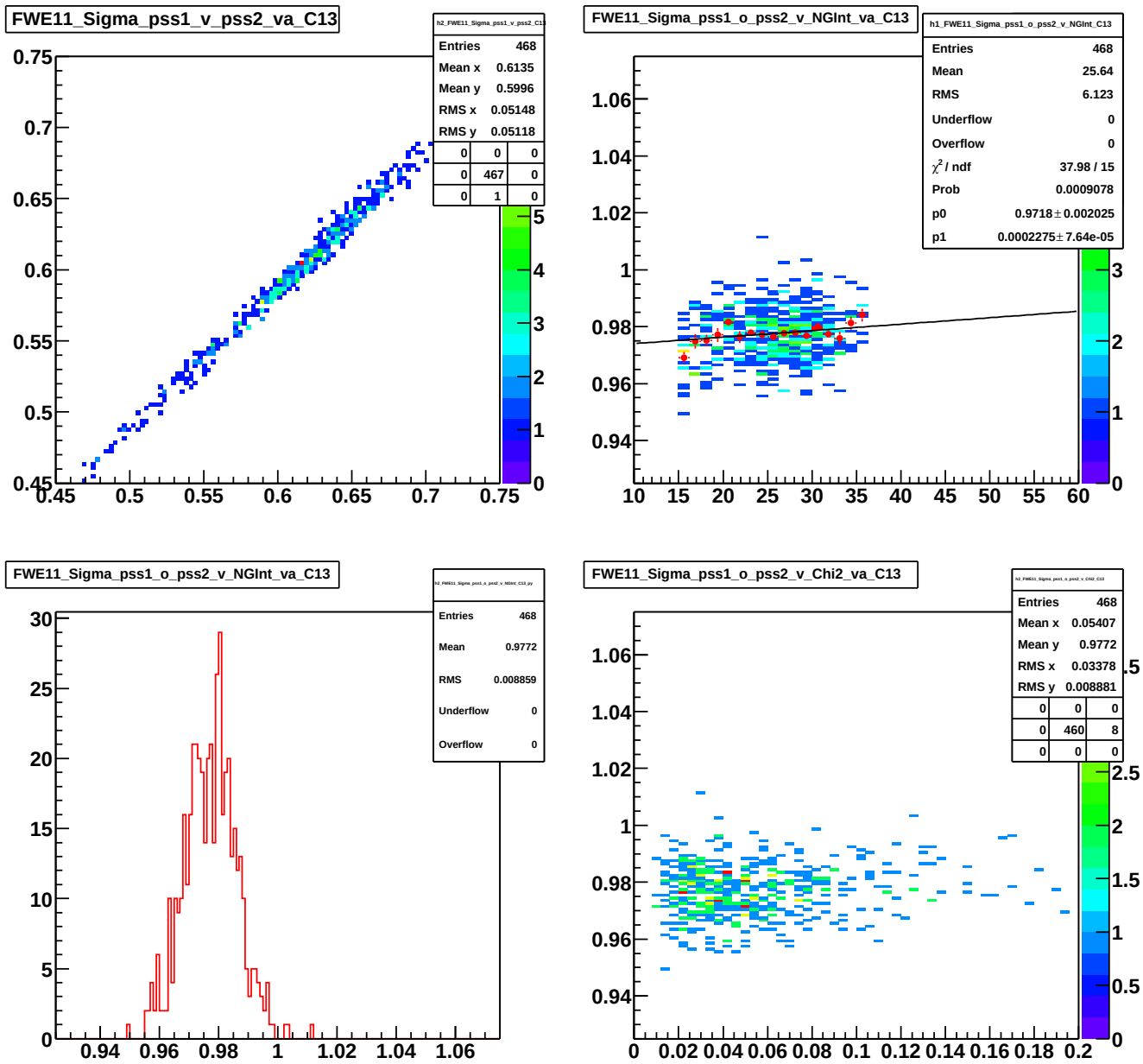

Figure 42: Antiproton beam, vertical detectors: Performance of the Flying Wire Detector at the E11 location during Tevatron Remove Halo case: Sigma of the bunch width distribution (in *mm*) of the pass 1 versus pass 2 of the FW detector; sigma of the bunch width distribution (in *mm*) of the pass 1 over pass 2 of the FW detector versus bunch intensity (ACNET variables T:FBI[A,P]NG) (in E9) together with an overlaid horizontal profile and a straight line fit; sigma of the bunch width distribution (in *mm*) of the pass 1 over pass 2 of the FW detector itself, sigma of the bunch width distribution (in *mm*) of the pass 1 over pass 2 of the FW detector versus front end measure of the goodness of fit.

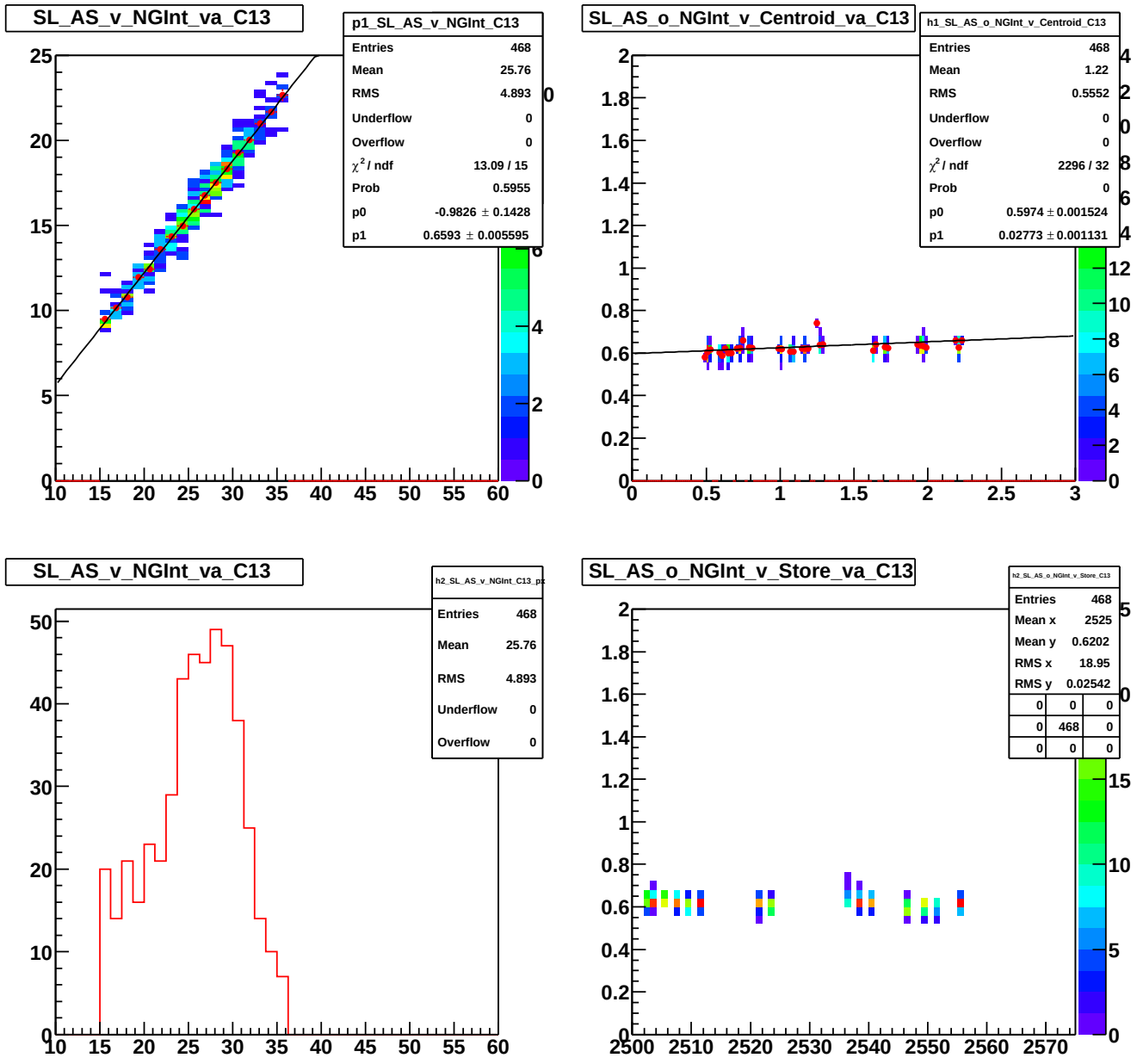

Figure 43: Antiproton beam, vertical detectors: Performance of the Synchrotron Light Detector at the C11 location during Tevatron Remove Halo case: Amplitude (in arbitrary units) times sigma of the bunch width distribution (in *mm*) of the raw SL detector distribution versus bunch intensity (ACNET variables T:FBI[A,P]NG) (in E9) with an overlaid horizontal profile of that distribution with a straight line fit; amplitude times sigma of the bunch width distribution (in *mm*) of the raw SL detector distribution over bunch intensity versus bunch E11 centroid (in *mm*) (based on the T:FW[E,H,V][A,P]CE ACNET variable) with an overlaid horizontal profile of that distribution with a straight line fit; bunch intensity; amplitude times sigma of the bunch width distribution (in *mm*) of the raw SL detector distribution over bunch intensity versus store number.

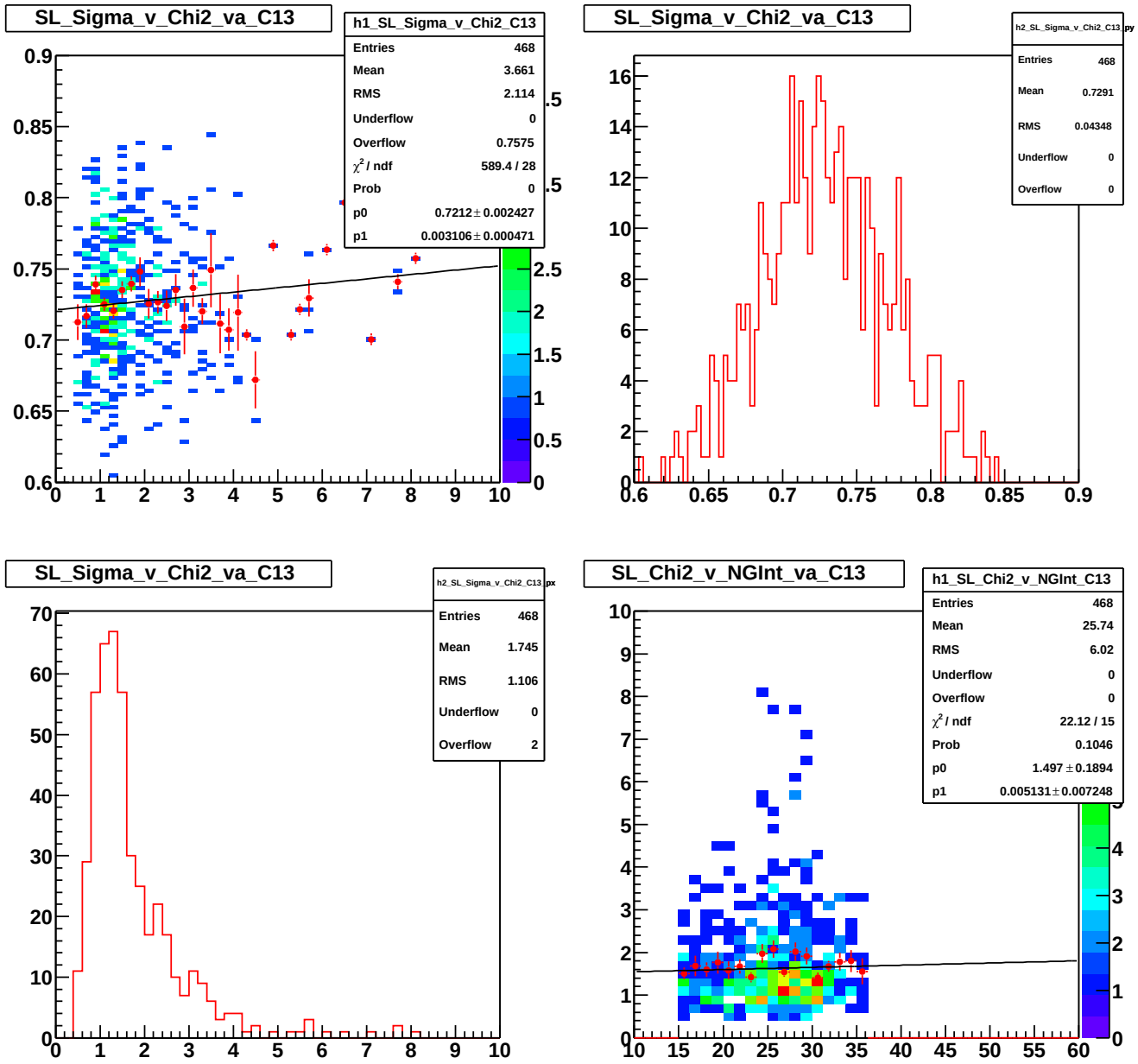

Figure 44: Antiproton beam, vertical detectors: Performance of the Synchrotron Light Detector at the C11 location during Tevatron Remove Halo case: Sigma of the bunch width distribution (in *mm*) as measured by the SL detector versus front end measure of the goodness of fit together with an overlaid horizontal profile and a straight line fit; sigma of the bunch width distribution (in *mm*) itself; goodness of fit itself; goodness of fit versus bunch intensity together with an overlaid horizontal profile and a straight line fit.

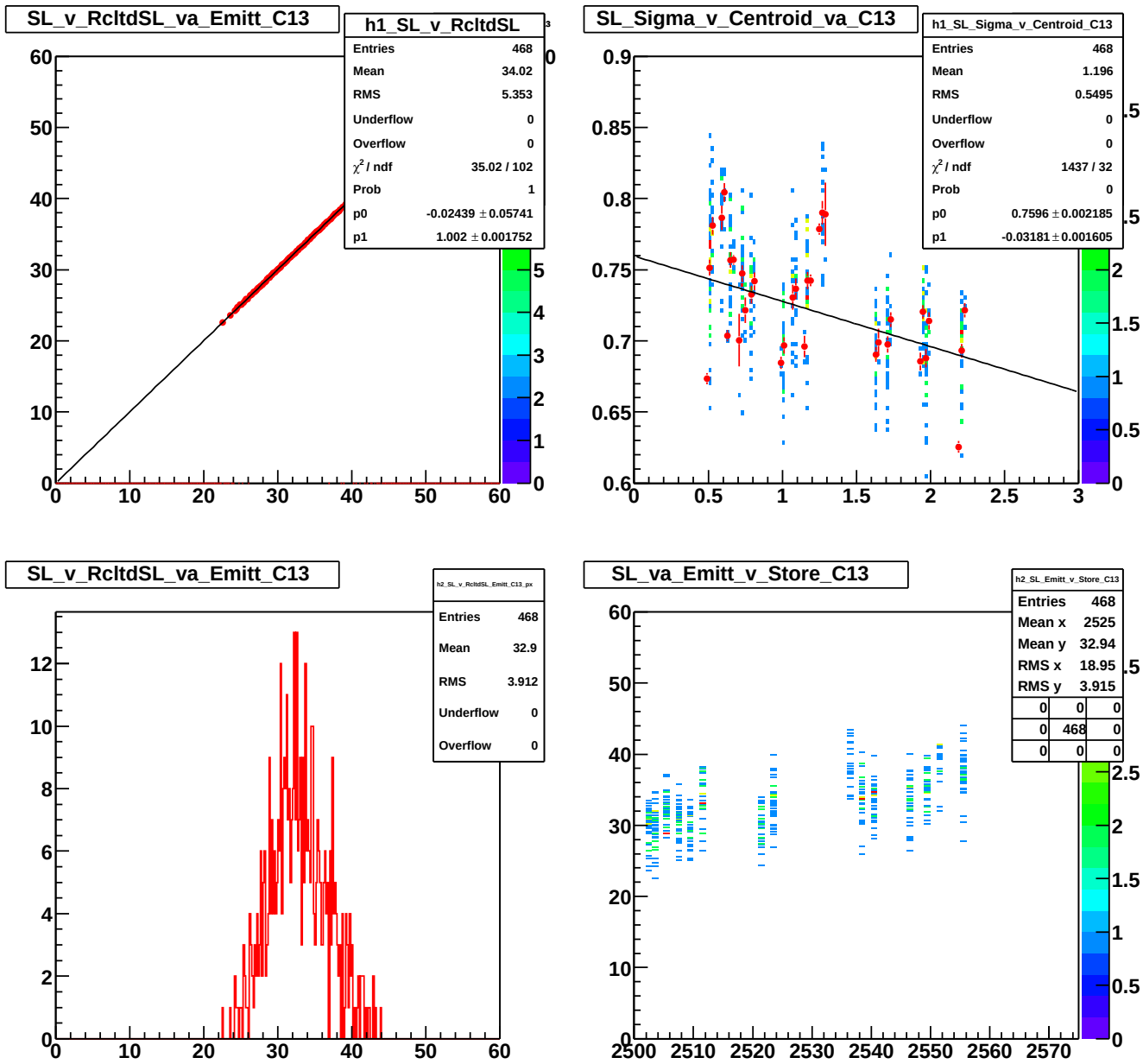

Figure 45: Antiproton beam, vertical detectors: Performance of the Synchrotron Light Detector at the C11 location during Tevatron Remove Halo case: Bunch emittance (in $\pi \cdot mm \cdot mrad$) as measured by the front end SL detector versus bunch emittance as recalculated using front end sigma of the bunch width distribution (in *mm*) (combined with SBD timing information in the horizontal cases) together with an overlaid horizontal profile of that distribution with a straight line fit; sigma of the bunch width distribution versus bunch E11 centroid (in *mm*) (based on the T:FW[E,H,V][A,P]CE ACNET variable) with an overlaid horizontal profile of that distribution with a straight line fit; bunch emittance; bunch emittance versus store number.

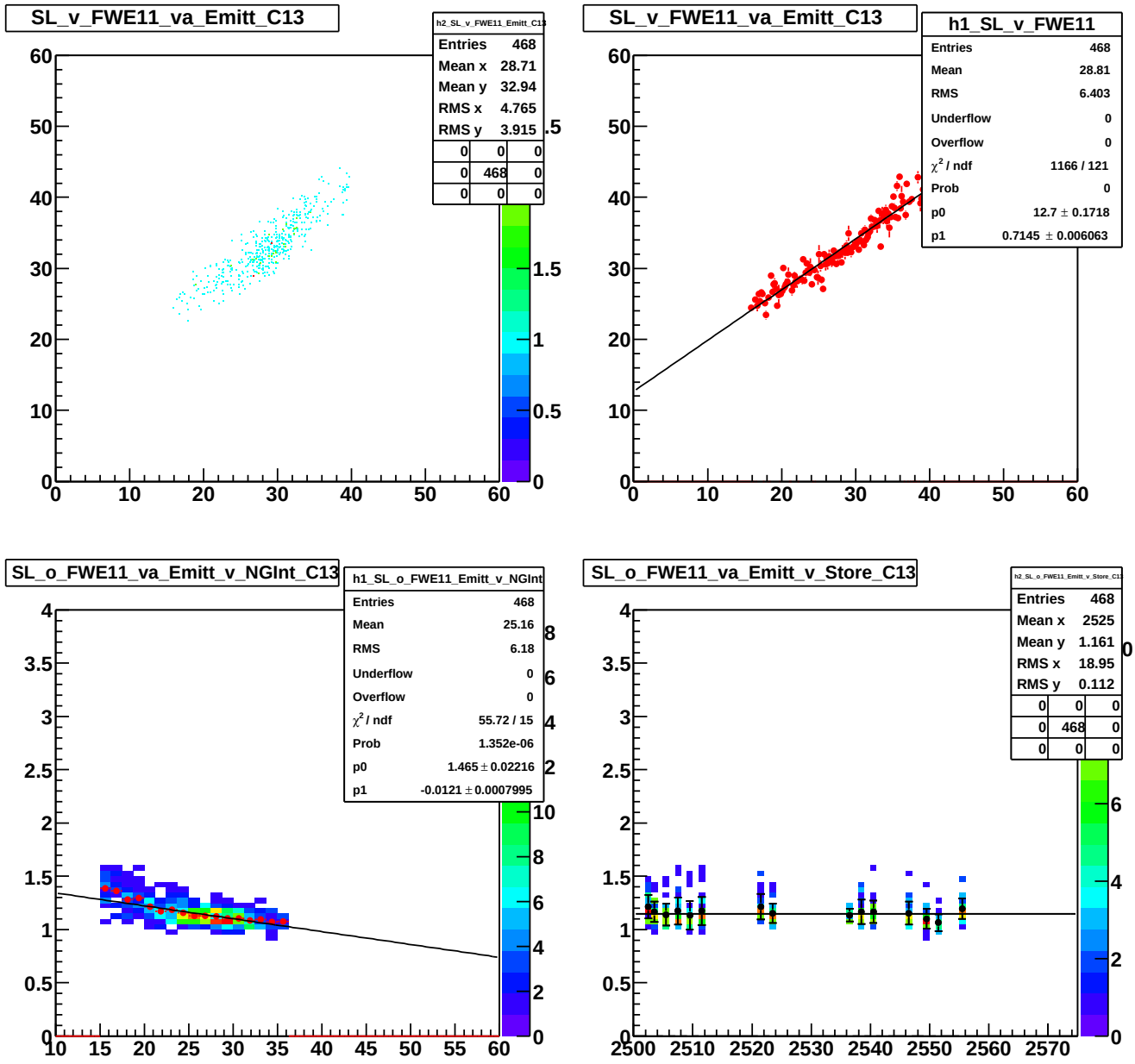

Figure 46: Antiproton beam, vertical detectors: Comparisons of Emittance measurements as done by Synchrotron Light Detector at C11 and Flying Wire Detector at E11 during Tevatron Remove Halo case: Bunch emittance (in $\pi \cdot mm \cdot mrad$) as measured by Synchrotron Light Detector versus bunch emittance as measured by the Flying Wire Detector at E11; horizontal profile of the previous distribution with a straight line fit; bunch emittance as measured by Synchrotron Light Detector over bunch emittance as measured by the Flying Wire Detector at E11 versus bunch intensity (ACNET variables T:FBI[A,P]NG) (in E9) together with an overlaid horizontal profile and a straight line fit; bunch emittance as measured by Synchrotron Light Detector over bunch emittance as measured by the Flying Wire Detector at E11 versus store number with overlaid averaged ratios for each store and a horizontal line fit.

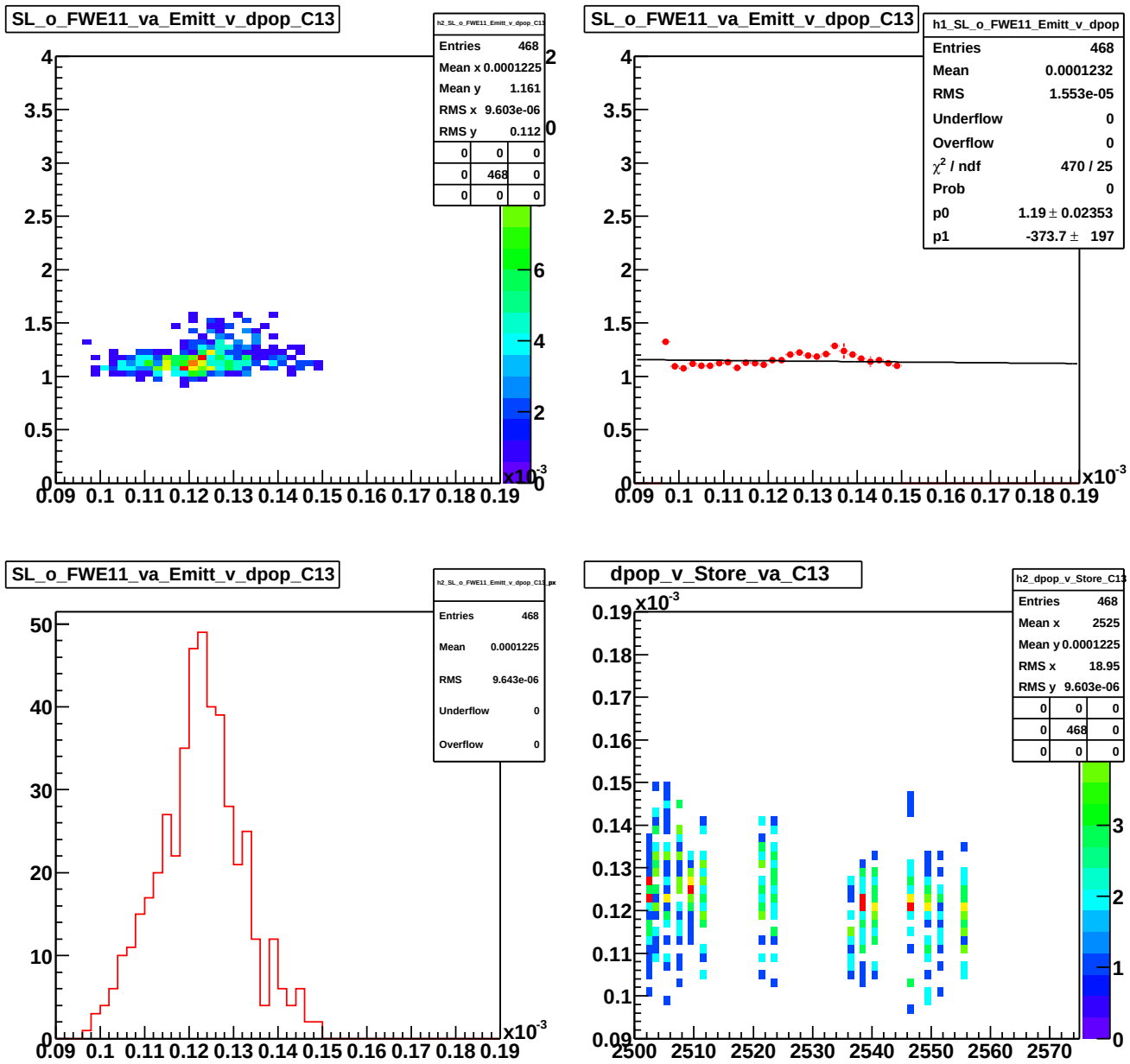

Figure 47: Antiproton beam, vertical detectors: Comparisons of Emittance measurements as done by Synchrotron Light Detector at C11 and Flying Wire Detector at E11 during Tevatron Remove Halo case: Bunch emittance as measured by Synchrotron Light Detector over bunch emittance as measured by the Flying Wire Detector at E11 versus recalculated $\delta p/p$ (based on δt the T:SBD[A,P]SS ACNET variable); horizontal profile of the previous distribution with a straight line fit; $\delta p/p$ itself; $\delta p/p$ versus store number.

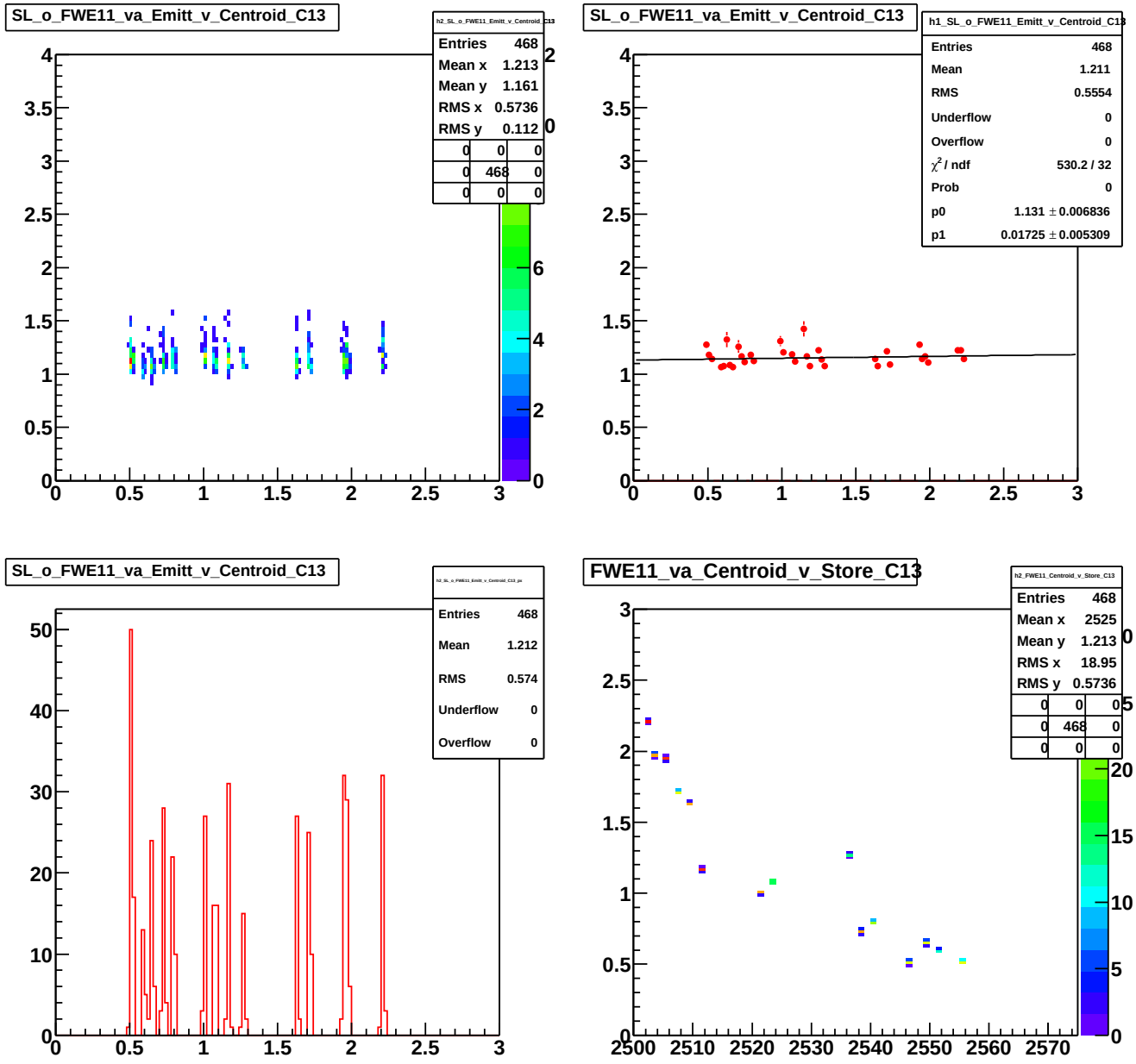

Figure 48: Antiproton beam, vertical detectors: Comparisons of Emittance measurements as done by Synchrotron Light Detector at C11 and Flying Wire Detector at E11 during Tevatron Remove Halo case: Bunch emittance as measured by Synchrotron Light Detector over bunch emittance as measured by the Flying Wire Detector at E11 versus bunch E11 centroid (in *mm*) (based on the T:FW[E,H,V][A,P]CE ACNET variable); horizontal profile of the previous distribution with a straight line fit; bunch E11 centroid itself; bunch E11 centroid versus store number.

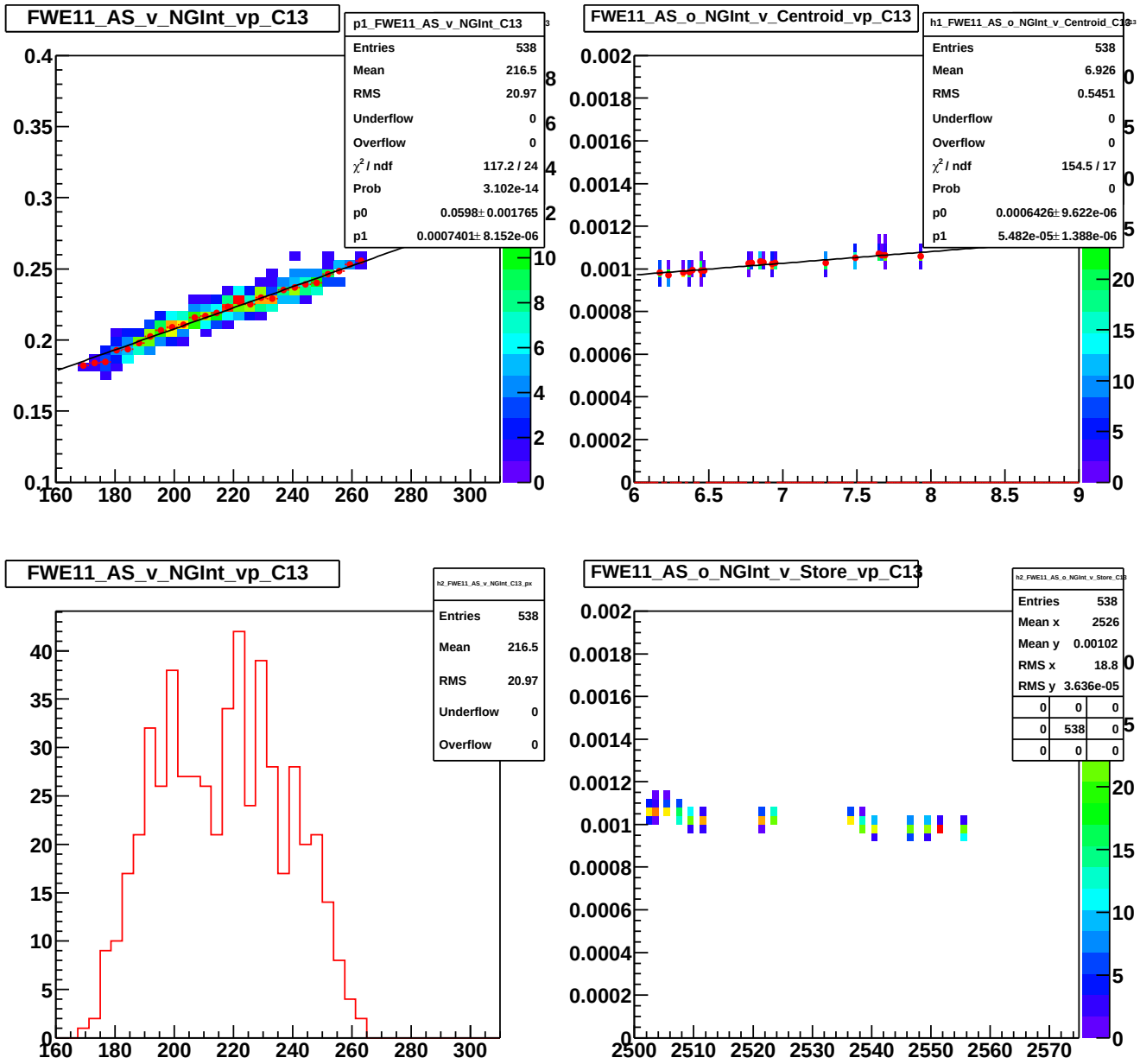

Figure 49: Proton beam, vertical detectors: Performance of the Flying Wire Detector at the E11 location during Tevatron Remove Halo case: Amplitude (in arbitrary units) times sigma of the bunch width distribution (in *mm*) of the front end FW detector data versus bunch intensity (ACNET variables T:FBI[A,P]NG) (in E9) with an overlaid horizontal profile of that distribution with a straight line fit; Amplitude times sigma of the bunch width distribution of the front end FW detector data over bunch intensity versus bunch E11 centroid (in *mm*) (based on the T:FW[E,H,V][A,P]CE ACNET variable) with an overlaid horizontal profile of that distribution with a straight line fit; bunch intensity; amplitude times sigma of the bunch width distribution (in *mm*) of the raw FW detector distribution over bunch intensity versus store number.

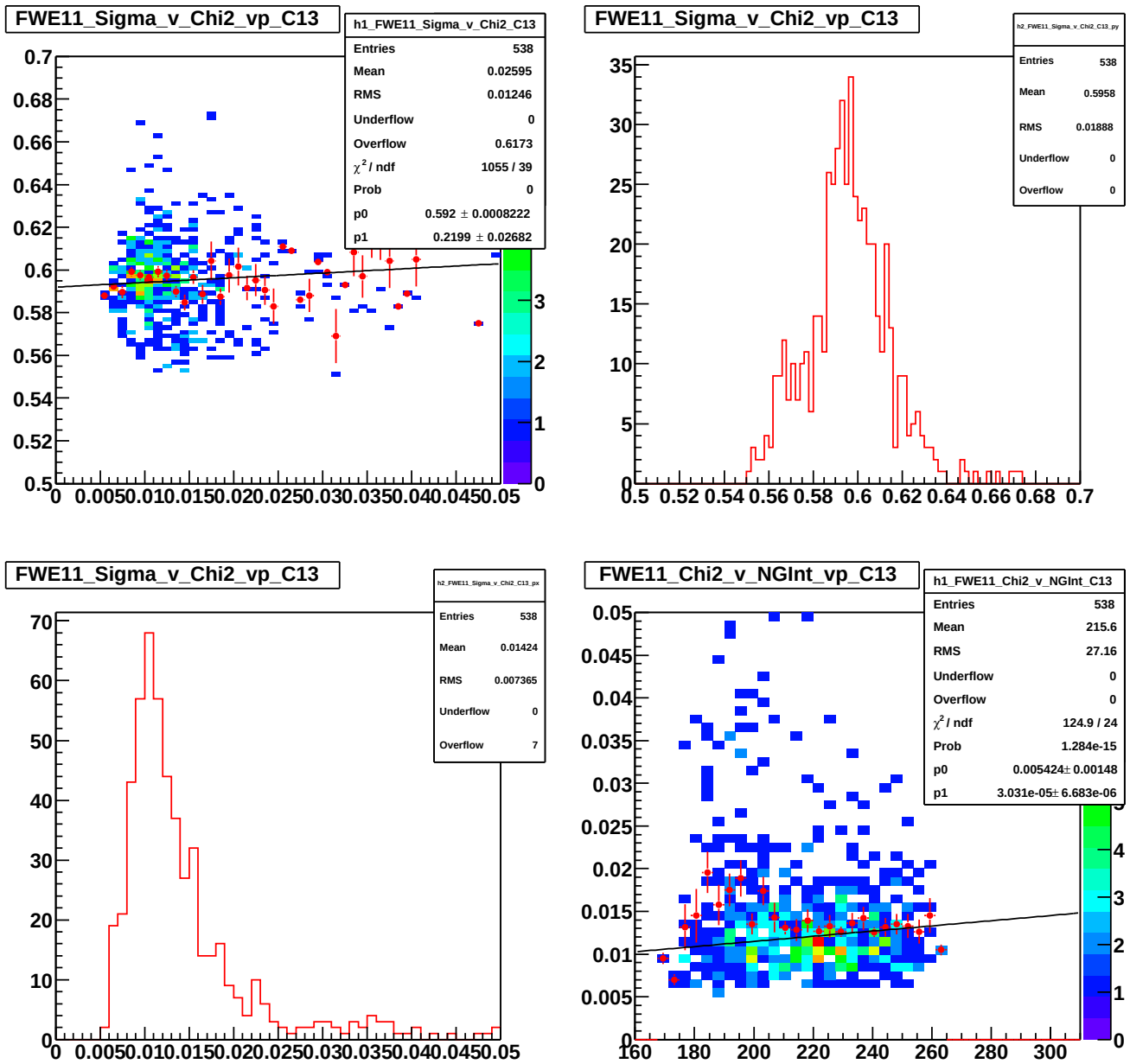

Figure 50: Proton beam, vertical detectors: Performance of the Flying Wire Detector at the E11 location during Tevatron Remove Halo case: Sigma of the bunch width distribution (in *mm*) as measured by the FW detector versus front end measure of the goodness of fit together with an overlaid horizontal profile and a straight line fit; sigma itself, goodness of fit itself; goodness of fit versus bunch intensity together with an overlaid horizontal profile and a straight line fit;

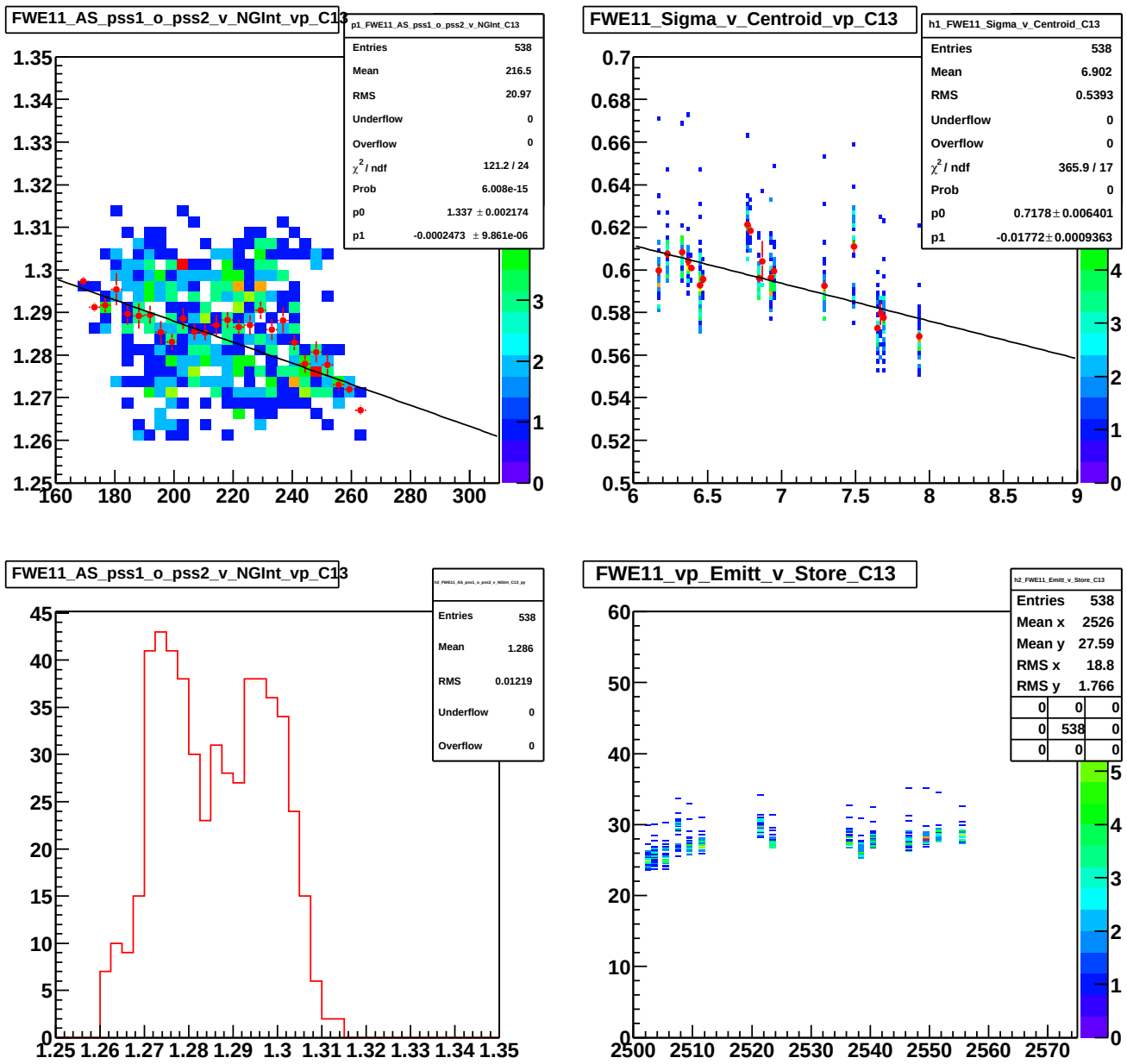

Figure 51: Proton beam, vertical detectors: Performance of the Flying Wire Detector at the E11 location during Tevatron Remove Halo case: Amplitude (in arbitrary units) times sigma of the bunch width distribution (in *mm*) of the pass 1 over pass 2 of the front end FW detector data versus bunch intensity (ACNET variables T:FBI[A,P]NG) (in E9) together with an overlaid horizontal profile of that distribution with a straight line fit; sigma of the bunch width distribution versus bunch centroid (in *mm*) (based on the T:FW[E,H,V][A,P]CE ACNET variable) with an overlaid horizontal profile of that distribution with a straight line fit; amplitude (in arbitrary units) times sigma of the bunch width distribution (in *mm*) of the pass 1 over pass 2 of the front end FW detector data itself, bunch emittance (in $\pi \cdot mm \cdot mrad$) versus store number.

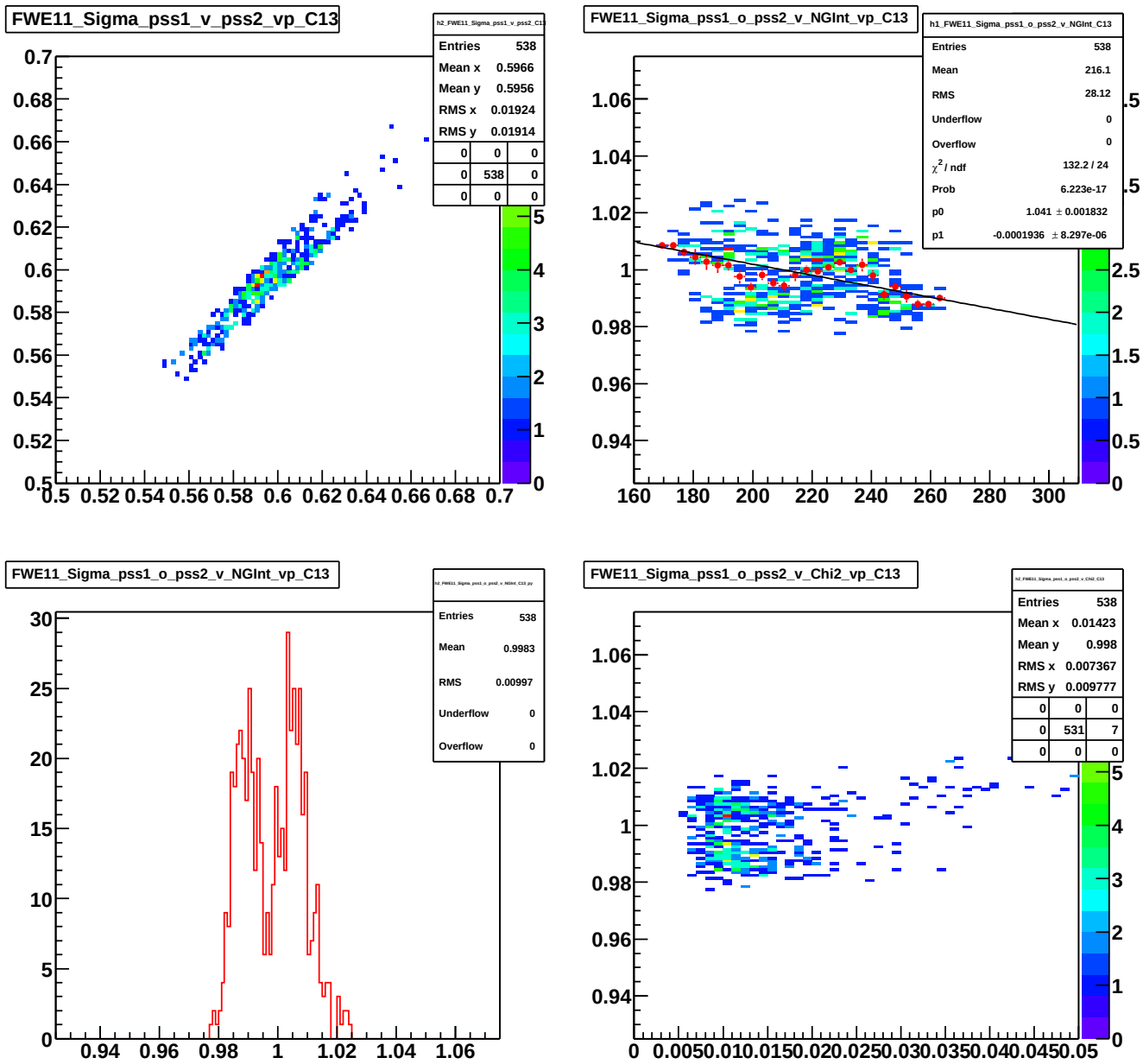

Figure 52: Proton beam, vertical detectors: Performance of the Flying Wire Detector at the E11 location during Tevatron Remove Halo case: Sigma of the bunch width distribution (in *mm*) of the pass 1 versus pass 2 of the FW detector; sigma of the bunch width distribution (in *mm*) of the pass 1 over pass 2 of the FW detector versus bunch intensity (ACNET variables T:FBI[A,P]NG) (in E9) together with an overlaid horizontal profile and a straight line fit; sigma of the bunch width distribution (in *mm*) of the pass 1 over pass 2 of the FW detector itself, sigma of the bunch width distribution (in *mm*) of the pass 1 over pass 2 of the FW detector versus front end measure of the goodness of fit.

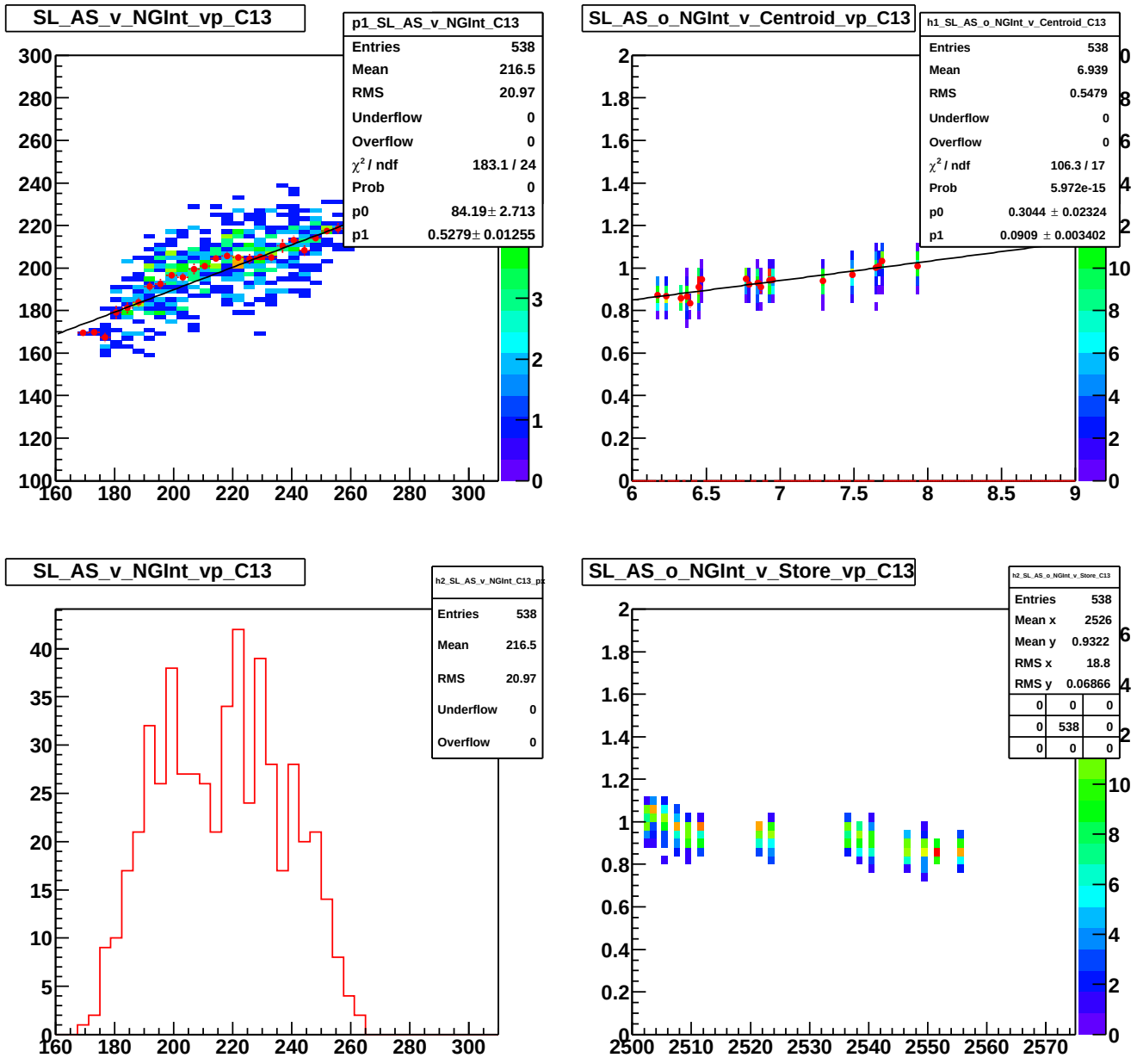

Figure 53: Proton beam, vertical detectors: Performance of the Synchrotron Light Detector at the C11 location during Tevatron Remove Halo case: Amplitude (in arbitrary units) times sigma of the bunch width distribution (in *mm*) of the raw SL detector distribution versus bunch intensity (ACNET variables T:FBI[A,P]NG) (in E9) with an overlaid horizontal profile of that distribution with a straight line fit; amplitude times sigma of the bunch width distribution (in *mm*) of the raw SL detector distribution over bunch intensity versus bunch E11 centroid (in *mm*) (based on the T:FW[E,H,V][A,P]CE ACNET variable) with an overlaid horizontal profile of that distribution with a straight line fit; bunch intensity; amplitude times sigma of the bunch width distribution (in *mm*) of the raw SL detector distribution over bunch intensity versus store number.

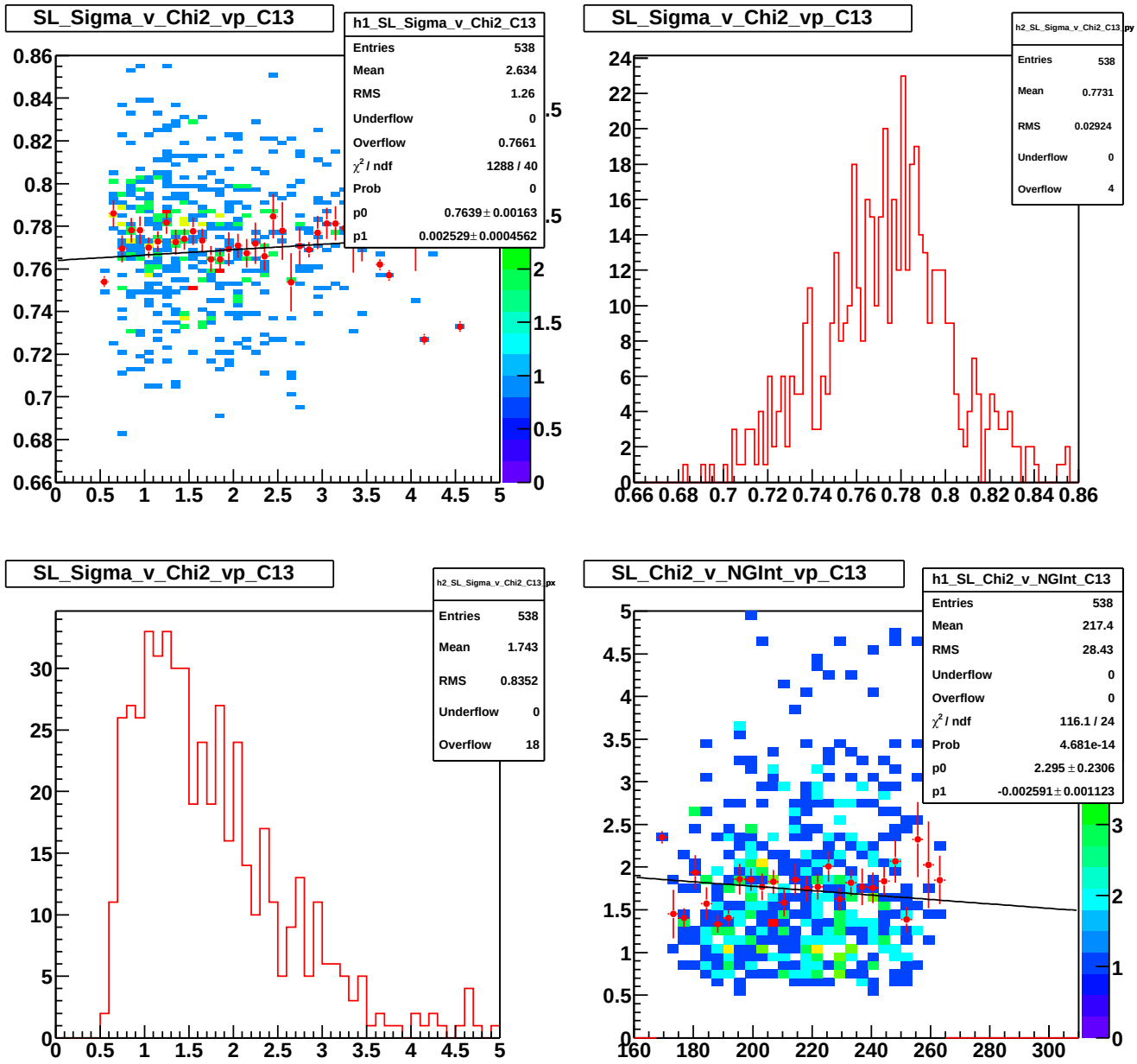

Figure 54: Proton beam, vertical detectors: Performance of the Synchrotron Light Detector at the C11 location during Tevatron Remove Halo case: Sigma of the bunch width distribution (in *mm*) as measured by the SL detector versus front end measure of the goodness of fit together with an overlaid horizontal profile and a straight line fit; sigma of the bunch width distribution (in *mm*) itself; goodness of fit itself; goodness of fit versus bunch intensity together with an overlaid horizontal profile and a straight line fit.

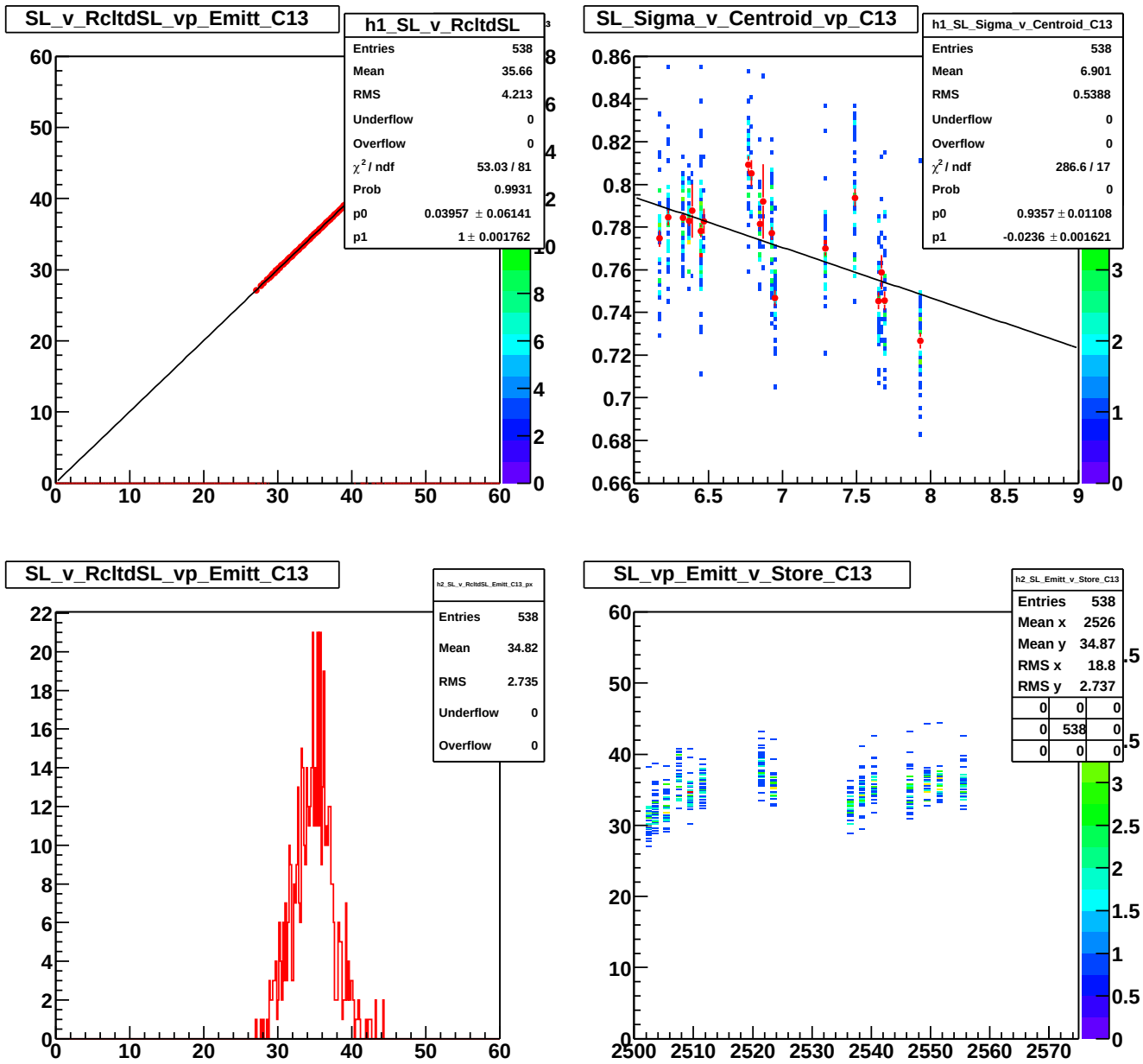

Figure 55: Proton beam, vertical detectors: Performance of the Synchrotron Light Detector at the C11 location during Tevatron Remove Halo case: Bunch emittance (in $\pi \cdot mm \cdot mrad$) as measured by the front end SL detector versus bunch emittance as recalculated using front end sigma of the bunch width distribution (in *mm*) (combined with SBD timing information in the horizontal cases) together with an overlaid horizontal profile of that distribution with a straight line fit; sigma of the bunch width distribution versus bunch E11 centroid (in *mm*) (based on the T:FW[E,H,V][A,P]CE ACNET variable) with an overlaid horizontal profile of that distribution with a straight line fit; bunch emittance; bunch emittance versus store number.

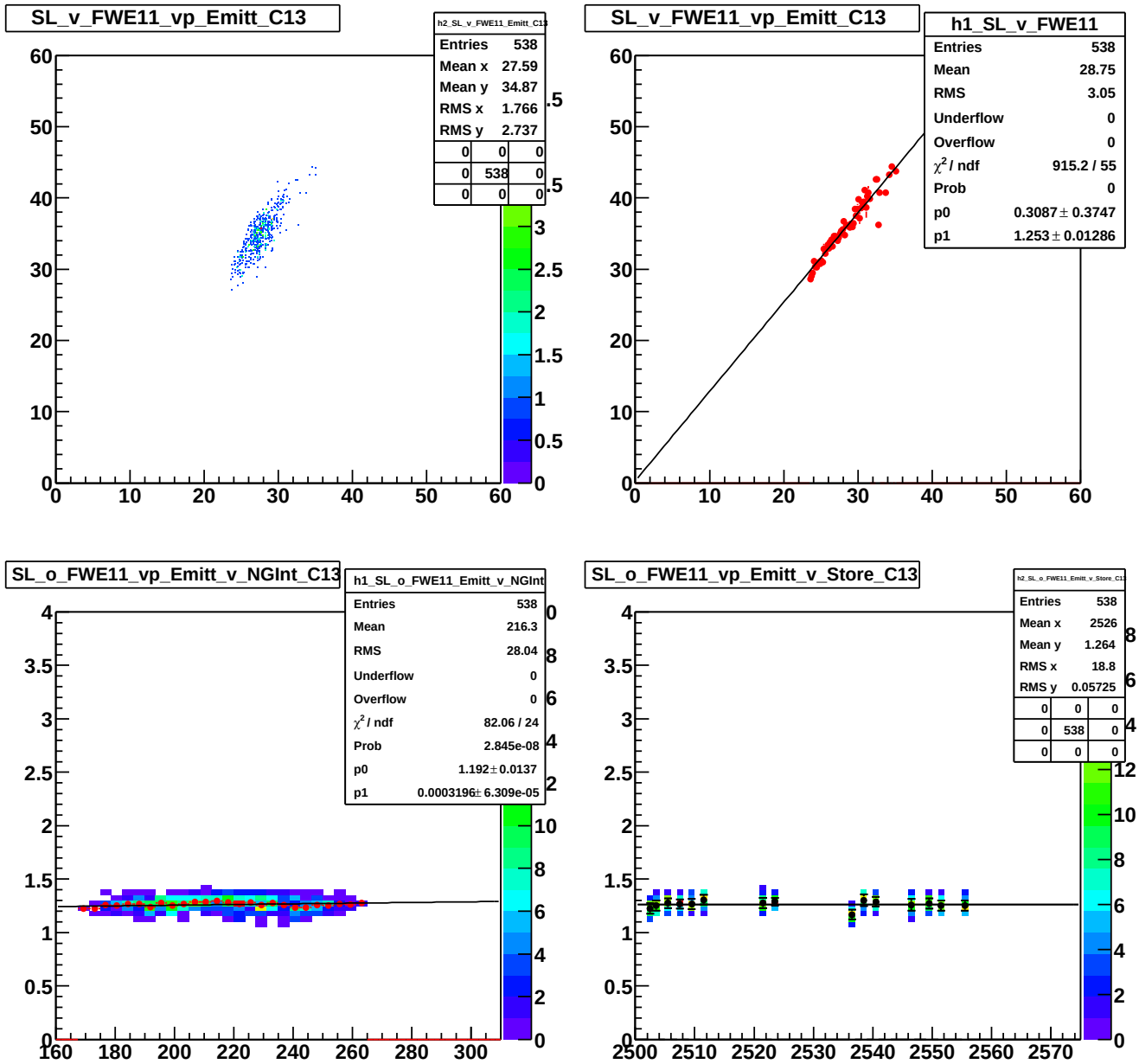

Figure 56: Proton beam, vertical detectors: Comparisons of Emittance measurements as done by Synchrotron Light Detector at C11 and Flying Wire Detector at E11 during Tevatron Remove Halo case: Bunch emittance (in $\pi \cdot mm \cdot mrad$) as measured by Synchrotron Light Detector versus bunch emittance as measured by the Flying Wire Detector at E11; horizontal profile of the previous distribution with a straight line fit; bunch emittance as measured by Synchrotron Light Detector over bunch emittance as measured by the Flying Wire Detector at E11 versus bunch intensity (ACNET variables T:FBI[A,P]NG) (in E9) together with an overlaid horizontal profile and a straight line fit; bunch emittance as measured by Synchrotron Light Detector over bunch emittance as measured by the Flying Wire Detector at E11 versus store number with overlaid averaged ratios for each store and a horizontal line fit.

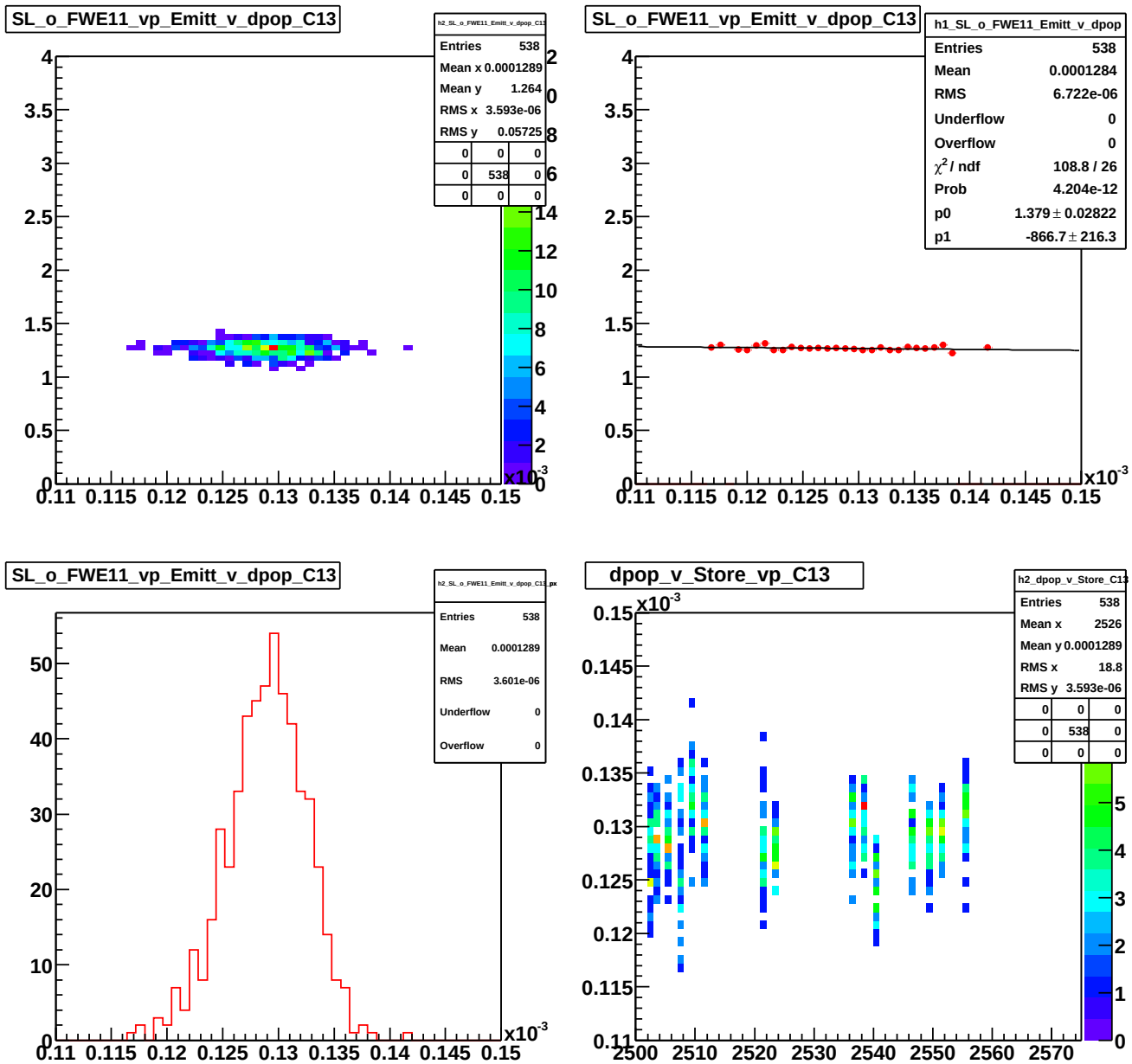

Figure 57: Proton beam, vertical detectors: Comparisons of Emittance measurements as done by Synchrotron Light Detector at C11 and Flying Wire Detector at E11 during Tevatron Remove Halo case: Bunch emittance as measured by Synchrotron Light Detector over bunch emittance as measured by the Flying Wire Detector at E11 versus recalculated $\delta p/p$ (based on δt the T:SBD[A,P]SS ACNET variable); horizontal profile of the previous distribution with a straight line fit; $\delta p/p$ itself; $\delta p/p$ versus store number.

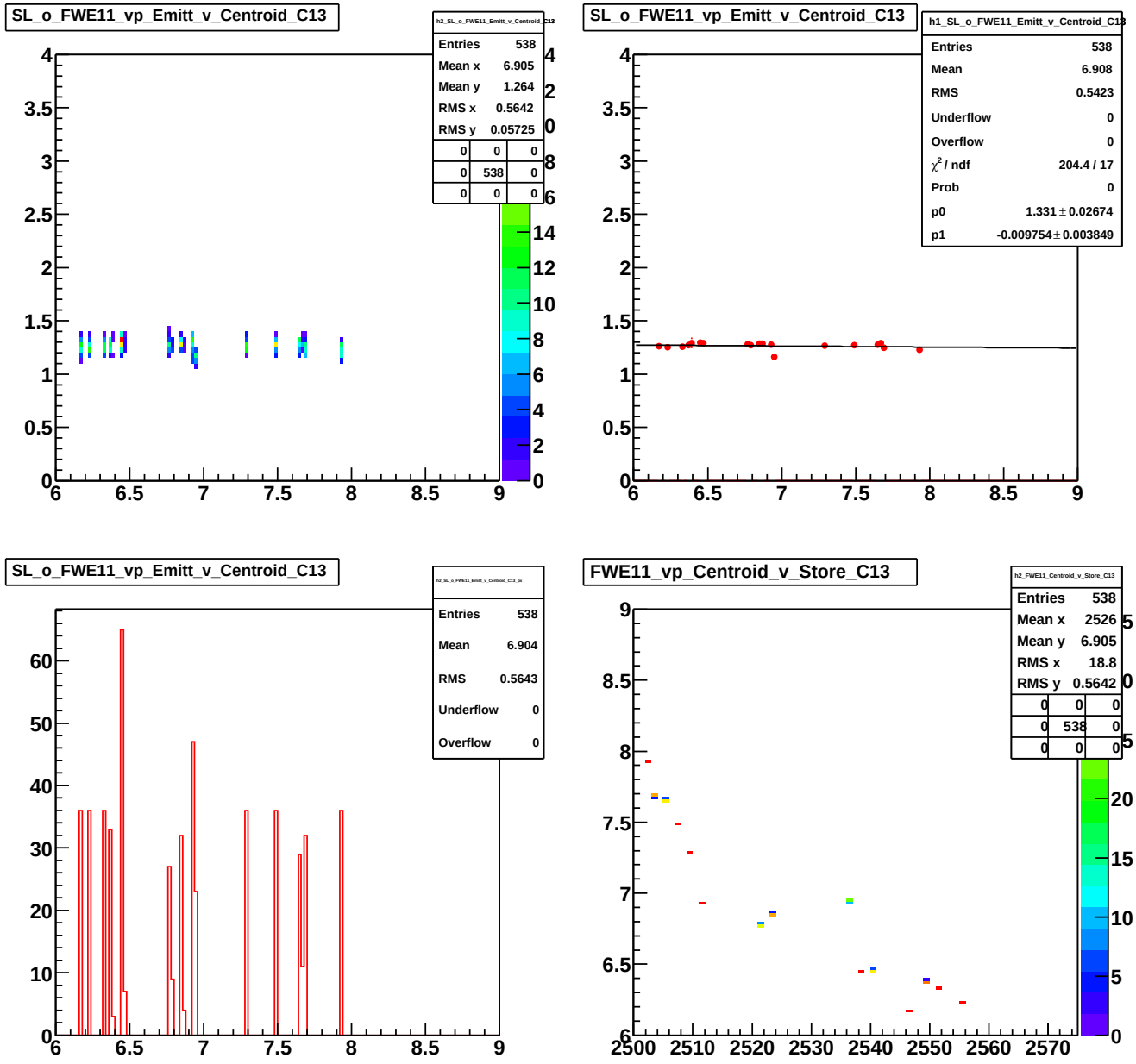

Figure 58: Proton beam, vertical detectors: Comparisons of Emittance measurements as done by Synchrotron Light Detector at C11 and Flying Wire Detector at E11 during Tevatron Remove Halo case: Bunch emittance as measured by Synchrotron Light Detector over bunch emittance as measured by the Flying Wire Detector at E11 versus bunch E11 centroid (in *mm*) (based on the T:FW[E,H,V][A,P]CE ACNET variable); horizontal profile of the previous distribution with a straight line fit; bunch E11 centroid itself; bunch E11 centroid versus store number.